TRIGGERED CARGO RELEASE FROM LIPOSOMES USING MEMBRANE-

SELECTIVE NANOPORE-FORMING PEPTIDES

AN ABSTRACT SUBMITTED ON THE TWENTY SECOND DAY OF NOVEMBER

TWO THOUSAND TWENTY-TWO TO THE DEPARTMENT OF BIOCHEMISTRY

AND MOLECULAR BIOLOGY IN PARTIAL FULFILLMENT OF THE

REQUIREMENTS OF THE GRADUATE SCHOOL OF TULANE UNIVERSITY FOR

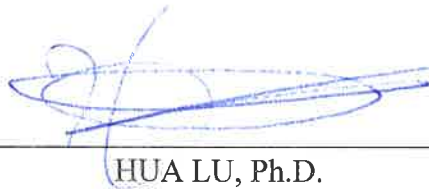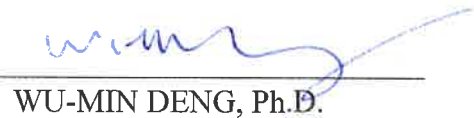THE DEGREE OF DOCTOR OF PHILOSOPHY BY

_____

LEISHENG SUN

APPROVED:

_____

WILLIAM C. WIMLEY, Ph.D., ADVISOR

_____   _____

HUA LU, Ph.D.   WU-MIN DENG, Ph.D.

_____   _____

HEATHER L. MACHADO, Ph.D.   JAMES JACKSON, Ph.D.

ABSTRACT

Here we developed a model of peptide-triggered cargo release from liposomes using peptides that have extraordinary selectivity for PC liposomes over mammalian cells. Such a model can be used when cargoes are encapsulated into stable liposomes, which can be permeabilized by peptides so that the cargoes are released immediately in the presence of cells. Previously, a novel family of α-helical pore-forming peptides called "macrolittins", was identified. These 26-residue peptides are products from two batches of screening iterative library. Macrolittins bind strongly to phosphatidylcholine (PC) liposomes, fold into α-helical secondary structure, and form macromolecule-sized pores, releasing macromolecular cargoes from PC liposomes at concentrations as low as 1 peptide per 1000 lipids. In this work, we show that macrolittins bind very weakly to cell membranes and have no measurable cytolytic activity against multiple human cell types even at a high peptide concentration. We show that this unprecedented selectivity for PC liposomes over cell plasma membranes can be explained, in part, by the sensitivity of macrolittin activity to physical chemical properties of the bilayer hydrocarbon core. We also find that macrolittins can cause PC liposome aggregation and fusion as well as increased fusion between PC liposome and cell membrane, but that these activities can be inhibited by inclusion of pegylated phospholipid within the membrane without affecting permeabilization. In the presence of cells, macrolittins release all liposome-entrapped cargoes (proteins and small molecule drugs) which are then readily uptaken by the cells. Triggered release occurs without any direct effect of the peptides on the cells, and without vesicle-vesicle or vesicle-cell interactions. To further investigate sequence-structure-function relationship of pore forming peptides, we made a series of targeted substitutions

and demonstrated the importance of two highly conserved acidic amino acids at the 4th and 8th positions in the macrolittin sequence. Finally, to further explore the basis for membrane selectivity, a library of elongated macrolittin analogues was synthesized and screened against liposomes of different membrane thicknesses. We find that variant hits have longer α-helical secondary structure, but have a preserved helical pattern of charged residues, which are required to partition into and form nanopores in thicker bilayers.

TRIGGERED CARGO RELEASE FROM LIPOSOMES USING MEMBRANE-

SELECTIVE NANOPORE-FORMING PEPTIDES

A DISSERTATION SUBMITTED ON THE TWENTY SECOND DAY OF

NOVEMBER TWO THOUSAND TWENTY-TWO TO THE DEPARTMENT OF

BIOCHEMISTRY AND MOLECULAR BIOLOGY IN PARTIAL FULFILLMENT OF

THE REQUIREMENTS OF THE GRADUATE SCHOOL OF TULANE UNIVERSITY
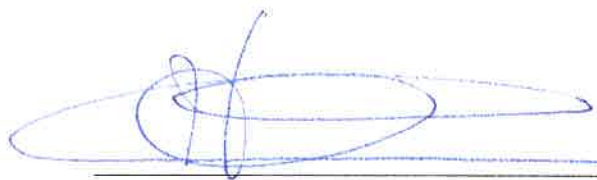
FOR THE DEGREE OF DOCTOR OF PHILOSOPHY BY
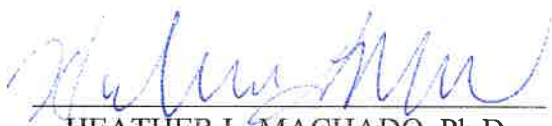
_____

LEISHENG SUN

APPROVED:

_____

WILLIAM C. WIMLEY, Ph.D., ADVISOR

_____   _____
HUA LU, Ph.D.   WU-MIN DENG, Ph.D.

_____   _____
HEATHER L. MACHADO, Ph.D.   JAMES JACKSON, Ph.D.

ACKNOWLEDGEMENT

With time flying fast, I have been studying at Tulane University for over five years and I am now about to finish this memorable and valuable journey at the end of this year. From 2017 to 2022, I learned a lot from academic courses and research projects in Biomedical Sciences Program in School of Medicine, and my hard works were recorded in my publications as a PhD student. Meanwhile. I made a lot of friends including my classmates, roommates and neighbors in New Orleans. I really enjoy the beautiful life during these five years in United States.

I was born in Changsha city at south part of China in 1992. I obtained my Bachelor degree in China Pharmaceutical University and my Master Degree at University of Minnesota, and my parents supported me for tuitions and living cost financially. Then I decided to pursue a PhD at Tulane University because I hope to learn more knowledge and skills about biomedical sciences to help patients who are suffering from diseases, and this decision was encouraged by my parents. Therefore, I would like to thank my parents to give me the great opportunities for advanced education. Thank you all!

Dr. Wimley is a popular advisor for many of my peer students due to his innovative research and helpful personality. No matter what kinds of results or news I get from projects, he is always positive and encouraging, and he would like to think about solutions for experiment optimization, which brings me comforts and confidence. It's hard to see someone so sophisticated and so successful in their focused domains while also being such a good instructor and also so optimistic. Thanks a lot for your patience and guidance during your mentorship. I really appreciate it!

My dissertation committee was amazing. In addition to my supervisor Dr. William Wimley, Drs Hua Lu, Wu-min Deng, Heather Machado, James Jackson are all helpful, insightful, giving me a lot of instructions and suggestions about academic research and job hunting. It is my genuine pleasure to talk with them during my PhD life.

When I joined the lab back in 2017, I was not familiar with the lab environment and did not know about the senior lab students. Drs. Shan Guha and Jenisha Ghimire introduced me to all the lab members and gave me instructions for some experiments. Dr. Eric Wu taught me a lot to use various equipment in the lab and helped me with important projects. Ryan helped me with my research when I am busy with other work... All of lab members are so friendly and helpful. So much love to them!

DEDICATION

To my family, my parents Zhiliang Sun and Libin Mo who have been supporting me since

I was born, and my cat Wenzy who has been staying with me for five years.

To those who always bring me encouragement and happiness.

TABLE OF CONTENTS

LIST OF FIGURES AND TABLES

CHAPTER 1: How macrolittins may trigger cargo release from liposomes.

Many biotechnological applications of membrane permeabilizing peptides have been described in the literature, including applications in drug delivery[1] and transfection,[2] as well as applications based on anticancer,[3] antibacterial[4] and antiviral activity.[5] To maximize the utility of membrane permeabilizing peptides we must identify peptides that are optimized for selectivity towards target membranes over bystander membranes. For example, membrane permeabilizing peptides could have utility in conjunction with liposome-associated drug delivery, which is used as a smart strategy to control drug delivery *in vivo*. Liposome encapsulation of small molecule drugs can extend drug release time, and reduce the acute systemic side effects of free drug.[6] Liposome encapsulation of macromolecular cargoes such as oligonucleotides, antibodies, enzymes, and other therapeutic proteins can improve stability and provide very long circulation time, in vivo, but spontaneous release of macromolecules can be very slow, if it happens at all. Further, drug-containing liposomes can accumulate specifically in diseased tissue, including tumors, due to enhanced permeability and retention.[7] They can also be targeted to specific tissues by other means,[8] but slow release of tumor-retained liposome-associated drugs could decrease free drug concentration and be less effective to tumor treatment.[9] In these circumstances, the utility of liposome encapsulation could be improved by fast release of vesicle contents, including macromolecules, by a nontoxic peptide.

Given that slow drug release from highly stable liposomes leads to poor therapeutic effect, there is a critical need for a strategy to accelerate drug and macromolecule release

from liposomes in a controllable manner. Researchers have been studying modification of liposomes for decades to optimize liposome delivery in vivo (**Fig. 1-1**). For example, PEGylation of lipids can be included in liposome membrane to inhibit interaction with cell or other macromolecules and increase circulation time in vivo. Compared to passive liposome accumulation at tumor site due to enhanced permeability and retention effect, active targeted delivery can be achieved by tethering antibody or ligand on liposome surface so that liposomes can bind cancer cell selectively. Importantly, liposome permeability has been designed to be sensitive to external triggers such as temperature, magnetic field, or light.[10, 11] In addition, internal triggers including enzyme, redox reaction, and pH at tumor microenvironment have been reported to release drug efficiently. However, there are some drawbacks with the current triggered release methods. Firstly, the synthesis of specialized lipids and preparation of liposomes specific to such controlled release is often complicated. For example, many thermosensitive liposomes include metallic nanoparticles within the artificial membrane.[12] Secondly, external stimuli such as specific pH must be localized to the affected tissue, thus locations in the body to be affected must be determined in advance and need to be accessible to external stimuli.[13] Thirdly, some liposomes with specific structures or compositions for potential stimuli can only encapsulate specific cargoes but not general macromolecular cargoes.[14] Lastly, some harsh stimuli might cause damage to cargoes encapsulated. Peptide-induced release has not been studied very often because most membrane-permeabilizing peptides also have cytolytic activity and do not release macromolecules, limiting their utility.[15] An ideal peptide as a stimulus for simple liposomes would potently permeabilize liposomes of a specific lipid composition, and release general macromolecule and small molecule cargos without

cytolytic activity against cell membranes. Unfortunately, peptides with these properties cannot be rationally designed or optimized because the structure and function of peptides in membranes cannot currently be described by quantitative sequence-structure-function relationship rules.[16] Peptide-membrane interactions are driven mostly by physical chemical interactions that act nonspecifically in the context of dynamic and heterogeneous fluid phase bilayer structure.[17]

To identify a peptide with high potency to permeabilize lipid membranes, we looked back at previous generations of evolved pore-forming peptides and found that a line of sequences starting from the bee venom peptide melittin might be promising. Melittin is the archetypal nonselective membrane permeabilizing peptide from cytolytic honeybee venom. It folds into an amphipathic α-helix by a process that is coupled to membrane partitioning.[18] Under most conditions, the melittin helix lies perpendicular to the bilayer normal where it causes permeabilization by transient, non-equilibrium disruption of membrane integrity.[19] By this mechanism, melittin similarly permeabilizes many different membranes, including those of eukaryotic cells,[20] bacteria,[21] viruses,[22] and fungi.[23] Against synthetic bilayers, melittin has similarly low selectivity, readily permeabilizing most fluid phase bilayers to small molecules, but not macromolecules, by forming small transient pores.[24]

Towards the goals of creating novel peptides with increased potency, controllability, and selectivity of membrane permeabilization, the Wimley lab has been generating gain-of-function analogs of melittin using multiple generations of synthetic molecular evolution - high throughput screening of iterative peptide libraries. The first-generation rational combinatorial library of 7,776 members was based on the sequence of melittin.[25] Gain-of-

function analogs were identified by screening this library for potent, equilibrium pore formation and release of small molecules for phosphatidylcholine (PC) liposomes (**Fig. 1-2A**). The most active analog, MelP5, is much more potent to cause small molecule leakage from PC liposomes compared to melittin (**Fig. 1-2B**) despite sharing 77% sequence identity. In addition, MelP5 enables the passage of macromolecules across PC membrane bilayer at low concentrations where melittin and other pore-forming peptides do not.[26] However, MelP5, similar to the parent peptide melittin, is not strongly membrane selective, and is highly cytolytic against multiple mammalian cell lines.[27] Subsequently, MelP5 was used as a template for a second generation library consisting of 18,432 members. In this generation, acidic residues were allowed in six sites with i to i+3 and i to i+4 helical spacings which placed them along the polar face of the amphipathic α-helix of MelP5 (**Fig. 1-2C**). Library members were screened simultaneously for both small molecule and macromolecular poration by measuring release of a small molecule dye of 400 Da and a dextran of 40 kDa. In this screening, the most potent macromolecular poration activity at pH 7, was selected, without selecting for pH dependence. As a result, the "macrolittins"[28] were identified. The macrolittins are a novel family of peptides that induce macromolecular poration in PC bilayers at neutral pH at a strikingly low peptide to lipid ratio (P: L) of ~1:1000, **Fig. 1-2B**. We know of no other peptide with the activity of the macrolittins, except the pHD peptides at pH ≤ 6.[29] In this work, we study three macrolittins, M70, M159 and M204 which have very similar sequences and activities (**Fig. 1-2A**). The potency of macrolittins to permeabilize PC liposomes are confirmed by macromolecule leakage assay, and this high potency is relevant to deep and large-size pores on PC membrane surface (**Fig. 1-3**). The macrolittins have three acidic amino acids (aspartate or glutamate)

out of six that were possible in the library. The macrolittins also have two basic amino acids with a preference for lysine. By design, the acidic and basic residues, and other polar residues such as threonine and glutamine, are found on one face of the amphipathic α-helix (**Fig. 1-2C**).

The lipid vesicles used in these screens was prepared from the lipid 1-palmitoyl-2-oleoyl-sn-glycero-3-phosphocholine (POPC) which contains one saturated chain of 16 carbons and one unsaturated chain of 18 carbons with a single C=C bond. This lipid recapitulates many of the physical chemical properties of mammalian cell plasma membranes, and thus has been widely used for decades as a model system to study mammalian cell plasma membranes.[30] In this dissertation, we test the hypothesis that two generations of synthetic molecular evolution specifically against POPC vesicles have produced some selectivity of macrolittins for POPC bilayers over mammalian cell membranes. Thus, we can determine if a peptide-triggered cargo release model will be established, in which different cargoes are encapsulated into liposomes in the presence of cells, and cargoes are released and uptake by cells immediately when ideal peptides permeabilize the liposomes efficiently (**Fig. 1-4**). We also characterize the mechanism of selectivity for specific membranes, and also demonstrate how to evolve membrane selectivity into the macrolittins.

This dissertation is organized into the following chapters. In **chapter 2**, we show that macrolittins have no cytolytic activity against various mammalian cell lines even at high concentration. To further clarify the interactions between macrolittins and cells, we investigate the effect of L or D type M159 on mammalian cells under different conditions. In **chapter 3**, we discover that unlike MelP5, macrolittins cannot only permeabilize PC

liposomes but also cause PC liposome aggregation and fusion with high potency. Thus, we test the potential factors which affect peptide selectivity by comparing peptide sequence between M159 and the parent peptide MelP5 as well as the difference between synthetical PC membrane and cell membrane. Testing this idea also provides an opportunity to test how closely the POPC model system mimics real mammalian cell membranes. In **chapter 4**, we demonstrate translational potential, *in vitro*, by showing that macrolittins readily trigger release of both macromolecules and small molecules from PC liposomes in the presence of cells, without affecting the cells directly. We expect that the extraordinary membrane selectivity of the macrolittins for PC liposomes over mammalian cell plasma membranes will be used in the triggered release of liposomal drugs in future translational studies. Lastly in **chapter 5**, to further investigate sequence-structure-function relationship of peptide, we make a new peptide library based upon M159 sequence to screen peptide candidates that permeabilize lipid liposomes with thinner or thicker membrane compared to PC.

Figure 1-1
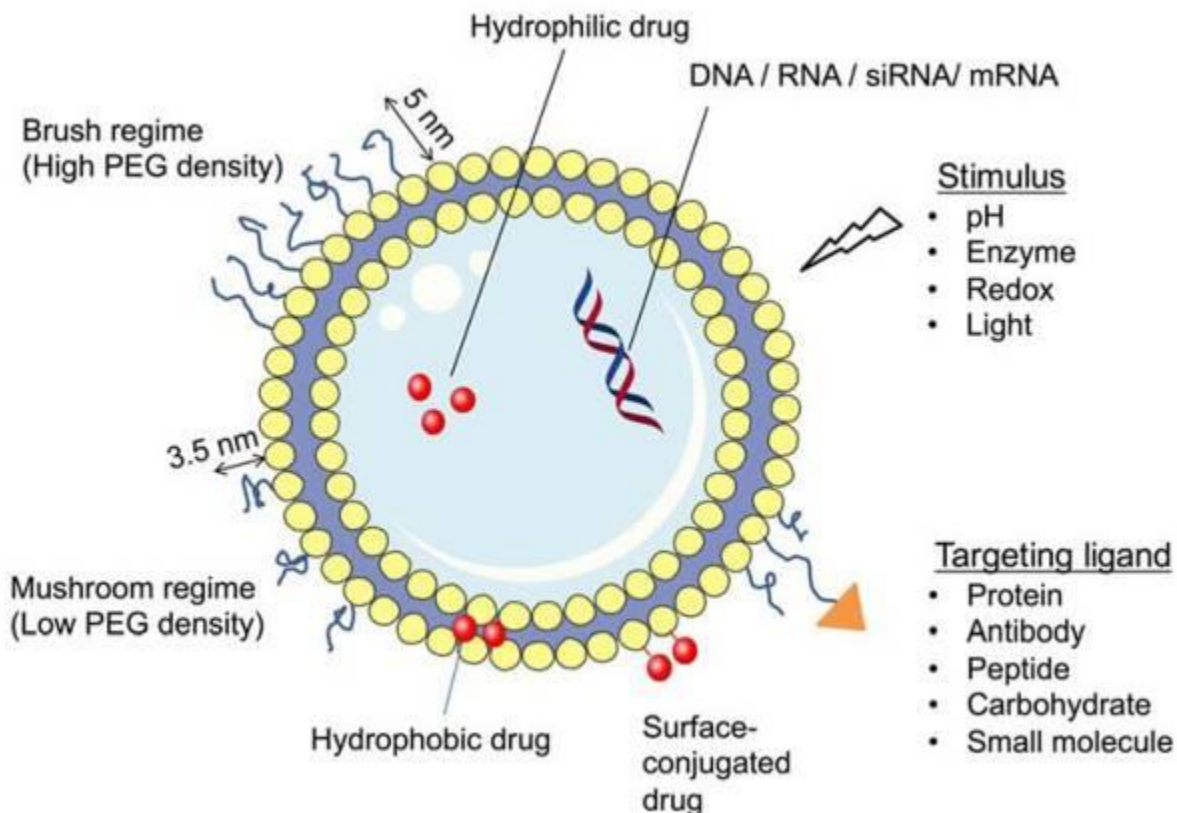
Figure 1-1. Modification of liposomes. Drug loading: hydrophobic drugs can be incorporated within bilayer membrane while hydrophilic drugs can be encapsulated into the aqueous core. The length of PEGylation (For example PEG2000) can be adjusted to modify the stealth features of the liposome formulation to protect from degradation or incorporation by cells. Ligands (protein, antibody, peptides, etc.) can be introduced or tethered to present on the liposome surface to achieve specific binding to cell markers or antigens at tumor sites. Drug release can be triggered by designing strategies with sensitivity to specific stimuli including pH, enzyme, redox, light and magnetic field. Adapted from Lee Y, et al., 2017[10]

Figure 1-2
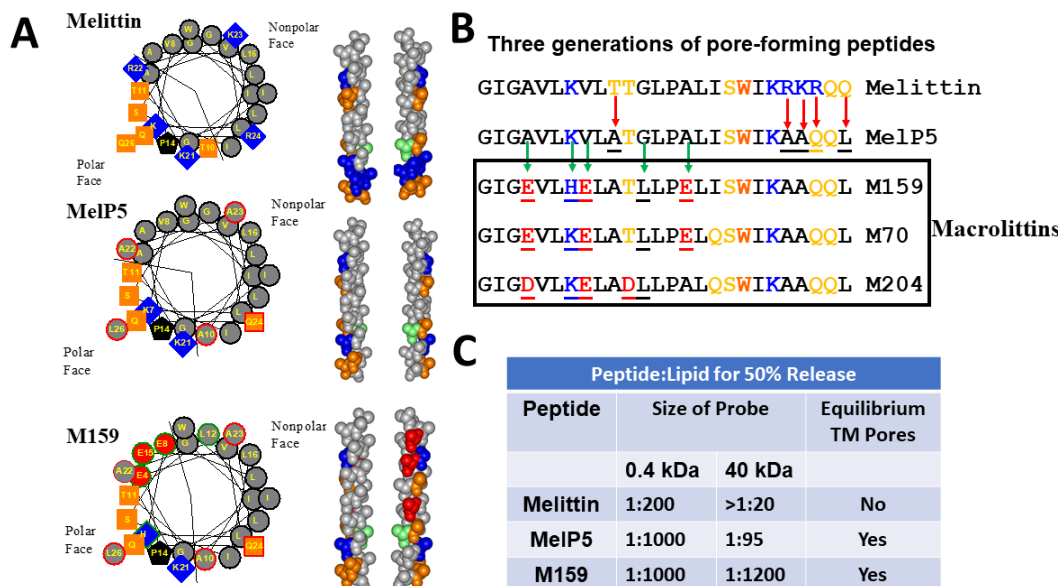
Figure 1-2. Synthetic molecular evolution of the macrolittins. **A**. In the first generation, a library based on the non-selective, transient pore former melittin, from Honeybee venom, was created and was used in a screen based on lipid vesicle leakage to select highly potent equilibrium pore forming peptides. The most active gain-of-function variants is called MelP5. In the second generation a library based on MelP5 was made and was screened in lipid vesicles for highly potent macromolecular poration, thereby identifying the macrolittins. The 5 residues that are different between Melittin and MelP5 are shown by red arrows and the five residues that are different between MelP5 and the macrolittin M159 are shown by green arrows. Residue colors are black for hydrophobic, red for acidic, blue for basic, and orange for polar & uncharged. **B.** Summary of gains of function over the two generations of evolution. The macrolittins are unprecedented in their ability to release macromolecules from phosphatidylcholine (PC) vesicles at very low peptide:lipid ratios (P:L). **C.** All three generations have pore-forming activity due to amphipathic structure in

membranes. MelP5 has a more ideal amphipathic helix along its length compared to melittin while the M159 has three additional acidic residues on its polar face and has a broader polar face compared to melittin and MelP5. (Figure and legend are adapted Sun, Hristova and Wimley, Nanoscale, 2021[31])

Figure 1-3
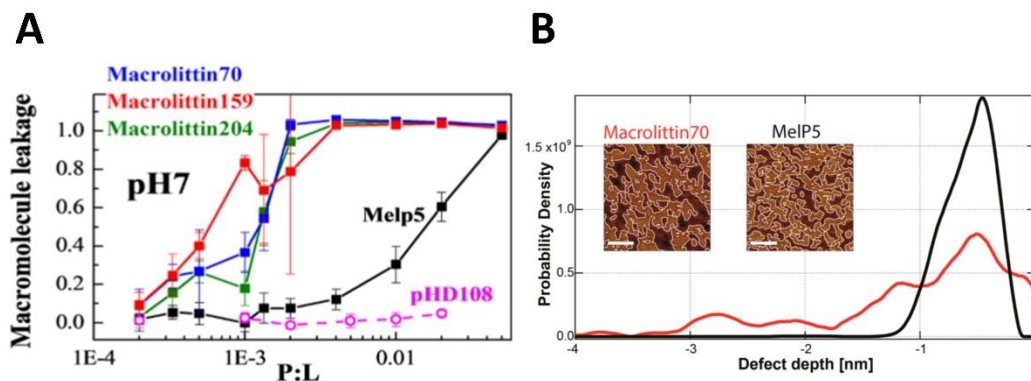
Figure 1-3. Confirmation of macrolittin potency. **A**macrolittin**. Macrolittin**-induced leakage of a 40kDa dextran from PC vesicles. Experiment at pH 7, all three macrolittins have significantly higher potency to TAMRA-biotin-dextran leakage than MelP5. **B.** Histograms of bilayer defect depths by atomic force microscopy for both peptides (macrolittin70 in red; MelP5 in black). Inset: Images with white contours outlining defect areas. scale bars = 50 nm. Adapted from Sijia L, et al., 2018[28]

Figure 1-4
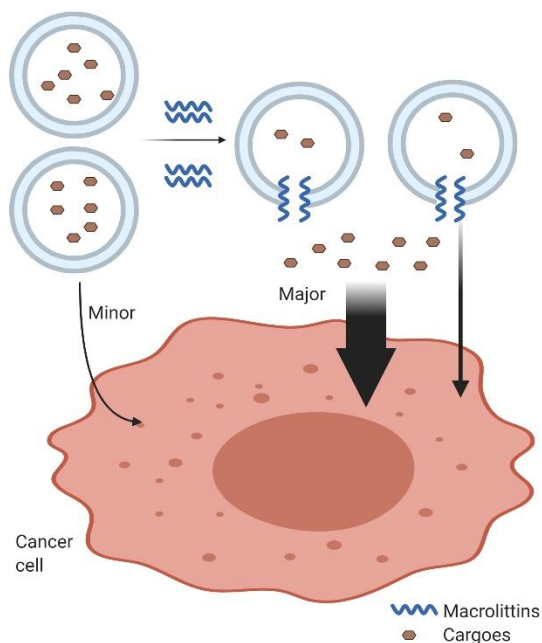
Figure 1-4. Peptide-triggered cargo release model. General cargoes such as small molecule drugs or macromolecular proteins are encapsulated into liposomes and incubated with cells. A few liposomes will be uptake by cell via potential endocytosis pathway. Upon adding candidate membrane-permeabilizing peptides, which bind liposome and make pore on its PC membrane, the cargoes are release and uptake by cells immediately with little interaction between peptides and cell plasma membranes. (Figure and legend are adapted from Sun, Hristova and Wimley, Nanoscale, 2021[31])

CHAPTER 2: Macrolittins are not toxic to cells under normal conditions

INTRODUCTION

Researchers found that the bee venom peptide melittin targets a range of both normal and cancer cells, including cancer cells from leukemia, lung, renal, liver, bladder and prostate cancers.[32] Therefore, some researchers have been optimizing melittin for anti-cancer therapies. For example, melittin was reported to significantly inhibit the epidermal growth factor-induced invasion and migration of non-small cell lung cancer cells, and subcutaneous injection of melittin at doses of 1 and 10 mg/kg significantly suppressed non-small cell lung cancer tumor growth by 27 and 61%, respectively[33]. Later the daughter peptide MelP5 was identified by screening a peptide library based on melittin. Both melittin and MelP5 can cause small molecule leakage from PC liposomes while only MelP5 enables the passage of macromolecules across bilayers. Interestingly, only 0.5-5 μM melittin or MelP5 can cause hemolysis of red blood cell and nucleated cell death, suggesting a high cytolytic potency.[27] These findings indicate that melittin and MelP5 can permeabilize both synthetic PC membranes and cell plasma membranes without selectivity.

Here we study the membrane selectivity of the third generation of membrane-permeabilizing peptides, described in Chapter 1, called macrolittins which have the highest potency to enable both small molecule and macromolecule passage across synthetical bilayer membranes. Prior to this work, the cell toxicity of macrolittins was unknown. In this dissertation, our goal is to discover a peptide with selectivity for pure PC membranes

over the cell plasma membrane. After several generations of evolution against PC liposomes, we hypothesized that the macrolittins could have the desired specificity.

Firstly, we focused on direct physical interaction between peptides and cells. Specifically, the percentage of peptide binding to cell membrane and peptide uptake by cells. Secondly, when we study interactions between peptide and cells, there are many cell culture conditions including full culture media (enough nutrients), serum starvation media and harsh culture (serum and amino acid depletion),[34] all of which might influence the effect of peptide on cell toxicity. Thirdly, in addition to cell toxicity, the peptides might make a difference in other cell activities including cell apoptosis, cell autophagy and cell endocytosis, and we expect these cell activities are within normal level because they can determine the health condition of cells. Lastly, the chirality of the peptide could be important since most of the amino acids recognized by proteases in the body are natural L-type amino acids. D-amino acid peptides have greater therapeutic potential because they are more resistant to degradation than L-peptides.[35] Therefore, D-peptides are likely to exert different effects on cells.

In this chapter, we utilize a variety of assays and techniques to evaluate the effects of macrolittins and its parent peptide MelP5 on cell toxicity and activities under different conditions. D-amino acid macrolittins are also investigated for peptide tracking and cell activity compared to L-type peptide. Although we cover many aspects of peptides and cell activities, we do not study all the pathways with detailed mechanisms and all cell culture conditions. However, we are making progress in investigating and understanding the activities of these peptides in mammalian cells.

MATERIALS AND METHODS

Peptide synthesis

All peptides were synthesized by Biosynthesis Inc. and were validated by mass spectrometry and HPLC. Stock solutions of 1.2 mM peptides were prepared with 0.025% acetic acid. Concentrations were determined by measuring the absorbance of the single tryptophan on each peptide. The average of three absorbance measurements at 280 nm on a NanoDrop 2000c (Thermo Fisher Scientific) was used to calculate the concentration. Peptide powders were stored frozen until use and peptide solutions were stored at 4 °C.

M159-TAMRA conjugation

The fluorescent dye TAMRA was conjugated to M159-GGC using a maleimide-thiol reaction. Appropriate amounts of pHD108-GC and TAMRA-maleimide (tetramethylrhodamine-5-maleimide, Invitrogen T6027) were weighed out and dissolved together to make 1.5 mM M159-GGC and 6 mM TAMRA-maleimide in degassed 10 mM phosphate buffer. Some maleimide crystals remained. The reaction was tracked with HPLC over 3 hours at room temperature, at which time the reaction was deemed complete. The conjugate was then purified with HPLC and the molecular weight was verified with mass spectrometry.

High pressure liquid chromatography

Peptide and peptide-dye conjugate were analyzed and purified using reversed-phase HPLC. The stationary phase was a 100mm x 4.6mm C-18 column from Kromasil (Bohus, Sweden). The mobile phase was composed of a gradient of distilled water (with 0.1% trifluoroacetic acid) and acetonitrile (with 0.1% trifluoroacetic acid) with a flow rate

of 1mL/min. Peptides were detected using tryptophan fluorescence (285ex/340em) and absorbance of 220nm and 280nm.

MALDI mass spectrometry

Peptide and peptide-dye conjugate synthesized were mass verified using a Bruker Autoflex III MALDI-TOF mass spectrometer (Bruker Daltonics, Billerica, MA). Mass spectra data were collected in both linear and reflector mode with positive ion detection. Typical sample preparation for MALDI-TOF data was performed by making stock solutions of 70% Acetonitrile: water + 30% water with 0.1% trifluoroacetic acid saturated with α-Cyano-4-hydroxycinnamic acid matrix (20 mg/mL). 10 µL stock solution was mixed with 1 µL peptide/peptide-dye solution, deposited onto the MALDI target plate and allowed to evaporate via the dried droplet method.

Cell culture

HeLa cells, HepG2 cells, and Raw 264.7 cells were purchased from ATCC. Cells were cultured at 37 °C with 5% CO_2 in Dulbecco's Modified Eagle's Medium (DMEM) (Gibco) supplemented with 10% fetal bovine serum (FBS) (Gibco), 1% antibiotic–antimycotic (Gibco), and 1% non-essential amino acids (Gibco). Cells were passaged 1: 5 at 90% confluency.

Alamar blue cytotoxicity assay

HeLa cells, HepG2 cells, A549 cells and Raw 264.7 cells at 80%-90% confluency were seeded per well on a 96-well clear and thin bottom TC plate in complete media and incubated overnight at 37°C and 5% CO_2. Cells were then washed with pH 7.4 serum free media and MelP5, M70, M159 or M204 were added to cells in pH 7.4 serum free media,

100 µL total volume. Cells were incubated for 3 hours and Alamar blue was added to 1% and incubated for 3 hr at 37°C then read at 550ex/590em.

Human serum and erythrocytes

Fresh human serum (OTC) and human O+ erythrocytes were obtained from Interstate Blood Bank, Inc. RBCs were subjected to four cycles of centrifugation at $1000g$ with resuspension in fresh DPBS. Following the final wash step, the supernatant was clear and colorless. RBC concentration was determined using a hemocytometer.

Cell binding

Suspensions of human red blood cells or RAW 264.7 macrophage cells were prepared at increasing cell densities and mixed with stock 20 µM peptide. The suspensions were rocked gently for 30 minutes at RT prior to centrifugation at $10\,000g$. The peptide remaining in the supernatants was measured with analytical reverse phase HPLC by comparing native tryptophan fluorescence peak areas with controls of known concentration.

Dextran uptake assay

HeLa cells at 80% confluency washed once with PBS and treated with different peptides and 100 µg/mL 10 kDa dextran-AF488 in 50 µL complete media for 30 min, 37°C. Cells were not washed and then examined with confocal microscopy.

Serum and amino acid starvation

Cells were washed once with PBS and media was replaced with EBSS (Thermofisher) and incubated for indicated time, 37°C. Cells were then washed and harvested for Wester-blot or were subject to fluorescence microscopy.

Confocal microscope

Dye labeled molecules are observed using a confocal scanning Nikon Eclipse Ti2 inverted microscope using a 60× oil-immersion objective. Hoechst dye staining cell nucleus was excited using a 360 nm laser. NBD, Alexa Fluor® 488, Bodipy dyes were excited using a 488 nm laser. Rhodamine and TAMRA was excited using a 543 nm laser.

Cell apoptosis assay

Hela cells at 80% confluency were wash with PBS and incubated with peptides and 2 μM NucView® 488 caspase-3 substrates as well as cell nuclear Hoechst dye (Thermo-fisher) in different culture medium for up to 4 hours at 37°C and 5% CO_2 in Biotek Cytation 5. Fluorescence images were taken every 30 min, and the fluorescence intensity of caspase-3 substrates was quantified and normalized by dividing fluorescence intensity of Hoechst dye.

Western-blot

Cells were harvested by trypsinization and centrifugation at 1400 rpm for 5 min. Cell pellets were resuspended and lysed by RIPA buffer containing protease inhibitor (Thermo-fisher), followed by shaking for 30 min at 4°C. Lysed cell solutions were centrifuged at 16000 g for 10 min at 4°C. The proteins in the supernatant were quantified by BCA assay kit (Thermo scientific). 15μg protein was loaded for each well in the NuPAGE 10% Bis-Tris gel (Invitrogen), and then enough MES SDS running buffer (Invitrogen) was added to cover sample wells. Samples were electrophoresed for 45 min at 200 V. Then proteins in the gel were transfered onto nitrocellulose membranes (Invitrogen) by transfer machine (Invitrogen) for 7 min. The membrane was blocked by 5% milk in 1% PBST for 1h. Then primary antibodies including anti-LC3B and anti-GAPDH (Santa Cruz Biotech) were added and shaking at 4°C overnight. The membrane was washed and

incubated with secondary antibodies (goat anti-rabbit or goat anti-mouse HRP, Thermo Scientific). Then the membrane was incubated with HRP chemiluminescent (Substrate reagent kit, Invitrogen) and exposed by ChemiDoc Imaging System. Images were processed with ImageJ.

Endosomal pathway investigation by using inhibitors

Around 90,000 HeLa cells were plated on a 48-well plate overnight at 37°C 5% CO_2. Cells were washed once with PBS and inhibitor was added in serum free media, 120 µL, 30 min at 37°C. Optimal concentrations of inhibitors was determined previously by using a sub-cytotoxic concentration as determined by Alamar blue. Concentrations are as follows: 12µg/mL methyl-β-cyclodextrin (MBCD), 5ug/mL filipin III, 30ug/mL EIPA, 20uM wortmannin, 0.4mM dynasore, 30ug/mL chlorpromazine. D-M159-TAMRA was then added directly to wells to make 2 µM final peptide concentration. Cells were incubated with peptide for 45 min at 37°C. Cells were washed once in PBS then trypsinized. 500 µL complete media was then added, transferred to a 1.5 mL tube, spun down, then resuspended in eBioscience viability dye e780 at 1:1k dilution in serum free media, 75 µL final volume, for 10 min at room temperature. Cells were washed with 500 µL serum free media, spun down, then resuspended in 500 µL FACS buffer then analysed using flow cytometry. At least 10k live cell events were collected per sample.

Flow cytometry

Cells were transferred to a filter-topped flow cytometry tube and analyzed on a BD LSR II flow cytometer. Cells displaying normal morphologies were gated and analyzed for ef780 fluorescence and TAMRA fluorescence using the 633 nm and the 543 nm laser, respectively.

RESULTS

Peptide toxicity to cells coupled to cell binding

To determine if macrolittins have toxicity against mammalian cell lines, we measured macrolittin-induced permeabilization of cells. This was performed by Alamar blue measuring the cytolytic toxicity of three macrolittins (M70, M159, M204) against various human cell types; human red blood cells (**Fig. 2-1A**), HeLa ovarian epithelial cells, HepG2 liver epithelial cells (**Fig. 2-1B&C**) and Raw 264.7 macrophages (**Fig. 2-1D**). Remarkably, despite their extraordinary activity against POPC vesicles, all three macrolittins have no measurable toxicity against any cell lines, and did not permeabilize cell plasma membranes, even at a high concentration (100 μM). By contrast, the parent peptide MelP5 and the natural bee venom peptide melittin cause complete cell lysis at 2-5 μM concentrations (**Fig. 2-1**).[36]

Generally, binding to cell surface is the prerequisite for a specific molecule to exert its effect on cells[37], To determine if the lack of macrolittin activity in cells is coupled to a lack of cell membrane binding, we next conducted label-free binding assays to measure whole cell binding of macrolittins.[38] We firstly developed the HPLC method to identify the single, clear peak of M159 (**Fig. 2-2A**) or MelP5 (**Fig. 2-2B**) and quantified them. Subsequently, peptides were incubated with cells and centrifuged, the supernatants containing free peptides were subject to HPLC quantification. Our results, in **Fig. 2-2C**, indicate that M159 binds weakly, or not at all, to human red blood cells and to Raw 264.7 macrophages. In contrast, MelP5 peptides binds strongly to both cell types. MelP5 binding to red blood cells could not be measured directly because of interference from released hemoglobin which has high intensity of fluorescence on HPLC, but our observation that

MelP5 can permeabilize these cells at < 5 µM concentration shows that it must bind well. Consistent with the lack of toxicity and lack of binding, our images from confocal microscopy indicate that dye-labeled dextran (10 kDa), which does not significantly into cells without cell membrane permeabilization, remains excluded from cells in the presence of any concentration of M159 (up to 100 µM) or the inert negative control peptide, 100 µM Oneg.[39] By contrast, incubation of cells with even a low concentration of MelP5 can permeabilize cell membranes and enable dextran to enter into cells (**Fig. 2-3**). Collectively, these results show that M159 does not partition strongly into human cell membranes and does not permeabilize or disrupt the plasma membranes of human cells, even at high peptide concentration.

Toxicity of D-M159 on cells under different conditions

To further evaluate the toxic effect of M159 on mammalian cells, we used D type peptide which cannot be easily degraded by proteases, and we performed the toxicity experiments under starvation conditions under which we can expect the peptides to have maximum effect. Starvation was accomplished by changing the complete medium into harsh starvation medium EBSS containing only glucose (depletion of serum, amino acids and growth factor), which is used to induce cell endocytosis and autophagy in a short time.[40] Hela cells and A549 cells, a lung cancer cell line, were selected to determine if co-treatment of M159 and starvation for 3 hours have cell-specific effect. Our results show that for Hela cell line, interestingly, high concentration of D-M159 (100 µM) is highly toxic to cells in harsh starvation condition (70% of cell death), while peptides alone or L-M159 with cell starvation does not cause cell toxicity significantly (**Fig. 2-4A**). In contrast, the results for A549 reveal that 100 µM D-M159 only has little toxicity to cells in harsh

starvation conditions and other treatments have no toxicity (**Fig. 2-4B**). These results suggest that there are interactions between D-M159 and cells at starvation condition, leading to cell death, specific for Hela cells.

Effects on D-M159 on different cell activities

Cell death occurs when a cell is unable to carry out its functions. It can be divided into programmed cell death (apoptosis) and necrotic cell death.[41] The images of starved cells treated with D-M159 show that the morphology of dead cells includes blebbing, cell shrinkage and nuclear fragmentation, which are characteristics of cell apoptosis.[42] To confirm the type of cell death induced by co-treatment of D-M159 and starvation, we performed Caspase-3 cleavage assay. During cell apoptosis, caspase-3 is activated and cleaves the indicator peptide, DNA-dye linked DEVD. Caspases cleave the peptide, and then the cleaved DNA dye binds to DNA at cell nucleus which is detected with high sensitivity[43] (**Fig. 2-5**). Real-time detection and imaging were utilized to quantify the level of cell apoptosis when Hela cells were incubated with caspase-3 reagent, cell nucleus dye, and different treatment of M159 and starvation. Our images at 4 hours show that L-M159 at both concentrations (50, 100 µM) and starvation treatment induced cell apoptosis signal at some extent (**Fig. 2-6A**). By contrast, D-M159 at both peptide concentrations and starvation treatment induced around 2-fold increase of cell apoptosis level (**Fig. 2-6A**), and the increase of apoptosis is dependent on time and concentration according to the quantification figure (**Fig. 2-6B**). Collectively, these results suggest that at least cell death is coupled to cell apoptosis induced by high concentration of D-M159 and harsh starvation condition. L-M159 does not cause cell death and apoptosis even with cell starvation condition, which is consistent with previous L-M159 cell binding results.

Autophagy is cytoplasmic, characterized by the formation of large endo-lysosome that digests organelles in a specific sequence prior to the destruction of the nucleus.[44] Autophagy is generally induced by a variety of stresses such as starvation. Excessive autophagy or inhibition of autophagy flux might cause damage to cell, leading to apoptosis.[45] Here, for the apoptosis or cell death assay, we have already induced cell autophagy by cell starvation for 3 hours. However, the role of D-M159 has not been identified in the autophagy event. To determine the effect of M159 on cell experiencing autophagy, we quantified cell autophagy level by comparing the autophagic marker LC3 expression using Western-blot. In addition, we used Bafilomycin A1 which inhibits the fusion of late-endosome and lysosome to block LC3 II digestion and autophagy flux.[46] In this autophagy assay, we only used 50 µM L-M159 or D-M159 to decrease the potential cell death. The blotting result indicates that treatment of starvation and bafilomycin increase the expression and accumulation of LC3II, suggesting that the autophagy is induced by starvation but autophagy flux is inhibited due to bafilomycin effect compared to starvation treatment alone in which the autophagy flux is not inhibited and LC3 II accumulation is decreased (**Fig. 2-7A**). Treatment with L-M159 or D-M159 alone did not induce autophagy significantly, and this effect is comparable bafilomycin treatment alone. However, when cells are subject to starvation and autophagy induction, L-M159 or D-M159 causes LC3 II accumulation compared to starvation alone treatment (**Fig. 2-7A, B**). Collectively, these results suggest that macrolittins have mild inhibitory effect on cell autophagy flux, leading to abnormal autophagy activity and cell death, consistent with previous results that D-M159 and starvation caused cell apoptosis.

L-M159 did not bind to cell plasma membrane and had no toxicity against cells in starvation condition while combination of D-M159 and starvation caused cell death, we deduct that D-M159 could exert some effects within cells. To track the trace and fate of D-M159 in cells, we firstly modified D-M159 by adding three amino acids glycine-glycine-cysteine at C-terminus, and then conjugated 5-Carboxytetramethylrhodamine (TAMRA) dye by maleimide thiol reaction on cysteine (**Fig 2-8A**). After purification and separation by HPLC, the molecular weight of D-M159GGC-TAMRA was identified as 3539.1 g/mol by mass spectrometry, thus D-M159 was labeled with TAMRA successfully (**Fig 2-8B**). Endocytosis is the main pathway that molecules are internalized and uptaken by cells.[47] Since macrolittins do not bind to or permeabilize cell membranes, we hypothesize that D-M159 is uptaken by cells via endocytosis pathway. We selected two endocytosis markers: transferrin and low-density lipoprotein (LDL) which are all uptaken by cells via receptor-mediated endocytosis.[48] Therefore, cells were incubated with D-M159GGC-TAMRA and endocytosis markers (AF488 labeled transferrin or LDL) for 3 hours and observed by confocal microscope. The images showed that D-M159 was visualized as puncta within cells and there were co-localizations between D-M159 and both markers, although not a highly co-localized extent, suggesting that at least D-M159 could be uptake by cells via endocytosis (**Fig. 2-9**), probably as a bystander of receptor-mediated endocytosis.

To further investigate the D-M159 endocytosis pathway, we used a variety of selective endocytosis inhibitors to determine the specific endocytosis that M159 adopted. Generally, there are 4 major classes of molecule uptake pathway: macropinocytosis, phagocytosis, clathrin-mediated, caveolae-mediated pathways. Here we do not test entry via phagocytosis because this pathway is involved with large particles such bacteria and

viruses during infection.[49] Specifically, methyl-beta-cyclodextrin (MBCD) inhibits both caveolae and clathrin vesicles formation on cell membrane by depleting cholesterol.[50] Chlorpromazine (CPZ) inhibits clathrin-mediated endocytosis because it is a selective inhibitor of the clathrin adapter protein AP2.[51] Filipin disrupts caveolae structures and inhibits their normal formation.[52] Wortmanin inhibits PI 3-kinase that interrupts clathrin-mediated endocytosis.[53] Dynasore inhibits dynamin function which is critical for clathrin vesicle scission from the plasma membrane and caveolae dynamics.[54] Lastly, ethyl-isopropyl-amiloride (EIPA) inhibits micropinocytosis process by blocking sodium channels.[55] Importantly, the mechanisms of some of these inhibitors might overlap and the inhibitors are known to inhibit at least one pathway, a complicated effect which depends a lot on cell type, inhibitor concentration and time of treatment (**Fig. 2-10A**). We used flow cytometry to quantify the entry of labeled D-M159. The concentrations for all of inhibitors were not toxic to cells (>80% viability) and only viable cells were selected for gating (**Fig. 2-10C**), and the gating strategy for D-M159 quantification is shown in **Fig. 2-10D**. Our final results in histogram indicate that the uptake of D-M159 is highly dependent on dynamin-assisted endocytosis pathway (both clathrin- and caveolae-mediated endocytosis. **Fig. 2-10B**). While macropinacytosis inhibition has no obvious effect on D-M159 endocytosis by cells.

DISCUSSION

In this chapter, we are focusing on the interaction between candidate peptide macrolittins and mammalian cells. Very interestingly, even high concentration of M159 has no toxicity to various mammalian cells while its parent peptide MelP5 or prototype

peptide melittin has highly potent ability to permeabilize cell plasma membrane, despite the fact that all these three peptides share similar amino acid sequences. We then concluded that peptide-cell membrane binding pattern could explain the toxicity because M159 did not bind mammalian cells compare to the high affinity of MelP5 to cell membrane.

Subsequently, we studied other cell activities to determine any other effect of M159 on cells given the fact that this peptide is not toxic. Apoptosis is a form of programmed cell death that happens frequently in multicellular organisms, and the induction of apoptosis is highly regulated by activation mechanisms, by which it leads to the death of the cell once the process is initiated.[56] Previously, melittin was reported to inhibit the proliferation of osteosarcoma 143B cells and induce apoptosis by up-regulating the expression of Bax and Caspase-3 and down-regulating the expression of Bcl-2 proteins.[57] Here we tested D type M159 because it is unable to be degraded in the endo-lysosome system within cells.[58] In addition, we subject cells to starvation condition to potentially increase molecule uptake by cells.[59] This harsh condition and high concentration of D-M159 are required to cause cell death, specifically, cell apoptosis because single peptide or starvation treatment could not decrease cell viability, suggesting that starvation might increase M159 uptake by cells despite it having little binding to cell plasma membrane. Notably, this toxic effect of D-M159 was cell specific because a lower toxicity was observed in A549 cells.

Endocytosis is an important process by which various substances can be brought into cells, increasing the communication between cell and its microenvironment outside the cell. The endocytic pathway of mammalian cells consists of distinct membrane compartments, which internalize molecules from the plasma membrane and recycle them

back to the surface, or sort them for degradation.[60] Since only D-M159 rather than L-M159 has toxicity at high concentration, we deducted that L-M159 might be degraded by protease within cell, for example, digested by enzymes in endo-lysosome system. Thus, we hypothesized that D-M159 was uptake by cell endocytosis and caused cell apoptosis perhaps by acting within the endosome or autophagosome. Our dye labeled D-M159 partly co-localized with endosome markers as small puncta aggregates within cells. Then we determined the specific endocytosis pathway for D-M159 uptake, which required dynamin to form vesicles according endocytosis inhibitors assay by flow cytometry. However, the conclusion for endocytosis pathway has caveats, because we added three more amino acids at C-terminus of D-M159 for labelling, leading to possible changes in the whole peptide structure or function; secondly, these inhibitors have overlapping mechanisms with others depending on concentration and time incubated.

We are also interested in the effect of D-M159 on cell autophagy, which is a natural, conserved degradation of the cell that removes unnecessary or dysfunctional components through a lysosome-dependent mechanism.[61] Autophagy can be a protective activity during some infections and stress condition, while overly extended autophagy can lead to cell death. We found that D-M159 remained in endo-lysosome system and hypothesized that it could make a difference in cell autophagy. To this end, we detected autophagy level by marker LC3 with previous D-M159 treatment. The results indicated that M159 can inhibit the autophagy activity induced by starvation, similar to bafilomycin but with a lower potency. To clarify the mechanism of M159 exerted on autophagy, future experiments will be need including using other autophagy, lysosome markers and testing of lysosome functions.

Figure 2-1
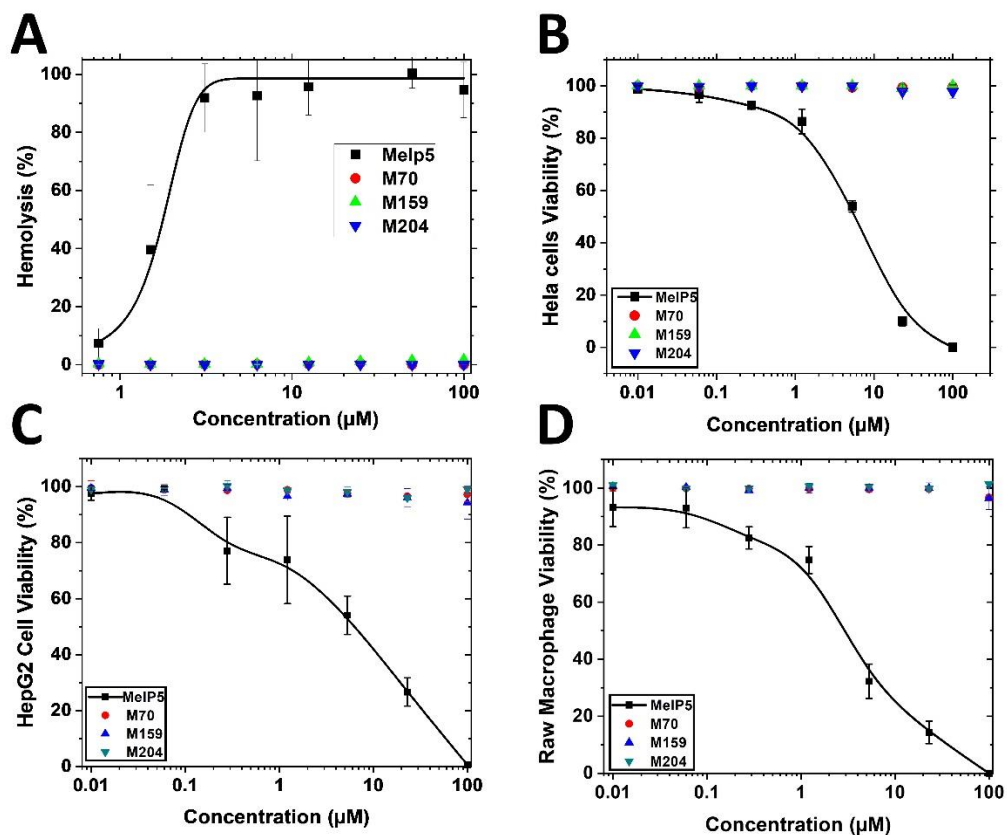
Figure 2-1. Toxic effects of macrolittins and MelP5 on human cells. **A.** Lysis of human red blood cells. Serially diluted MelP5 and three macrolittins were incubated with human RBCs for 1 h. Release of hemoglobin was measured using optical absorbance of the cell supernatant at the heme absorbance wavelength of 410 nm. **B-D.** Viability of mammalian nucleated cells. Serially diluted peptides were incubated with Hela cells (B), HepG2 cells (C) and Raw macrophages (D) for 3 h and then washed off. After 24 h, cells were subjected to the cell toxicity assay using Alamar Blue reagent (ex/em = 540/590 nm). (Figure and legend are adapted from Sun, Hristova and Wimley, Nanoscale, 2021[31])

Figure 2-2
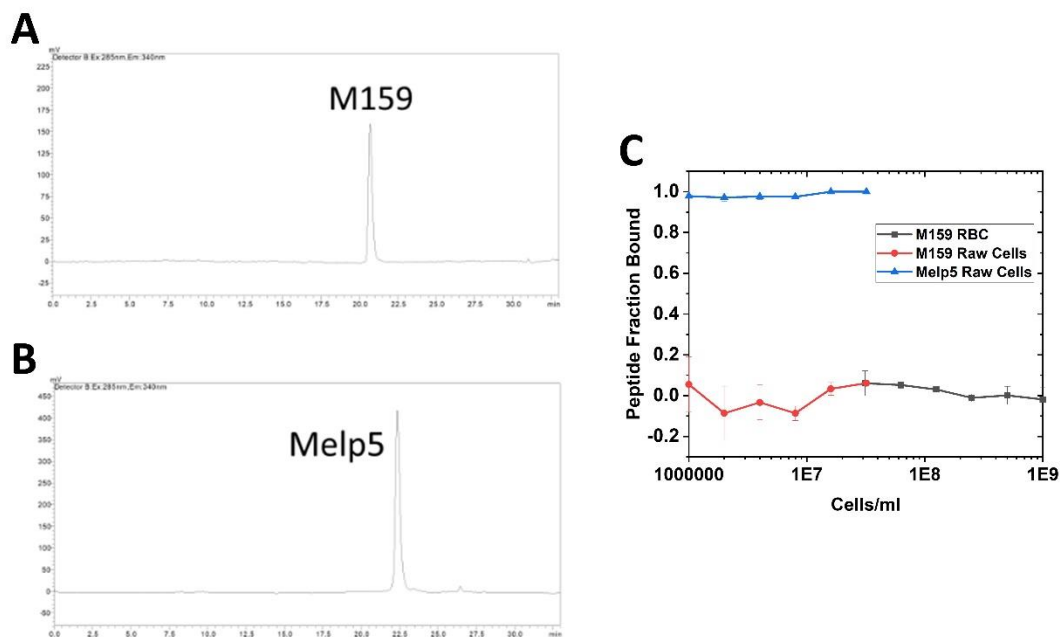
Figure 2-2. Measurement of peptide binding to Raw 264.7 cells and human red blood cells. 20μM pure peptide M159 (**A**) and MelP5 (**B**) were loaded by HPLC, and the clear peaks revealed the appearance of peptide and can be quantified to calculate peptide amount using tryptophan fluorescence (ex285/em340). **C.** 20 μM MelP5 or 20 μM M159 were incubated with increasing concentrations of cells indicated for 30 min, followed by centrifugation of the cells. Peptide remaining in the supernatant was analyzed by HPLC, and the peptide peak area was compared to that of an identically treated sample without cells to obtain fraction bound. (Figure and legend are adapted from Sun, Hristova and Wimley, Nanoscale, 2021[31])

Figure 2-3
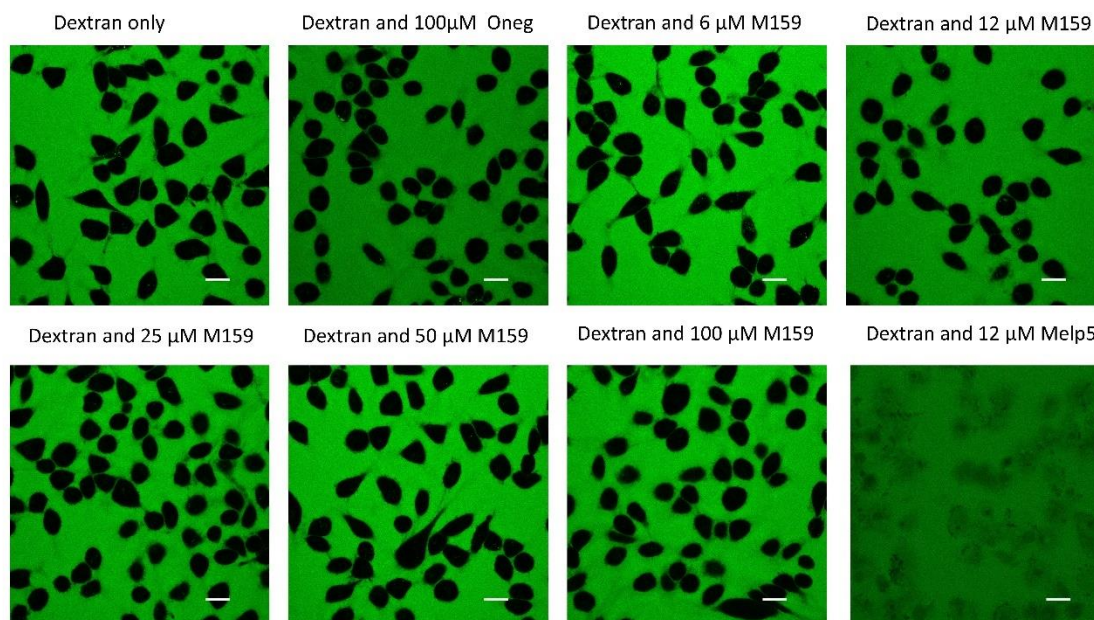
Figure 2-3. Peptides and cells. Hela cells were incubated with 100 µg/mL 10 kDa AF-labeled dextran and inert peptide Oneg, increasing concentrations of M159 (6-100µM), 12 µM MelP5 for 30 min, then cells were observed using confocal microscopy without washing (from left to right: dextran alone; dextran and ONEG; dextran and different concentrations of M159; dextran and MelP5, the concentrations are shown in the figure). Scale bar = 20 µm. (Figure and legend are adapted from Sun, Hristova and Wimley, Nanoscale, 2021[31])

Figure 2-4
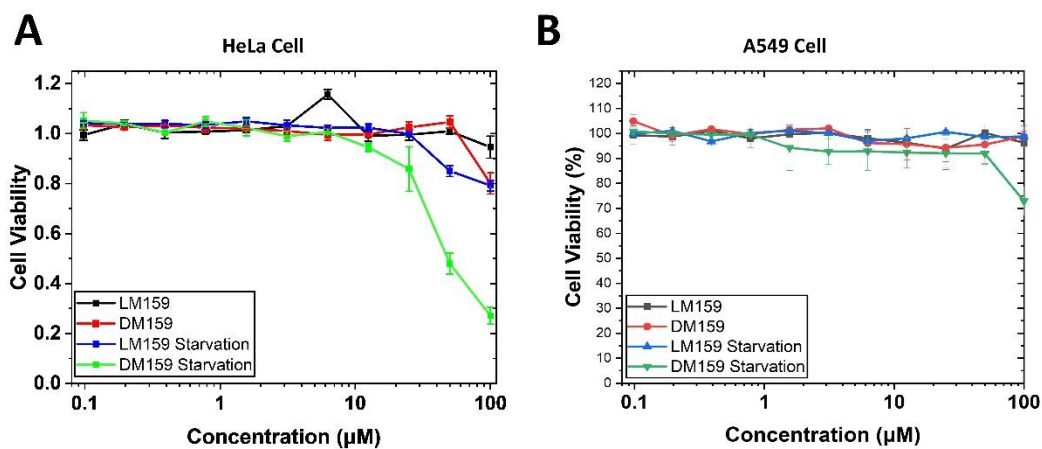
Figure 2-4. The toxic effect of L or D type M159 on cells at different conditions. Viability of mammalian nucleated cells. Serially diluted L-M159 or D-M159 were incubated with Hela cells (**A**), A549 cells (**B**) at complete medium or harsh starvation medium (EBSS) for 3 h and then washed off. After 24 h, cells were subjected to the cell toxicity assay using Alamar Blue reagent (ex/em = 540/590 nm).

Figure 2-5

After caspase cleavage in apoptopic cells, the high-affinity DNA dye
is released and will fluoresce upon binding to DNA
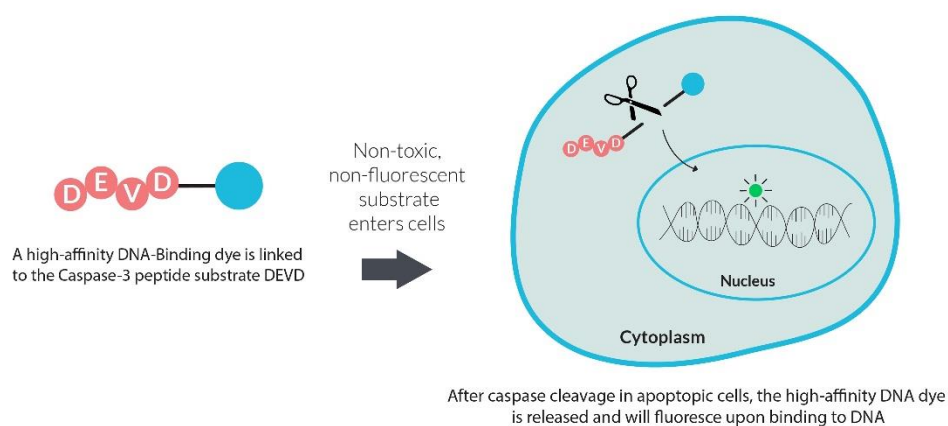
Figure 2-5. NucView® caspase-3 substrates are based upon fluorogenic DNA dyes that have been conjugated to the caspase-3/7 recognition sequence (DEVD). In the presence cells, the substrate is non-toxic, non-fluorescent and can penetrate the plasma membrane and enter the cytoplasm. During apoptosis, caspase-3/7 cleaves the substrate and releases the high-affinity DNA dye leading to nuclear fluorescent staining. Consequently, NucView caspase-3 substrates allow detection of caspase-3/7 activity and visualization of morphological changes in the nucleus during apoptosis (Adapted from Biotium Inc. https://biotium.com/technology/nucview-caspase-3-substrates)
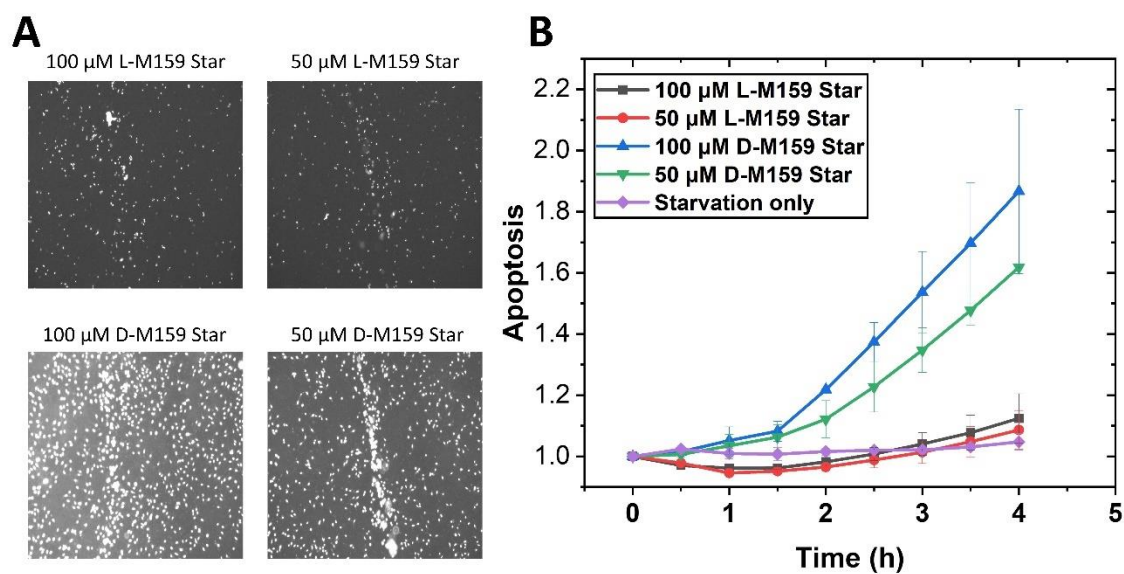
Figure 2-6

Figure 2-6. D-M159 caused cell apoptosis under starvation condition. Different concentrations of L-M159 or D-M159 were incubated with 80% confluent Hela cells with NucView® caspase-3 substrates and Hoechst dye at complete medium or harsh starvation medium (EBSS) for up to 4 hours. Biotek Cytation 5 was used to image the cells with fluorescence every 30 min until 4 hours. **A.** Images were taken at 4 hours indicating the fluorescence of NucView® caspase-3 substrates (ex488/em520), and the treatments are indicated. **B.** Quantification of cell apoptosis value: the intensity of substrate fluorescence divided by cell nuclear dye Hoechst fluorescence intensity for each image. (Star=Starvation)

Figure 2-7
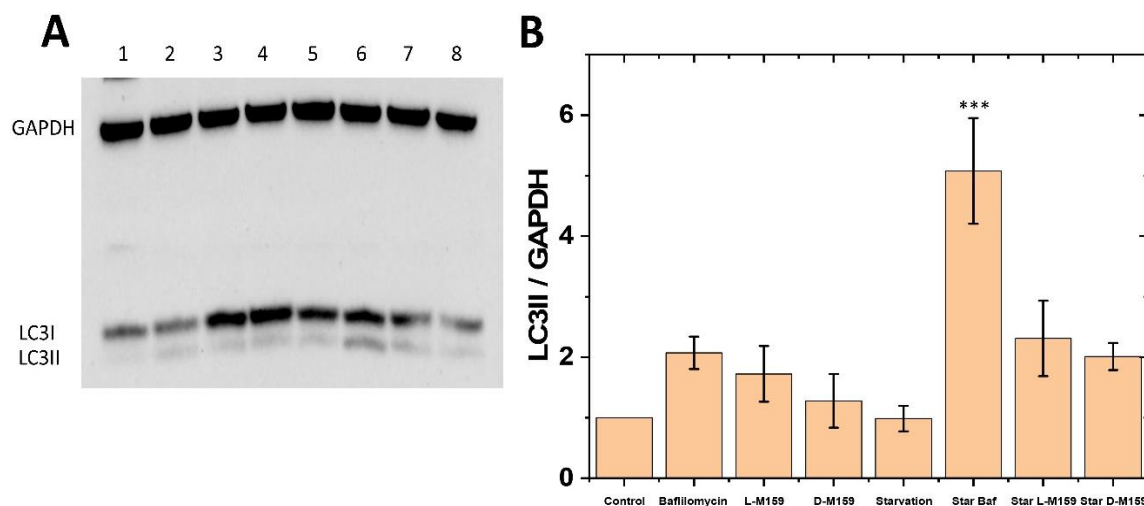
Figure 2-7. Effect of M159 on cell autophagy. **A.** Cells with different treatments for 3 hours were loaded on SDS-PAGE gel and run Western-blot. GAPDH antibody was used as detect housekeeping GAPDH protein and LC3B antibody detected autophagy marker LC3 protein (lane 1: no treatment; lane 2: 200nM Bafilomycin A1; lane 3: 50 μM L-M159; lane 4: 50 μM D-M159; lane 5: starvation; lane 6: starvation and 200nM Bafilomycin A; lane 7: starvation and 50 μM L-M159; lane 8: starvation and 50 μM D-M159). **B.** Quantification of cell autophagy level: LC3II expression divided by expression of GAPDH. The treatments are shown in the histogram. Data were processed with ImageJ.

Figure 2-8
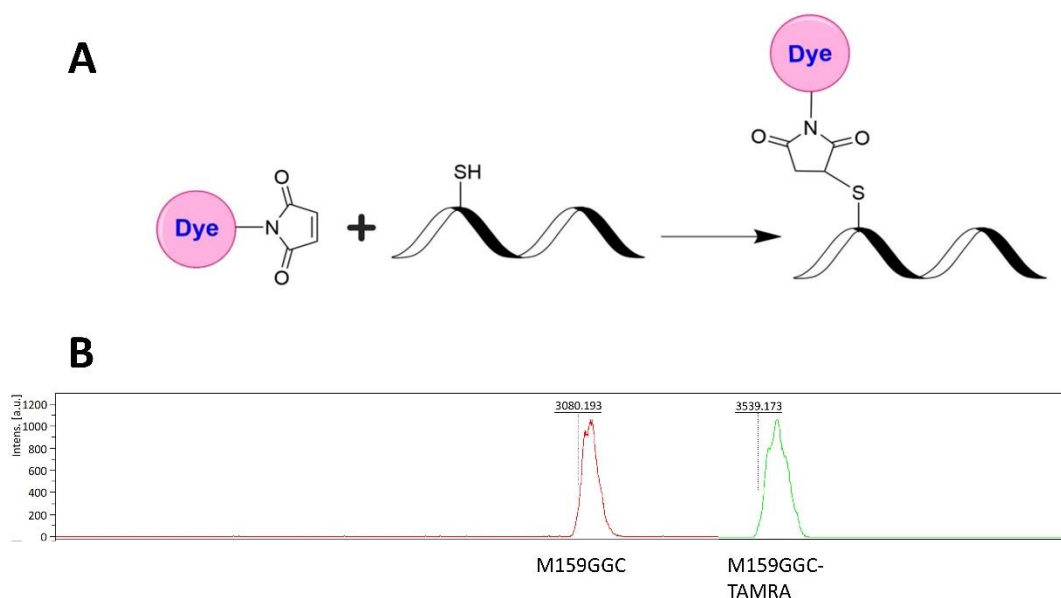
Figure 2-8. Conjugation of TAMRA dye to M159. Three additional amino acid GGC were added at C-terminus of M159. **A.** TAMRA dye was conjugated at C-terminus of M159GGC by maleimide thiol reaction (Adapted from https://www.aatbio.com/products/tide-quencher-2ws-maleimide-tq2ws-maleimide?unit=2059). **B.** M159GGC and M159GGC-TAMRA were separated and subject to Mass spectrometry (MALDI-TOF) with correct molecular weight.

Figure 2-9
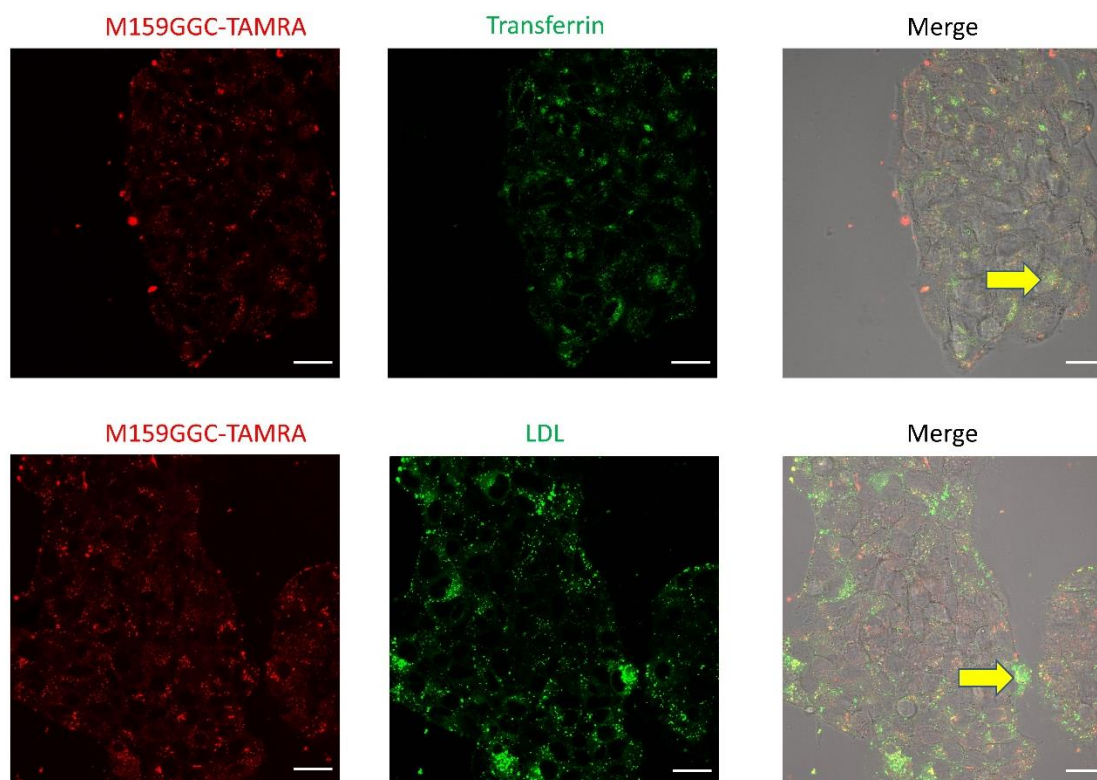
Figure 2-9. Co-localization between labeled M159 and endocytosis marker. 2 µM M159GGC-TAMRA and AF488-Transferrin or AF-488-LDL (low density lipoprotein) were incubated with HepG2 cells for 30 min, and then cells were washed with PBS and observed by confocal microscope. Top images show co-localization between M159GGC-TAMRA and transferrin while bottom images show co-localization between M159GGC-TAMRA and LDL. Right images show merged image with brightfield, and yellow arrow indicates potential co-localization. (scale=20 µm)
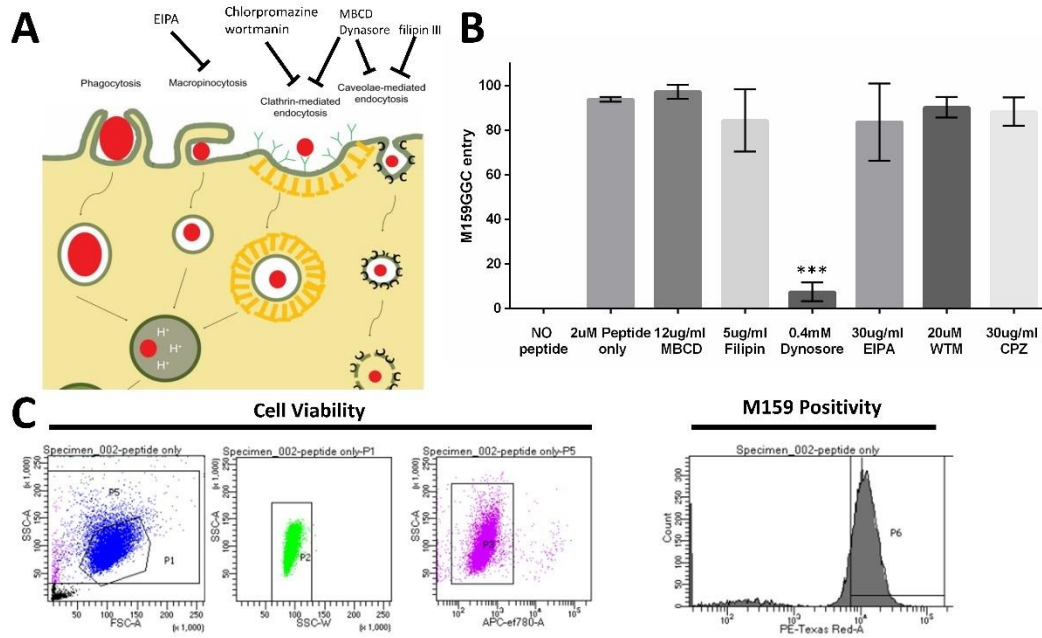
Figure 2-10

Figure 2-10. M159 uptake by specific endocytosis pathway. **A.** We used a variety of selective endocytosis inhibitors to determine M159 uptake pathway. Image is adapted from Harish, 2013[62]. **B.** This histogram concludes the results from flow cytometry indicating that uptake of M159 requires dynamin-dependent endocytosis. The gating strategy is shown in (**C**) where only viable cells are analyzed.

CHAPTER 3: Mechanisms underlying peptide selectivity

INTRODUCTION

Peptide-membrane interactions have been studied for a long time and these interactions are involved in a variety of important biological activities, such as the mechanisms of antimicrobial defense, viral translocation across the membrane, vesicle fusion, functions of membrane proteins, transport of active peptides, interruption of membranes, and others. Membrane-active peptides comprise a large family of diverse peptides with a broad range of biological activities and, thus, continuously attract growing interest for their wide biomedical applications.[63]

When peptides interact with lipid membranes, structural changes occur in both peptides and membranes. Therefore, the process of these changes is very complicated, requiring both theoretical and simulation as well as experimental studies of peptide-membrane interactions. For many years, researchers have studied the relationship between the structure of the peptide and the mechanism of interaction with different lipids. Although a detailed explanation for all peptide-lipid interactions still remains elusive, some sequence-structure-functions rules have been described for specific lipids experimentally. In addition, the key point is to use this knowledge of peptide-lipid relationships to understand the biological functions of membrane active peptides and lipid species within membranes. Further, it is important to utilize the rules to design peptides with selective functionalities in potential therapeutic applications.

In the previous chapter, the results indicate that there is a significant difference in cell toxicity between M159 and MelP5 despite the fact that they share very similar amino acid sequences. The previous publications showed that the secondary structure of these two peptides were different under some conditions. Specifically, circular dichroism results show that M159 adopts α-helix secondary structure in the absence and presence of lipid vesicles, while MelP5 only adopts α-helix secondary structure in the presence of POPC vesicles. In the absence of membranes, MelP5 is random coil. Yet, there are also similarities. For example, both peptides insert across POPC membranes perpendicularly to form pores. However, M159 can form large-size pores on lipid bilayers and enable macromolecule passage across the membrane much more potently than its parent peptide MelP5, suggesting a difference in POPC lipid binding affinity or structure in membranes. By contrast, MelP5 is highly potent to permeabilize cell plasma membrane and causes cell death at low concentration, while macrolittins do not permeabilize cell membranes even at high concentration, suggesting a difference in cell membrane binding affinity.

In this chapter, we will explore the mechanisms underlying the lipid membrane selectivity of M159 and MelP5, and we will focus on two parts: the lipid membrane composition and the peptide sequence. Here, we compare pure synthetic POPC membranes and cell plasma membranes, where the major differences include net charge, the presence of macromolecules on the membrane surface, the presence of cholesterol within the membrane, and the dynamic thickness of lipid membranes. To this end, we mimic those individual differences by preparing liposomes with different compositions and conduct leakage assays. Thus, we can determine which factors in the membrane are associated with differences in peptide activity. To assess the role of peptide sequence, we compare

individual amino acids differences between MelP5 and M159 and use variants whose sequence is "between" M159 and MelP5. In this way, we can compare their activities to identify the critical residues involved with peptide-membrane selectivity.

In addition to leakage assay by peptide permeabilization, we also study liposome aggregation and fusion to probe the effects of the peptides on membrane architecture. Similarly, the peptides MelP5 and M159 have selectivity in their ability to induce the aggregation of liposomes with specific lipids. Interestingly, both liposome leakage and aggregation can occur at the same time. Here we determine the relationship between leakage and aggregation. Because liposome aggregation is not desirable in long-term stability during manufacturing and in vivo delivery, we design new "stealth" liposomes to inhibit aggregation while leakage is not affected.

In summary, in this chapter we focus on mutual selectivity between peptide and lipid membranes by investigating the sequence-structure-function relationship of peptides. A series of biophysical experiments including binding, circular dichroism, liposome leakage and aggregation are conducted to explain their functional difference such as cell toxicity. The results and rules revealed in this chapter will be highly useful in the design of next-generation gain-of-function peptides with in the future.

MATERIALS AND METHODS

1-Palmitoyl-2-oleoyl-sn-glycero-3-phosphocholine (POPC), 1-palmitoyl-2-oleoyl-sn-glycero-3-phospho-(1′-rac-glycerol) (POPG), 1,2-dioleoyl-sn-glycero-3-phosphoethanolamine-N-[methoxy(poly-ethyleneglycol)-2000] (PEG2k-PE), 1,2-dimyristoleoyl-sn-glycero-3- phosphocholine (diC14:1PC), 1,2-dieicosenoyl-sn-glycero-

3-phosphocholine (C20:1PC), phosphoethanolamine-N-(7-nitro-2-1,3- benzoxadiazol-4-yl) (NBD-PE), 1,2-dioleoyl-sn-glycero-3-phosphoethanolamine-N-(lissamine rhodamine B sulfonyl) (Rhodamine-PE) and Cholesterol were purchased from Avanti Polar Lipids. Labeled low density lipoprotein (BODIPY™ FL LDL), 8-aminonaphthalene-1,2,3-trisulfonic acid (ANTS) and p-xylylenebis (pyridinium bromide) (DPX) were purchased from Thermo Fisher Scientific. TAMRA-biotin-dextran (TBD) was synthesized as described elsewhere.[64]

Liposome preparation

Large unilamellar vesicles of 100 nm diameter were prepared with different compositions of synthetic lipids. For vesicles without entrapped contents (empty vesicles), lipids in chloroform were dried under vacuum overnight, resuspended in pH 7 buffer (10 mM sodium phosphate, 100 mM KCl, pH = 7) to 30–50 mM concentration, and extruded at least 10 times through 100 nm polycarbonate membranes. Empty vesicles were used for light scattering, lipid exchange, vesicle fusion, confocal microscope, electric microscopy. Lipid concentration was measured by Stewart Assay.[65] For TBD-entrapping vesicles, dry lipid films were resuspended in buffer containing 1 mg of TBD and the solutions were subject to 10 freeze–thaw cycles using liquid nitrogen. After extrusion, vesicles were incubated on high-capacity streptavidin agarose to remove unencapsulated TBD. For ANTS/DPX vesicles, dried lipid films were resuspended in 12.5 mM ANTS and 45 mM DPX. Upon extrusion, unencapsulated ANTS and DPX were separated from the vesicles by size exclusion chromatography with Sephadex G-100 resin. (Method is adapted.[31])

Minimum inhibitory concentration (MIC) determination

E. coli (ATCC 25922) and *S. aureus* (ATCC 25923) were used in the experiments. 100 ml bacteria solutions (400000/well) were incubated with different peptides at gradient concentrations overnight at 37 °C. The MIC in 96-well plate was measured by a plate reader (OD value). Values of less than 0.1 were considered sterilized.

Light scattering assays

2 mM liposomes with different lipid compositions were incubated with M159 or MelP5 for 3 h and 24 h at peptide-to-lipid ratio (P : L) ranging from 1 : 10 to 1 : 10 000 in 96-well plates, and as a negative control, no peptide was added to liposomes. Absorbance of liposomes by light scattering was measured at 410 nm using a Biotek Synergy plate reader (BioTek, USA). The measurements were repeated three times. (Method is adapted.[31])

Fluorescence resonance energy transfer (FRET) Assays

0.4 mM Liposomes containing 0.5% NBD-PE and 0.5% rhodamine-PE dyes mixed with 1.6 mM pure POPC liposomes were incubated with MelP5 or M159 for 3 h and 24 h at P:L ranging from 1:10 to 1:10000 in 96-well plates. NBD fluorescence was monitored on a plate reader (ex/em = 480/520 nm), and lipid exchange percentage was calculated by the ratio of measured NBD fluorescence to NBD fluorescence from positive controls (2 mM POPC liposomes containing 0.08% NBD-PE and 0.08% rhodamine-PE), and as a negative control, no peptide was added to mixed liposomes. The measurements were repeated three times. Fractional lipid exchange was calculated as: (Method is adapted.[31])

$$f_{mixing} = (F_{sample} - F_{no\ peptide})/(F_{positive} - F_{sample}) \qquad \text{(Equation 1)}$$

Cryo-transmission Electron Microscopy

Liposome formulations were diluted with the HBS buffer to reach a total lipid concentration of 2 mM and were incubated with peptides for 24 h. Cryo-TEM imaging was

done on an FEI G2 F30 Tecnai TEM operated at 150 kV. To prepare the sample, a mesh copper grid (Electron Microscopy Sciences) was picked up with tweezers and mounted on the plunging station of an FEI Vitrobot. Five microliters of the solution were applied to the grid. The excess liquid was blotted by filter paper attached to arms of the Vitrobot for 2 s to form a thin film. The sample was then vitrified by plunging into liquid ethane. The vitrified sample was finally transferred onto a single-tilt cryo specimen holder for imaging. (Method is adapted.[31])

TAMRA-biotin-dextran leakage assays

Leakage of 40 kDa TBD was measured with FRET. Dextran vesicles with entrapped TBD were diluted to 1 mM, and streptavidin-AF488 (the donor fluorophore) was added to a final concentration of 20 nM. In a 96-well plate, peptide and vesicles were mixed P:L ranging from 1:10 to 1:10000 and then incubated while shaking at room temperature for 1 h before measuring FRET by donor fluorescence quenching on a Microplate Reader with ex/em = 495/ 519 nm. As a positive control for 100% leakage, 5 μL of 10% Triton-X100 was added to three wells, and as a negative control, no peptide was added to three wells. The measurements were repeated three times. Fractional leakage was calculated as (Method is adapted.[31])

$$f_{\text{TBD leakage}} = (F_{\text{no peptide}} - F_{\text{sample}})/(F_{\text{no peptide}} - F_{\text{triton}}) \qquad \text{(Equation 2)}$$

ANTS/DPX leakage assays

Small-molecule leakage was measured by quenching ANTS with DPX. ANTS/DPX leakage vesicles were diluted to 1 mM. On a 96-well plate, peptide and vesicles were mixed at P:L ranging from 1:10 to 1:10000 and then incubated with shaking at room temperature for 1 h before measuring ANTS fluorescence using a microplate reader

with ex/em = 360/519 nm. As a positive control for 100% leakage, 4 μL of 10% Triton X100 was added to three wells, and as a negative control, no peptide or Triton was added to three wells. The measurements were repeated three times. Fractional leakage was calculated as (Method is adapted.[31])

$$f_{\text{ANTS/DPX leakage}} = (F_{\text{sample}} - F_{\text{no peptide}})/(F_{\text{triton}} - F_{\text{no peptide}}) \quad \text{(Equation 3)}$$

Tryptophan binding

100 μL 10 μM peptides were prepared in HBS solutions in cuvettes. Liposomes with different lipid compositions were added with P:L ranging from 1:10 to 1:170. After 10 minutes of incubation at room temperature, tryptophan fluorescence spectra were measured on a spectrophotometer (HORIBA, Canada) and the peak fluorescence intensity was recorded at 333 nm (ex = 280 nm). Samples to correct for lipid scattering, including vesicles with pure tryptophan at P:L ranging from 1:10 to 1:170 was also measured. A scattering correction was made as described previously. The fitting curve and mole-fraction partition coefficient K_P, was obtained by fitting using the equation

$$I([L]) = 1 + (K_P[L])/([W] + K_P[L]) \quad \text{(Equation 4)}$$

Where K_P is a mole-fraction partition coefficient, I is the fluorescence fold increase compared to no lipid binding, [L] is the lipid concentration and [W] = 55.3 M is the molar concentration of water. The measurements were repeated three times. (Method is adapted.[31])

Circular dichroism (CD)

pH 5 and pH 7 POPC vesicles were prepared as above but without KCl. Samples were also prepared in buffer without KCl and at 30 μM peptide and +/- 0.5 mM POPC. CD was collected using a Jasco J-810 spectropolarimeter, flushed with N2. Scans were at 20

nm/sec, 3 accumulations, and samples were at room temperature. Quartz cuvette pathlength was 0.1 cm.

RESULTS

Membrane difference coupled to peptide selectivity

In this chapter, we are using both TAMRA-biotin dextran (TBD, a macromolecule) and ANTS/DPX small molecule leakage assays to evaluate the peptide potency to permeabilize liposomes with different lipid compositions (**Figure 3-1**). Macrolittins have a higher potency for triggering macromolecule release from synthetic POPC liposomes than MelP5 but have a much lower propensity to permeabilize human cell membranes (**Fig. 3-2A**). This selectivity exists despite the fact that 21 of their 26 residues (73%) are identical. To determine the factors contributing to this remarkable membrane selectivity, we tested hypotheses relevant to the differences between pure POPC liposomes and mammalian cell membranes.

Firstly, we hypothesized that the moderate anionic charge on the cell surface, contributed by glycoconjugates on lipids and proteins, plus any external anionic lipids such as phosphatidylserine (POPS) and phosphatidylglycerol (POPG),[66] might inhibit the macrolittins by interacting with the charges on the peptides at pH 7. In comparison, POPC is zwitterionic, with zero net charge. M159 has a net charge of about -1 at pH 7 while MelP5 has a charge of +3. We measured leakage of small molecules and macromolecules induced by MelP5 or M159 from liposomes containing 95% POPC and 5% anionic POPG to mimic an anionic charged surface. Inclusion of 5% anionic POPG did not significantly

change the potency of leakage for small or for large molecules induced by either M159 or MelP5 (**Fig. 3-3A&E**).[31]

Secondly, considering that mammalian cell plasma membranes contain between 20 and 40 mol % cholesterol,[67] we tested leakage from POPC liposomes containing 30 mol% cholesterol. Inclusion of cholesterol in liposomes modified acyl chain fluidity of bilayer membrane, significantly inhibited leakage of small and large molecules for M159, providing our first clue to the physical chemistry of its membrane selectivity. Interestingly, small molecule leakage for MelP5 was decreased only slightly by cholesterol, and macromolecule leakage was significantly increased by cholesterol, consistent with the toxic effect of MelP5 against mammalian cell membranes (**Fig. 3-3C&G**).[31]

Thirdly, to test the effect of bilayer thickness, we prepared liposomes with 100% PC lipids comprised of either diC14:1(9)PC or diC20:1(11)PC lipids. These di-unsaturated PC lipids, like POPC, are both in the fluid phase at room temperature with similar acyl chain fluidity. diC14:1-PC forms a thinner bilayer than POPC, while diC20:1-PC forms a thicker bilayer due to the length of fatty acid chain. **Fig. 3-3D&H** show TBD leakage from these two liposomes compared to POPC. Against thinner bilayers (diC14:1-PC) the potency for leakage of dextran by M159 decreased a small amount, compared to POPC. **Fig, 3-3D**. Against thicker bilayers (diC20:1-PC), the inhibition of M159 macromolecular poration was dramatic, **Fig. 3-3H.** MelP5 was less sensitive to bilayer thickness. In diC14:1PC its activity is similar to POPC and in diC20PC bilayers its activity was reduced, but not as much as M159.[31]

Lastly, to mimic the steric effects of the crowded carbohydrate layer on mammalian cell membranes[68] we made the same measurements using liposomes containing 95% POPC

lipids and 5% lipids with a covalently attached 2,000 Da polyethylene glycol (PEG2K-PE). At 5 mol% PEG2k lipids fully cover the surface of a lipid vesicle with a continuous layer of PEG in the "mushroom" configuration.[69] Inclusion of 5% PEG2K-PE did not change the potency of either small or large molecule leakage induced by either M159 or MelP5 (**Fig. 3-3B&F**).[31] Collectively, membrane properties that affect the hydrocarbon core of the membrane, including cholesterol content and membrane thickness, play roles in inhibiting M159 activity in cell membranes compared to POPC liposomes.

Liposomal aggregation and fusion induced by peptides

Pore-forming peptides often cause fusion and aggregation of lipid vesicles because they disrupt the normally strict segregation of polar and nonpolar moieties in the bilayer.[70] In an *in vivo* application of peptide-induced controlled release from vesicles, fusion and aggregation would be undesirable because peptide-destabilized vesicles can interact with cells and deposit lipids. They will also have altered shape and increased size and thus altered and unpredictable circulation times and clearance routes. For these reasons we measured the effects of macrolittins on POPC vesicle architecture. We first measured light scattering by optical absorbance, because scattering will increase if average particle size increases due to either aggregation or fusion.[71] The results, in **Fig. 3-4A**, indicate that M159 induces significant aggregation or fusion of POPC liposomes even at very low P:L, with a maximum light scattering at P:L ~ 0.015. By contrast, MelP5 caused little change in light scattering at any concentration. The decrease in light scattering from the peak with increasing P:L probably results from the partial solubilization of the bilayers by macrolittin at these high concentrations.[28] To test whether the macrolittin-induced increase in light scattering is due to membrane fusion, we measured lipid exchange using Förster resonance

energy transfer (FRET) between dye labelled lipids.[72] In this assay, one population of liposomes, doped with NBD-PE (donor) and Rhodamine-PE (acceptor) lipids, was mixed with an excess of liposomes lacking dye-labeled lipids. NBD fluorescence is quenched in the rhodamine-labelled vesicles, but its fluorescence will increase if fusion takes place due to dilution of the donor and acceptor lipids into the unlabeled liposomes. The measurements in **Fig. 3-4B** show that M159 causes significant vesicle fusion, and that MelP5 causes much less fusion. We express fusion in **Fig. 3-4B** relative to the equilibrium state of completely randomized lipids, which means acceptor lipids are diluted sixfold over the initial concentration. A single fusion event between two vesicles will lead to a two-fold reduction in rhodamine acceptor concentration. Subsequent fusion events dilute the acceptor by smaller increments.[31]

To further characterize the effects of M159 and MelP5 on vesicle architecture, we observed liposomes using confocal microscopy (**Fig. 3-4C**) and Cryo-electron microscopy (**Fig. 3-4D**). In confocal microscopy, individual dye-labelled liposomes with 0.1 μm diameter cannot be resolved, leading to a diffuse fluorescent background. However, after addition of M159, we observed the formation of very large (≥ 10 μm) irregular lipid structures. The size of the aggregates depended on peptide to lipid ratio when P:L < 0.003 (**Fig. 3-5**). Cryo-EM results, **Fig. 3-4D**, show that addition of M159 to 0.1 μm unilamellar POPC vesicles results in fused liposomes with greater diameter and formation of large multilamellar vesicles, verifying that membrane fusion is driving changes in membrane topology. MelP5 does not cause the formation of multilamellar vesicles.[31]

To determine if peptide-induced lipid aggregation and fusion has the same membrane selectivity as leakage, we performed light scattering and FRET assays using

liposomes containing 30% cholesterol. The results (**Fig. 3-6A&B**) showed that M159 causes only a small amount of aggregation and fusion in 30% cholesterol bilayers, matching its low macromolecular poration activity in the same bilayers. MelP5, on the other hand, induced more liposome aggregation and fusion in POPC bilayers containing 30% cholesterol (**Fig. 3-6A&B**) compared to POPC, just as it caused more leakage (**Fig. 3-3G**). To further test the effect of cholesterol on macrolittin fusion activity, we also tested for peptide-induced fusion and aggregation of low-density lipoprotein (LDL) particles, which are bounded by a cholesterol rich lipid monolayer.[73] We find that M159 does not cause aggregation and fusion of LDL particles, while MelP5 causes dramatic increases in LDL particle size (**Fig. 3-6C**), consistent with the selectivity of these peptides against lipid vesicles.[31]

Aggregation and fusion of liposomes upon interaction with macrolittins is undesirable for long-term stability of drug product and drug-release applications of macrolittins. Therefore, we tested whether fusion and aggregation can be inhibited, without changing pore formation and macromolecular cargo release. By these experiments, we also test the hypothesis that macromolecule release is due only to pore formation, and is not the incidental result of the changes in vesicle architecture that accompany fusion and aggregation. Earlier, in **Fig. 3-3B&F**, we showed that the addition of 5% anionic lipids or the addition of 5% PEG2k lipids to POPC do not inhibit macromolecular poration. At the same time, these lipids are expected to decrease or eliminate fusion and aggregation of vesicles, due to the added electrostatic and steric repulsion between membrane surfaces.[74] Our results show that addition of either 5 mol% POPG or 5% PEG2k-PE or both eliminate M159-dependent changes in particle size **(Fig. 3-7A)**, and significantly reduce fusion

between vesicles (**Fig. 3-7B**), specifically at low peptide concentrations. Yet, they do not change binding pattern of macrolittins (**Fig. 3-8**) and they do not change macromolecular poration (**Fig. 3-3**). Thus, fusion and aggregation are easily mitigated without any loss of membrane selectivity or macromolecular poration of liposomes.[31]

Membrane selectivity determined by peptide sequences

To identify the key residues that determine lipid membrane selectivity by peptides, we firstly compare the sequence of MelP5 and its non-toxic daughter peptides from the macrolittin family. There are five members in the macrolittin family and all of them have net charge of -1 while MelP5 has +2. We thus focus on the change of acidic amino acids at specific sites: the alanine at 4th of MelP5 is replaced with acidic amino acids (aspartic acid or glutamic acid) in all macrolittins and the valine at 8th of MelP5 is substituted by acidic amino acids in 4 out 5 macrolittins. In addition, the nonpolar isoleucine at 17th of MelP5 is substituted by polar glutamine in 4 out of 5 macrolittins. Therefore, we hypothesize that these 3 amino acid substitutions play roles in modifying the cell toxicity of the peptide variants. In this study, we choose macrolittin 159 (M159) from the macrolittin family, and we selected three peptide variants with single amino acid substitution: 4EA, in which the glutamic acid at 4th site in M159 is replaced by alanine, the native residue in MelP5; 8EV, in which glutamic acid at 8th site in M159 is substituted by valine, the native residue in MelP5; 17IQ, in which isoleucine at 17th site in MelP5 is replaced by glutamine (**Fig. 3-9**). We thus study the structural, biophysical and functional characteristics of these 5 peptides (MelP5, M159, M159-4EA, M159-8EV, MelP5-17IQ).

To test if the cell toxicity caused by these peptides changes after we substitute key amino acids, we chose HeLa cells as a nucleated mammalian cell line and red blood cells

to test cell viability and hemolysis after treatment with different peptides. Consistent with previous results, we found that MelP5 was highly toxic to HeLa cells at a low concentration while M159 had almost no toxicity even at high concentrations. The three variants yielded intermediate toxicities. The MelP5 variant 17IQ is more toxic than the two M159 variants 4EA and 8EV (**Fig. 3-10A**) and the 4EA and 8EV variants were more toxic than M159. For red blood cells, the hemolysis curves for three variants are similarly between the curves of MelP5 and M159 (**Fig. 3-10B**). We also measured the peptide toxicity to Gram negative bacteria *Ecoli* and Gram positive bacteria *S.aureus* (**Fig. 3-10C&D**) The minimal inhibitory concentration (MIC) measurements indicated that both MelP5 and its variant 17IQ had MIC of less than 40 µM of, and 17IQ had even lower MIC than MelP5 to both bacteria, while M159 and its two variants have little toxicity to both bacteria (MIC > 40 µM). These results revealed that these single amino acids are critical to determine peptide toxicity to different cells.

Considering that the natural venom toxin melittin is a membrane-permeabilizing peptide, and its variants MelP5 and M159 are all membrane active peptides, we are interested in the composition of those cell membranes. In addition, our previous results showed that cholesterol content and membrane thickness played roles in resisting peptide attack. Particularly, MelP5 is more active in PC membranes containing cholesterol while the activity of M159 is inhibited in the presence of cholesterol. Therefore, we investigated the sequence-membrane activity relationship. We performed molecule leakage assays with different lipid compositions to compare membrane-permeabilizing activity induced by variants. The vesicle compositions include 100% pure PC, 70% PC plus 30% cholesterol to mimic cell membrane, and membranes of different thickness (thin C14 and thick C20)

to mimic varying membrane thicknesses. For small molecule (ANTS/DPX) leakage from 100% pure PC vesicles, the leakage curves are not significantly changed among these peptides (Figure 3A). When vesicle membrane contains 30% cholesterol, those three variant curves are between MelP5 leakage curve and M159 leakage curve (**Fig. 3-11A**). For macromolecule (40kDa TBD) leakage from vesicles containing 100% pure PC, 70% PC plus 30% and pure 100% C14, all three variant curves are between MelP5 curve and M159 cure (**Fig. 3-11C-E**). However, with the vesicles with thick lipid membrane, the membrane permeabilizations of all five peptides were all highly decreased, and 100% leakage of TBD cannot be achieved even at high peptide concentrations (**Fig. 3-11F**). These results indicated that the cellular target of these peptide cell toxicity is mainly the cell membrane, and that critical single amino acids substitutions play roles in the evolution of peptide detoxication.

Next, we studied another important feature of membrane-active peptides, lipid aggregation or exchange, due to fusion, induced by peptides. To investigate the effects of variants on vesicle architecture in different lipid compositions, we find that MelP5 and other variants caused little change in light scattering at any concentration for pure POPC liposomes (**Fig. 3-12A**). When vesicles contain 30% cholesterol, all the peptides can cause changes in light scattering at around P : L ~ 0.01, in which the variant 4EA caused maximum light scattering at P : L ~ 0.05 (**Fig. 3-12B**). However, with vesicles consisting of pure 100% C20PC lipids, the thicker bilayer, none of these peptides caused changes in light scattering even at high concentrations (**Fig. 3-12C**). To test whether the peptide-induced increase in light scattering is associated with membrane fusion, we measured lipid exchange using Förster resonance energy transfer (FRET) between dye-labeled lipids. For

100% PC vesicles, M159 induced significantly higher lipid exchange rate than other peptides from P : L ~ 0.001 (**Fig. 3-12D**). When 30% cholesterol was included, M159 caused significantly lower lipid exchange rate than all other peptides at around P : L ~ 0.01 (**Fig. 3-12E**). For C20PC vesicles, none of the peptides induce lipid exchange except at a very high concentration (**Fig. 3-12F**). Previously, we visualized the lipid aggregates induced by M159 or MelP5 by confocal microscopes. Here the images of aggregates of vesicle either in 100%PC or 70%PC30%Cholesterol induced by three variants (P : L = 0.01) indicated that for 100%PC vesicles, these variants induced lipid aggregates of small size (**Fig. 3-13**) while they caused huge aggregates of lipids in the present of cholesterol. The 17IQ variant yielded even more aggregates than the other two variants (Figure 5B). Above all, the light scattering results are consistent with lipid exchange results and images of aggregates, suggesting M159 is highly selective to pure POPC lipid bilayers, while MelP5 and the variants are more selective to for bilayers containing cholesterol.

The actions of peptides on vesicles, such as leakage and aggregation, only happen when peptides bind to vesicles. To investigate if the differences in peptide-lipid associations are caused by differences in peptide-lipid binding, we measured peptide binding capacity by detecting the intensity and peak wavelength changes of tryptophan and compared the binding curves of these peptides in different vesicle compositions. Up to 0.38 mM vesicles were titrated into 10 μM peptides drop by drop and binding curves were made. Our results showed that all the variants bind 100% PC vesicles immediately after adding lipids, and the curves tend to arrive at the plateau value around 0.4 mM vesicle concentration (**Fig. 3-14A**). These curves of 100% PC vesicles are similar to those of 100% C20 vesicles (**Fig. 3-14C**), suggesting that the thickness of phospholipids does not affect

peptide binding. However, vesicles containing 30% cholesterol decrease the intensity of tryptophan binding, more interestingly, the intensity tends to be zero for 17IQ variant, which might be explained by perturbance of cholesterol turbidity or unbound tryptophan in the peptide (**Fig. 3-14B**). For all three kinds of vesicles, the mole fraction partition coefficients for MelP5 and 8EV binding is over 10^6, indicating these peptides are essentially completely membrane bound (**Fig. 3-14D**). Finally. To examine the secondary structure of these variants in the presence of those types of vesicles, we used CD spectroscopy with and without the addition of vesicles. In the absence of lipid addition, we found that both MelP5 and its variant 17IQ exhibit a single minimum at ~ 200 nm, indicating a random coil secondary structure. While M159 and its variants 4EA and 8EV acquire the classical α-helical CD spectroscopy (**Fig. 15A**). With 100% PC vesicle or C20 vesicle addition, all the peptides exhibit α-helical secondary structures, consistent with similar binding curves between pure PC and C20 vesicles (**Fig. 15B&D**). However, when adding vesicles containing 30% cholesterol, MelP5, M159 and 4EA are still in α-helical secondary structures, while the intensity of 8EV and 17IQ is low, which is likely to be a result of aggregation/fusion of these vesicles (**Fig. 15C**).

DISCUSSION

Membrane selectivity

We are focusing on mutual selectivity between peptide and lipid bilayers by studying peptide-lipid interaction for this chapter. The differences in membrane selectivity between M159 and MelP5 can be quantified by comparing potencies in biophysical and functional studies; controlled release of macromolecules from POPC vesicles versus toxic

cytolysis of cell membranes. For the release of macromolecules from POPC, M159 is about 28-fold more potent than MelP5 and at least 100-fold more potent than melittin. On the other hand, M159 is at least 100-fold less potent than MelP5 or melittin against human cell membranes. After just two generations of synthetic molecular evolution, M159 is a at least 3,000-fold more selective than MelP5, and 10,000-fold more selective than melittin, for POPC over human cell plasma membranes.[31]

Mechanistic model of selectivity

There is a critical difference between the macrolittins and most other membrane permeabilizing peptides that provides an important clue to the mechanism of their membrane selectivity. The macrolittins release both small molecules and macromolecules from POPC bilayers with similar high potency, which is very unusual, as most membrane permeabilizing peptides, including melittin and MelP5, release small molecules at much lower P:L than they release macromolecules.[30] The majority of membrane permeabilizing peptides do not form explicit pores in membranes at all but act through what has been called "interfacial activity"[75] to form a continuum of transient, dynamic and heterogeneous permeabilization pathways through the membrane. Typically, the maximum size of released molecules increases with P:L, creating different potencies for small molecule and macromolecule release. The macrolittins, on the other hand, release small molecules and macromolecules at very similar P:L values meaning that they do not form small pores at low peptide and larger pores at higher peptide. At the same time, we have shown by atomic force microscopy that macrolittins form a wide range of nm-sized pores in POPC bilayers. Taken together, these observations show that macrolittins form only large pore structures, with a minimum pore size in the nm range.[28]

The effects of hydrocarbon core properties (i.e. cholesterol content and bilayer thickness) on the membrane selectivity of the macrolittins are probably the result of this unique large pore structure, which will have a very large peptide-membrane interface around the circumference of the pore. By evolving peptides over two generations in POPC vesicles for macromolecule release at low concentration, we have created a unique, pore structure that is especially well-suited to form large pores in POPC bilayers. Once inserted across the membrane, the peptides form the boundary between the large aqueous pore and the bilayer lipids by orienting their amphipathic helices with the polar surface, including the three acidic residues selected in the screen, oriented towards the pore interior and the hydrophobic surface oriented toward the membrane lipids. In this model, the free energy of the peptide-lipid and peptide-peptide interfaces will be critically important in pore stability, which may explain how pore stability is very sensitive to hydrocarbon core properties.

Key residues in peptide sequences

The key differences in amino acids between M159 and MelP5 are also studied here. We investigate how the toxin MelP5 is detoxified in the macrolittin which have significantly more PC permeabilizing activity. Specifically, we focus on the sequence-structure-function relationships by comparing the biophysical and functional features of MelP5, macrolittin and three toxin variants (4EA, 8EV, 17IQ) in which potentially key amino acids are substituted. We find that substitution of the acidic amino acids at the 4th or 8th site of M159 with non-polar amino acids present at these sites in MelP5 increased both the cell toxicity and the disruption of synthetic bilayers containing cholesterol implying that these residues contribute to the detoxification of melittin and MelP5, as well

as to the nanopore forming properties of the macrolittins. Substitution of leucine by glutamine at the 17th position of MelP5 decreased MelP5 toxicity, indicating how the toxicity of MelP5 is alleviated in the non-toxic M159 and related peptides.[29] Finally, according to the biophysical and functional results of these peptides, we will propose a theoretical model describing the relationship between the peptide-lipid pore structure and peptide sequence, which provides insights to enable the design or screening of even more useful melittin variants in the future.

Figure 3-1
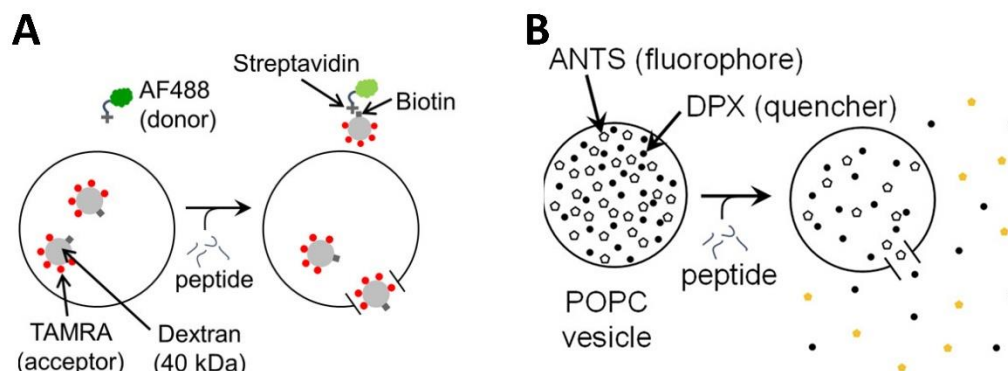
Figure 3-1. Molecule leakage assays. **A.** Illustration of macromolecule leakage assay. Peptides at gradient concentrations were incubated with streptavidin-AlexaFluor488 (SA-AF488) and liposomes with different compositions containing TAMRA-biotin-dextran (TBD) for 1 h. Upon TBD release induced by peptide poration, SA-AF488 can bind TBD, leading to FRET and reduced AF488 fluorescence intensity. **B.** Illustration of small molecule leakage assay. Peptides at gradient concentrations were incubated with encapsulated ANTS (fluorophore) and DPX (quencher) for 1 h, the dilution of ANTS and DPX leads to increased intensity of ANTS fluorescence. Schematics are adapted.[76]

Figure 3-2
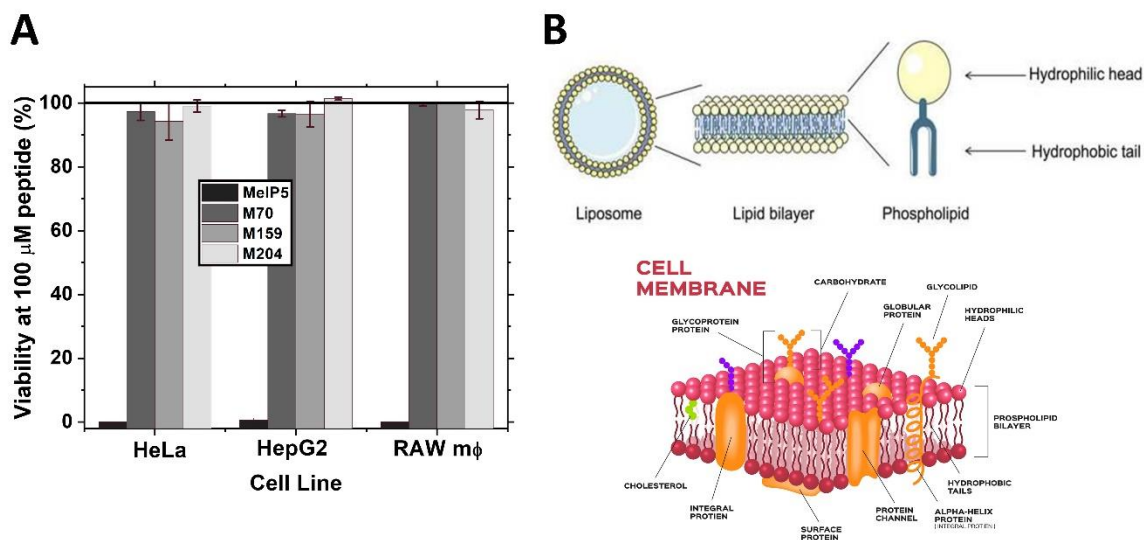
Figure 3-2. Different cell toxicity coupled to different membrane compositions. **A.** Effect of 100 µM of MelP5 and three macrolittins on Hela cells, HepG2 cells and RAW 264.7 macrophages. Peptides were incubated with cells for 3 h. After 24 h, cell viability was measured by Alamar Blue. **B.** The difference compositions between synthetical POPC liposomes (top) and mammalian cell membranes (bottom). Adapted from (Figure and legend are adapted from Sun, Hristova and Wimley, Nanoscale, 2021[31]) and https://nootropicgeek.com/phosphatidylserine-review/
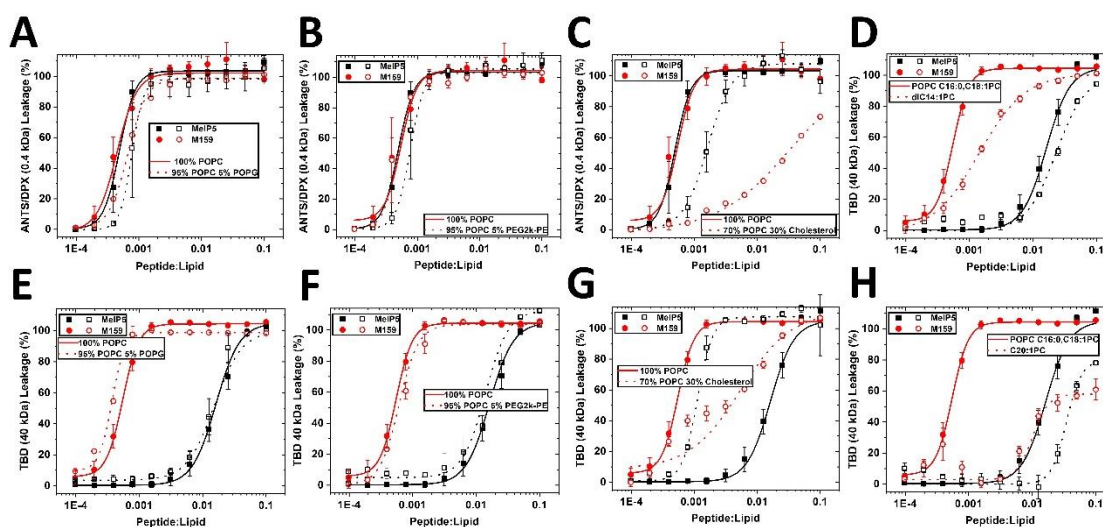
Figure 3-3

Figure 3-3. Mechanisms underlying membrane selectivity of macrolittins. **A-C**. ANTS/DPX small molecule leakage results. Peptides (MelP5 or M159) were incubated with liposomes containing 95% POPC and 5% POPG (A); 95% POPC and 5% PEG2k-PE (B); 70% POPC and 30% Cholesterol (C) encapsulated ANTS (fluorophore) and DPX (quencher) for 1 h respectively, in which peptides with liposomes containing 100% POPC were compared. Upon pore formation, the dilution of ANTS and DPX results in an increase in ANTS fluorescence monitored on a plate reader (ex/em = 350/519 nm). **D-H**. Macromolecular (TBD) leakage assay. Peptides (MelP5 or M159) were incubated with different compositions of liposomes 100% diC14:1PC (D); 95% POPC and 5% POPG (E); 95% POPC and 5% PEG2K (F); 70% POPC and 30% Cholesterol (G); 100% diC20:1-PC (H) containing TAMRA-biotin-dextran (TBD) for 1 h respectively, in which peptides with liposomes containing 100% POPC were compared. Upon macromolecular pore formation, the 40 kDa dextran leaks out of the liposomes and form a complex with streptavidin, causing FRET monitored on a plate reader (ex/em = 480/520 nm). For both leakage assays,

we chose a series of peptide to lipid ratio (from 1E-4 to 0.1) and Triton X100 was added to obtain the 100% leakage value as a positive control. (Figure and legend are adapted from Sun, Hristova and Wimley, Nanoscale, 2021[31])

Figure 3-4
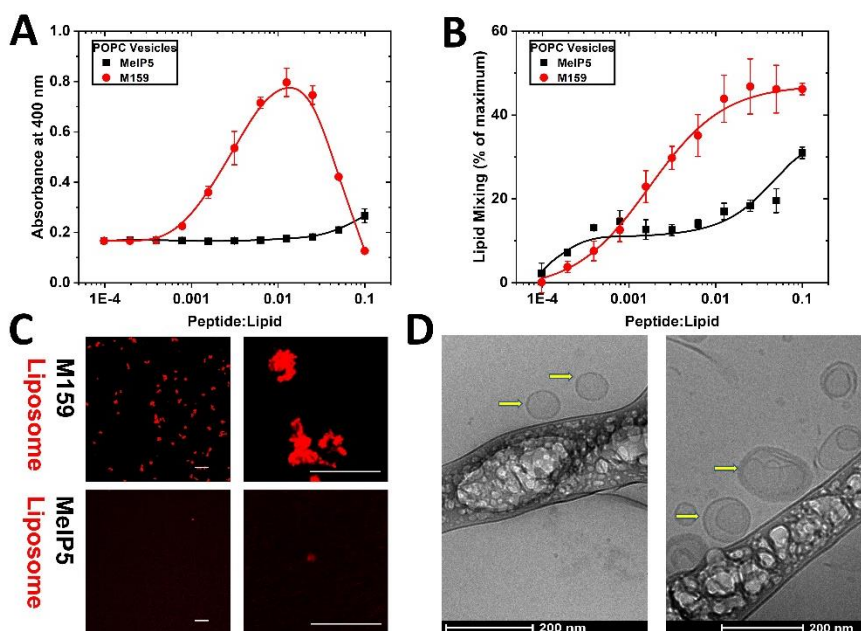
Figure 3-4. M159-induced aggregation and fusion between pure POPC liposomes. (A) Light scattering of POPC liposomes with peptide treatments. 2 mM POPC liposomes were incubated with MelP5 or M159 for 3 h at different peptide to lipid ratios. Optical absorbance, which reports on liposome light scattering, was measured at 410 nm by a plate reader. (B) Fluorescence resonance energy transfer (FRET) between dual labeled POPC liposomes and non-labeled POPC liposomes. 0.4 mM POPC Liposomes containing 0.5% NBD-PE and 0.5% rhodamine-PE dyes mixed with 2 mM pure POPC liposomes were incubated with MelP5 or M159 for 3 h at different peptide to lipid ratios. NBD fluorescence was monitored on a plate reader (ex/em = 480/520 nm), and lipid exchange percentage was calculated by the ratio of measured NBD fluorescence to NBD fluorescence from positive controls (2.4 mM POPC liposomes containing 0.08% NBD-PE and 0.08% rhodamine-PE). (C) Confocal images of POPC liposomes. 2 mM rhodamine labeled POPC liposomes were incubated with 60 μM MelP5 or M159 and they were observed using confocal microscopy

(ex/em = 512/560 nm). Top: M159 treatment; bottom: MelP5 treatment. (Scale bar = 20 µm) (D) Cryo-TEM images of POPC liposomes. 2 mM POPC liposomes were incubated with 60 µM MelP5 (left) or M159 (right) and they were visualized by Cryo-TEM. Liposomes are indicated by yellow arrows. (Figure and legend are adapted from Sun, Hristova and Wimley, Nanoscale, 2021[31])

Figure 3-5
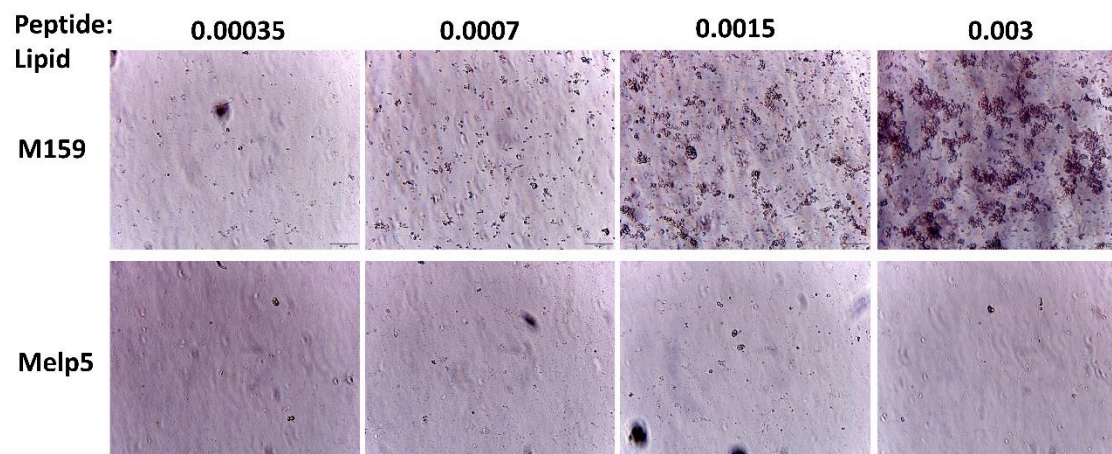
Figure 3-5. M159 induced pure POPC liposomes aggregation. Pure POPC liposomes were incubated with M159 or MelP5 at different peptide to lipid ratios for 3 h, then the mixtures were observed by an optic microscope. (Top panel: M159 treatment; bottom panel: MelP5 treatment. Peptide to lipid ratios were shown.). (Figure and legend are adapted from Sun, Hristova and Wimley, Nanoscale, 2021[31])

Figure 3-6
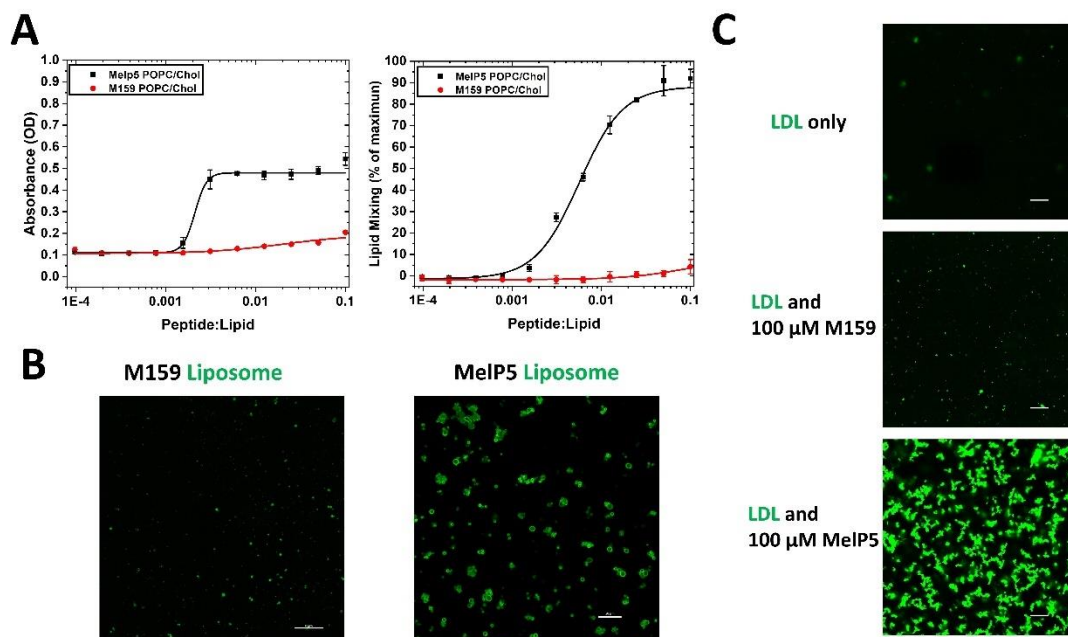
Figure 3-6. MelP5 induced aggregation between liposomes containing cholesterol. (**A**) Lipid light scattering was induced by MelP5 instead of M159 using liposomes containing 50% POPC and 50% Chol (left). Lipid exchange was induced by MelP5 instead of M159 using liposomes containing 50 POPC and 50 Chol (right). (**B**) 2 mM NBD labeled liposomes containing 70% POPC and 30% cholesterol were incubated with 20 µM MelP5 or M159 and they were observed using confocal microscopy (Left: M159 treatment; right: MelP5 treatment). (**C**) 10 µg/ml Bodipy-labeled LDL (ex/em = 488/512 nm) was incubated with 100 µM M159 or MelP5 for 3 h at 37 degrees. They were observed by a confocal microscope (top: LDL alone; middle: LDL and M159; bottom: LDL and MelP5). Scale bar = 20 µm. (Figure and legend are adapted from Sun, Hristova and Wimley, Nanoscale, 2021[31])

Figure 3-7
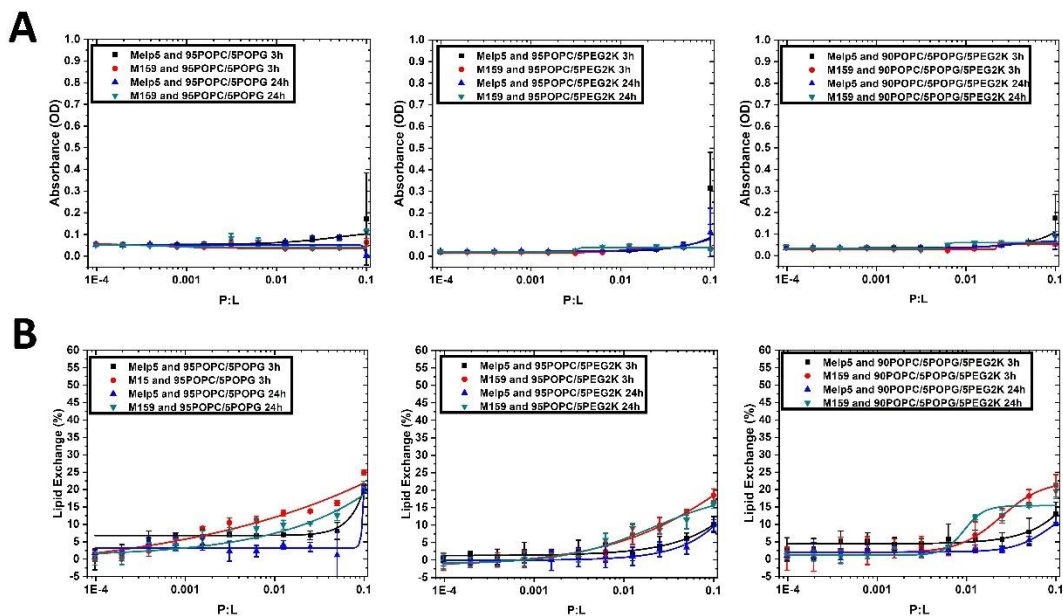
Figure 3-7. Peptide-induced lipid aggregation and remixing were blocked. **A.** Lipid aggregation of liposomes with peptide treatments was blocked by inclusion of 5% POPG (left), 5% PEG2K (middle) and 5%POPG plus 5%PEG2K (right) in POPC liposomes. **B.** Lipid exchange of liposomes with peptide treatments was blocked by inclusion of 5% POPG (left), 5% PEG2K (middle) and 5%POPG plus 5%PEG2K (right) in POPC liposomes.

Figure 3-8
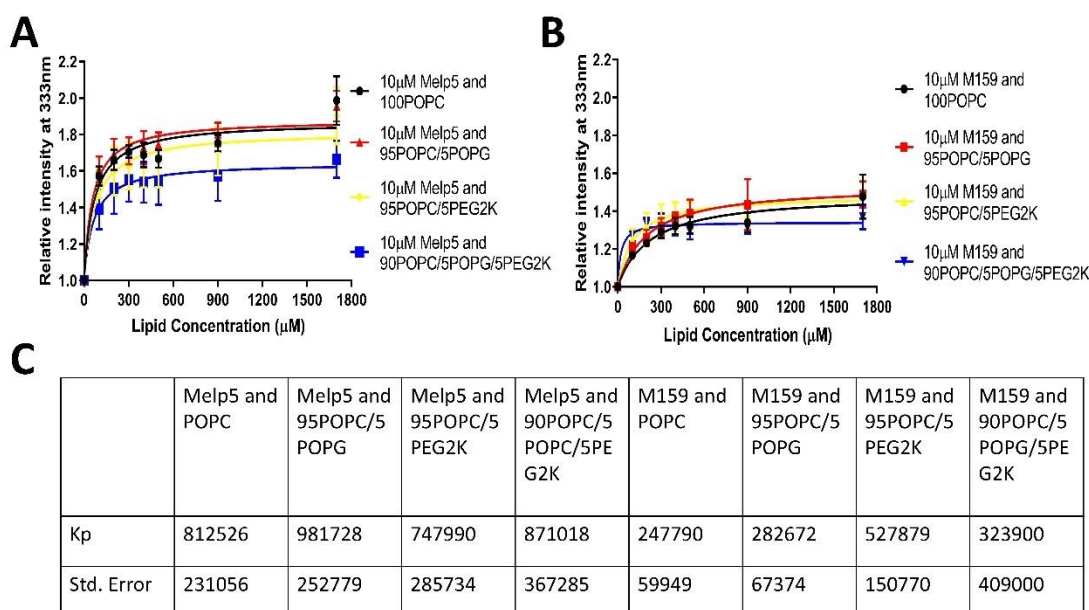
Figure 3-8. MelP5 or M159 binding to lipid bilayers, as indicated by tryptophan fluorescence intensity increase upon liposome additions. Different liposomes (100% POPC; 95% POPC, 5% POPG; 95% POPC, 5% PEG2K-PE; 90% POPC, 5% POPG, 5% PEG2K-PE) binding assay of 10 µM MelP5 (**A**) and 10 µM M159 (**B**) at a series of lipid concentrations. The relative fluorescence intensities were normalized to the maximal value (333nm) divided by tryptophan fluorescence intensity without lipid addition using a fluorimeter. Curves were fitted to Eq to determine the partition coefficient (K_p). (**C**) The measured K_p values and standard errors of peptides binding to liposomes were listed in the table (n = 3). (Figure and legend are adapted from Sun, Hristova and Wimley, Nanoscale, 2021[31])

Figure 3-9

A

Peptide Names	Peptide Sequences	Net Charges
Melittin	GIGAVLKVLTTGLPALISWIKRKRQQ	+5
Melp5	GIGAVLKVLATGLPALISWIKAAQQL	+2
Melp5 17Q	GIGAVLKVLATGLPALQSWIKAAQQL	+2
Macrolittin 159	GIGEVLHELATLLPELISWIKAAQQL	-1
Macrolittin 159 4A	GIGAVLHELATLLPELISWIKAAQQL	0
Macrolittin 159 8V	GIGEVLHVLATLLPELISWIKAAQQL	0

B

Figure 3-9. Bee venom toxin and its variants. **A.** List of the amino acid sequences and net charges of main toxin melittin and its variants. Acidic (red), basic (blue) and polar (yellow) residues are shown to highlight amphipathicity. **B.** Helical Wheel projections of the peptides tested or discussed in this work.

Figure 3-10

Figure 3-10. Toxicity of peptides on human cells and bacteria. **A.** HeLa cells were incubated with different peptides shown at about 80% confluency for 3 h, then the cells were subject to cell toxicity assay. **B.** Hemolysis of human red blood cells. Serially diluted peptides were incubated with human RBCs for 1 h. Release of hemoglobin was measured using optical absorbance of the cell supernatant at the heme absorbance wavelength of 410 nm, and % lysis against human erythrocytes was shown. A culture of *Ecoli* (**C**) or *P. aeruginosa* (**D**) in log phase growth in TSB media was treated with serial dilutions of five peptides and then MICs for each peptide were determined.

Figure 3-11
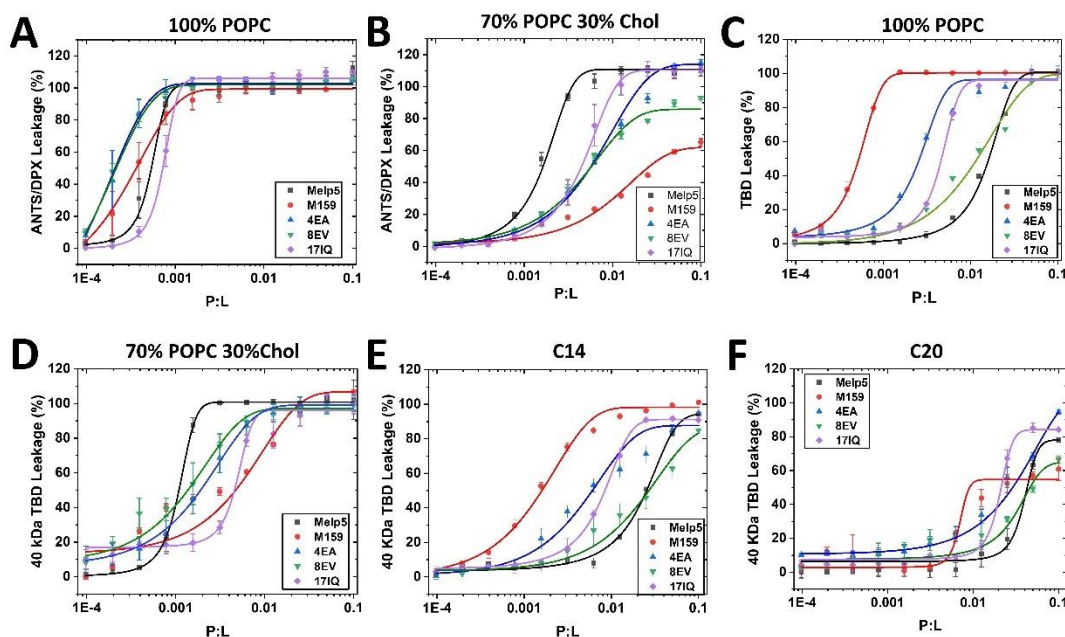
Figure 3-11. Leakage of different vesicles induced by peptides. **A-B**. ANTS/DPX small molecule leakage results. Peptides were incubated with liposomes composed of 100% POPC (**A**) or 70% POPC and 30% Cholesterol (**B**). Vesicles contained encapsulated ANTS (fluorophore) and DPX (quencher). Results are measured after 1 hour. **C-F**. Macromolecular TAMRA-Biotin-Dextran 40 kDa (TBD) leakage assay. Peptides were incubated with different compositions of liposomes, 100% POPC (**C**); 70% POPC and 30% Cholesterol (**D**); 100% diC14:1-PC(**E**); 100% diC20:1-PC (**F**). Vesicles contain entrapped TBD and AlexaFluor488-streptavidin is added to the external solution. Results are shown after 1 hour incubation. In all experiments, Triton X100 was added to obtain the 100% leakage value as a positive control.

Figure 3-12
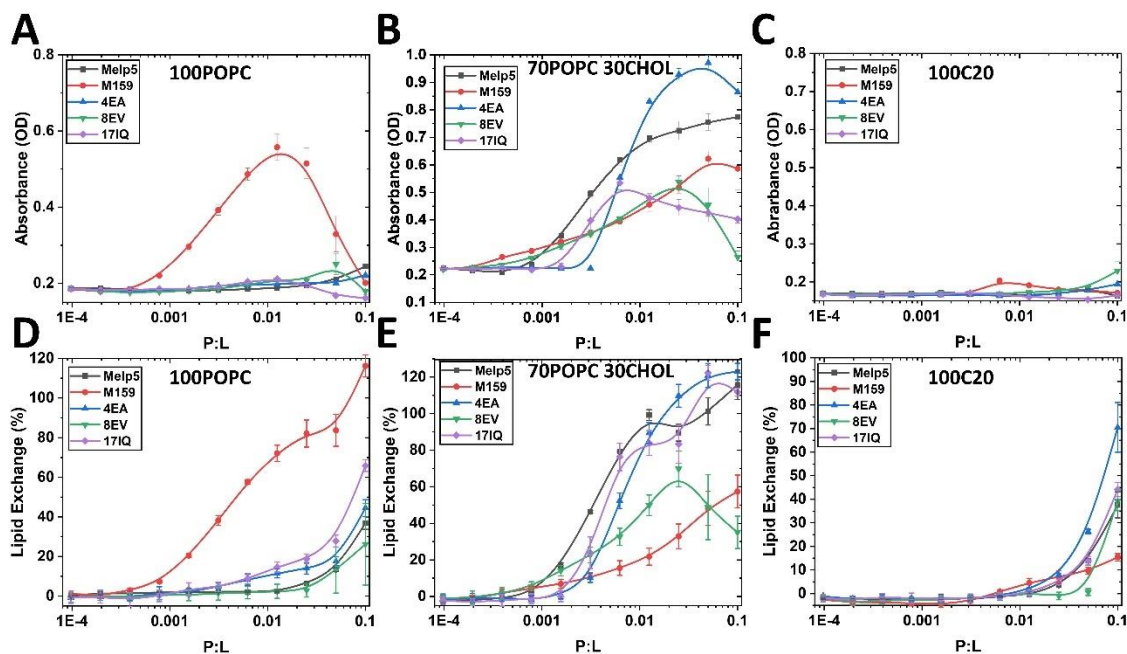
Figure 3-12. Peptide-induced aggregation and lipid exchange between vesicles. **A-C**. Light scattering of vesicles consisting of 100% POPC (**A**); 70% POPC and 30% Cholesterol (**B**); 100% diC20:1-PC (**C**) incubated with peptides. 2 mM vesicles were incubated with peptides for 3 h at different peptide-to-lipid ratios. Optical absorbance was measured at 410 nm on a plate reader. **D-E**. FRET between dual labeled vesicles and non-labeled vesicles with the composition 100% POPC (**D**); 70% POPC and 30% Cholesterol (**E**); 100% diC20:1-PC (**F**). 0.4 mM vesicles containing 0.5% NBD-PE and 0.5% rhodamine-PE dyes mixed with 2 mM vesicles were incubated with peptides for 3 h at different peptide-to-lipid ratios. NBD fluorescence was monitored on a plate reader and lipid exchange percentage was calculated by the ratio of measured NBD fluorescence to NBD fluorescence from positive controls.

Figure 3-13
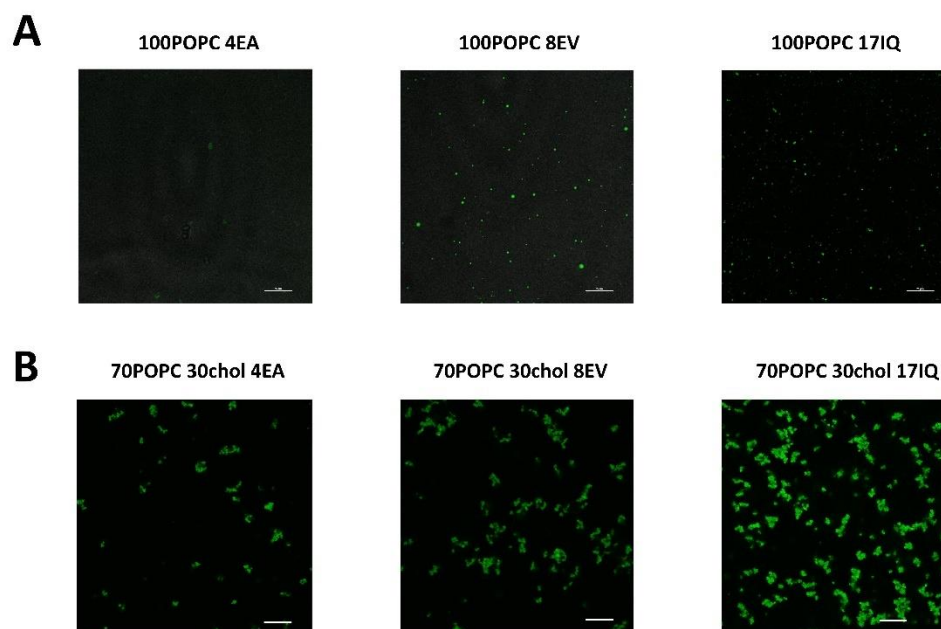
Figure 3-13. Confocal microscopy images of vesicle aggregates. 2 mM NBD-labeled vesicles consisting of 100% POPC (**A**) or 70% POPC and 30% Cholesterol (**B**) were incubated with 60 μM peptides shown for 1 h and were observed using confocal microscopy (scale bars = 20 μm).
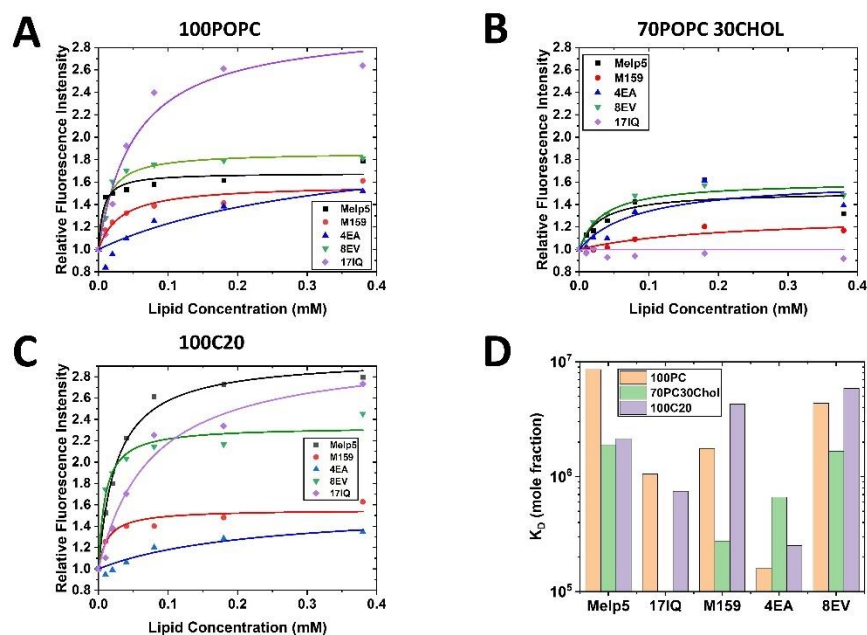
Figure 3-14

Figure 3-14. Membrane binding of toxin variants. 10 µM Peptides bind lipid bilayers, as indicated by tryptophan fluorescence intensity increase upon liposome additions. Peptide binding curve with vesicles of 100% POPC (**A**); 70% POPC and 30% Cholesterol (**B**); 100% diC20:1-PC (**C**) are fitted and shown. The relative fluorescence intensities were normalized to the maximal value (at 333 nm), divided by tryptophan fluorescence intensity without lipid addition. Curves were fitted to Eq 4 to determine the partition coefficient (K_D). (**D**) The measured K_D values are measured accordingly.

Figure 3-15
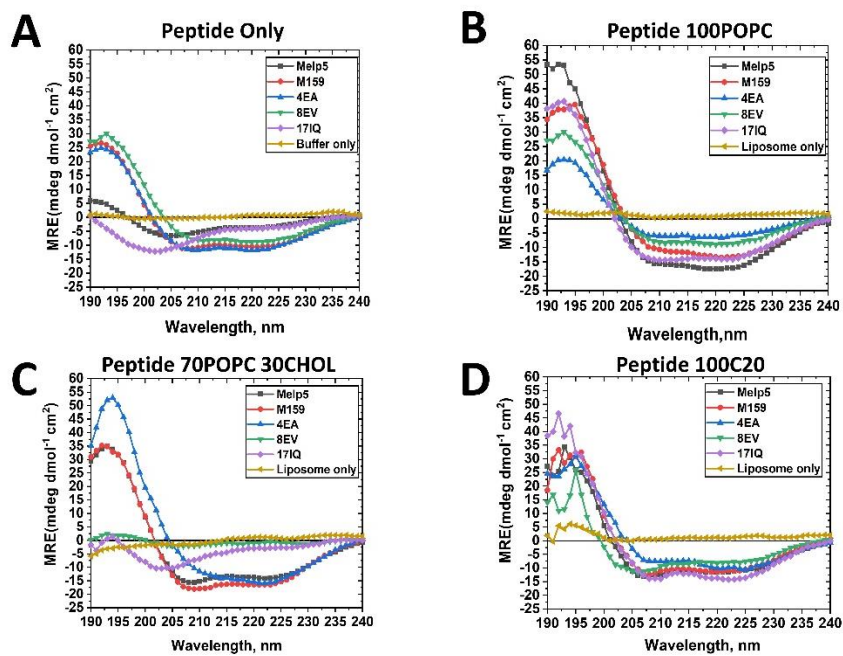
Figure 3-15. Secondary structure of venom variants. 25 µM different peptides were measure in the absence of vesicles (**A**) or in the presence of 1 mM vesicles consisting of 100%POPC (**B**); 70%POPC and 30%Cholesterol (**C**); 100% diC20:1-PC (**D**) at room temperature using a JASCO 810 CD spectrometer. The blank control is buffer only or liposome only without peptides.

CHAPTER 4: Peptide-triggered cargo release model

INTRODUCTION

Liposome encapsulation of small molecule drugs can extend drug release time, and reduce the acute systemic side effects of free drug.[6] Liposome encapsulation of macromolecular cargoes such as oligonucleotides, antibodies, enzymes, and other therapeutic proteins can improve stability and provide very long circulation time, in vivo, but spontaneous release of macromolecules can be very slow, if it happens at all. Further, drug-containing liposomes can accumulate specifically in diseased tissue, including tumors, due to enhanced permeability and retention.[7] They can also be targeted to specific tissues by other means.[8] But slow release of tumor-retained liposome-associated drugs could decrease free drug concentration locally and be less effective to tumor treatment.[9] In these circumstances, the utility of liposome encapsulation could be improved by fast release of vesicle contents, including macromolecules, by a nontoxic peptide.

From previous chapters, we identified that the candidate peptide macrolittins, namely M159 had selective potency of permeabilization against synthetic POPC liposomes over cell plasma membrane (no toxicity) partly due to different physiochemical properties of hydrocarbon cores of the bilayers. Although M159 could also induce pure POPC liposome aggregation, we designed a strategy (liposome PEGylation) to block this undesirable effect while maintaining its high potency to permeabilization. The last requirement for this potential peptide-triggered drug release model is to determine if M159 enables cargo release from liposomes in the presence of cells. Researchers found some

peptides such as MAP and penetratin are rapidly degraded both extracellularly and intracellularly giving rise to several degradation products.[77] Consistently, our previous results indicate that M159 is subject to cell endocytosis and degraded within cells. Therefore, the effect of mammalian cell environment on stability of M159 and its permeability effect should be investigated.

Given the fact that M159 induces pure POPC liposome aggregation and fusion, the interaction between POPC and cell plasma membrane caused by M159 cannot be ignored although interaction between POPC liposome can be inhibited. Even without M159, individual liposomes might be uptake by mammalian cells by either endocytosis or phagocytosis,[78] eliminating the permeabilizing effect of M159 on liposomes. In this chapter, we will firstly determine the interaction between liposome and cells with/without M159 on relevant time scales. And we will take measures to inhibit M159-induced liposome uptake by cell in order to focus on M159-triggered cargo release in cell environment.

Subsequently, we will select the cargoes to be encapsulated. Previously, we chose TBD as macromolecule and ANT/DPX as small molecule cargoes. Herein we are more interested in potentially therapeutic cargoes encapsulated in liposomes with high stability. Although we adopt different liposomes and purification methods according to different cargoes, the candidate peptide M159 can permeabilize those liposomes to all similar sized cargoes. Notably, to distinguish the effect of M159 induced liposome leakage and liposome fusion with cell plasma membrane, we will use a labeled lipid as a control which can insert cell membrane spontaneously. For both cargoes, we will visualize cargo uptake by cells and quantify the effect of cargoes released to assess the efficiency and effectiveness of this peptide-triggered cargo release model.

Finally, we will further investigate the effect of M159 on other lipid nanoparticles in addition to liposomes. For example, Lipofectamine 3000 reagents have been very popular and widely used as a general cell transfection product. Although we do not know its exact formulation and composition because they are trade secrets, it is known to consist of positively charged lipids, which can associate with negatively charge nucleic acid and form compact nanoparticles. We will test the cell transfection efficiency of plasmids in the presence of lipofectamine and M159. Currently, the potential triggered-cargo release model has only been tested in vitro at cell level, but future animal studies are planned.

MATERIALS AND METHODS

Lipofectamine 3000 reagents and Cholera Toxin Subunit B (Recombinant) with Alexa Fluor™ 488 Conjugate (Labeled CTX) was purchased from Thermo Fisher Scientific. 1,2-dioleoyl-sn-glycero-3-phosphoethanolamine-N-(lissamine rhodamine B sulfonyl) (Rhodamine-PE) and Cholesterol were purchased from Avanti Polar Lipids. Doxorubicin HCl was purchased from Cayman Chemical Company. Chloroform, ammonium thiocyanate, and other salts and buffer materials were purchased from Fisher Scientific or Sigma-Aldrich. Plasmid labeling was completed by Label IT Nucleic Acid Labeling Kits (Mirus)

Liposome-cargo preparation

For labeled CTX vesicles, dried lipid films were resuspended in 20 µg/ml labeled CTX. Upon extrusion, unencapsulated labeled CTX were separated from the vesicles by size exclusion chromatography with Sephadex G-100 resin. For Doxorubicin-containing liposomes, a remote loading method was used.16 POPC and cholesterol (mol/mol = 7/3)

were dried under vacuum overnight. The resulting lipid film was hydrated with 300 mM (NH4)2HPO4 solution by gentle mixing, then the generated vesicles were extruded over 10 times through 100 nm polycarbonate membranes. Liposomes were passed through a Sephadex G-100 resin column equilibrated with an isotonic HEPES buffered saline (HBS) including 140 mM NaCl, 10 mM HEPES ([4-(2-hydroxyethyl)-piperazino]- ethanesulfonic acid, pH 7.4) to replace the extra-liposomal solution. The eluted liposomes were diluted with isotonic HEPES buffer to yield a final lipid concentration of 5 mM. Subsequently, doxorubicin HCl was added to the liposomal dispersion to achieve a drug to lipid ratio of 1/3 (mol/mol). The loading process was carried out at 4 °C for 12 h. The separation of liposomes from free DXR was performed by ultracentrifugation. Ultracentrifugation was performed at 130 000g for 3 h at 20 °C (Beckman Airfuge, USA), and the supernatant was removed. The liposome pellet was redispersed in HBS at pH 7.4.

Flow cytometry

After HepG2 cells were treated with liposomes and/or peptides at around 80% cell confluency, the incubation solution was aspirated and cells were released with 100 µl 0.025% Trypsin for 3 min at 37 °C; 500 µl DMEM containing 2% FBS. 20 mM HEPES was used to suspend the cells. Cells were transferred to a filter-topped flow cytometry tube and analyzed on a BD LSR II flow cytometer. Cells displaying normal morphologies were gated and analyzed for labeled CTX fluorescence and rhodamine-labeled lipid fluorescence using the 488 nm and the 543 nm laser, respectively.

Doxorubicin Leakage Assays

40 µl Doxorubicin-containing liposomes were incubated with peptides at different concentrations for 1 h and were subject to ultracentrifugation at 130000 x g for 10 min at

room temperature, then doxorubicin in the supernatants were quantified photometrically at 495 nm. Complete liposome lysis was treated with 5 µl 4% Triton X-100, and as a negative control, no peptide was added. Fractional leakage was calculated as

$$f_{DOX\ leakage} = (F_{sample} - F_{no\ peptide})/(F_{triton} - F_{no\ peptide}) \qquad \text{(Equation 5)}$$

Cell transfection

Hela cells at 80% confluency were transiently transfected with GFP plasmid (Addgene) by Lipofectamine 3000 according to reagent kit instruction with/without M159 incubation. After 24 h, cells were subject to confocal microscope or Western-blot to visualize GFP expression or quantify GFP proteins respectively.

RESULTS

Blocking peptide-induced liposome-cell membrane interaction

In the last chapter, we found that M159 induced liposome aggregation and fusion potently, but that this effect can be inhibited by inclusion of 5% POPG or 5% PEG2K as shown by light scattering measurements (**Fig. 4-1A**) and FRET assays (**Fig. 4-1B**). At the beginning of this chapter, we test the effects of macrolittins on liposome-cell interactions. We incubated cultured human HeLa cells with dye-labelled liposomes made from 100% POPC, POPC + 5% POPG, or POPC + 5% PEG2k-PE. Cells were first incubated for 1 hr. with liposomes only or with liposomes followed by M159. Cells were washed and imaged by confocal microscopy. When cells were incubated with liposomes in the absence of peptides, very little dye-labelled lipid remained associated with the cells (**Fig. 4-1C**) indicating no spontaneous liposome- cell membrane interaction. When M159 was added to POPC vesicles and cells, many large (≥ 5 µm) bright particles were observed associated

with the cell surfaces. A few smaller particles had also been taken up into the cells. Our interpretation of these images is that M159 induced the formation of large lipidic aggregates which then adhered to the surfaces of the cells and were subsequently uptake by cell endocytosis. Liposomes made from POPC containing 5% POPG behaved like POPC in this experiment, leaving many lipidic particles associated with cell surfaces after washing (**Fig. 4-1C**). This is in contrast with the observation that M159-induced aggregation of POPC vesicles in buffer is inhibited by 5% POPG (**Fig. 4-1A&B**). In contrast, the confocal images showed that liposomes containing 5% PEG2K-PE, in the presence of M159, interact very little with cells compared to liposomes containing pure POPC (**Fig. 4-1C**). Based upon these experiments, we conclude that inclusion of 5% PEG2k lipids in POPC vesicles will prevent any fusion or aggregation in the presence of cells and probably in vivo as well. Therefore, in the cell culture experiments that follow below, we will use POPC + 5 mol% PEG2k-PE to prevent liposome cell interactions.[31]

M159 releases cholera toxin subunit B from liposomes in cell culture

To support our long-term strategy of utilizing macrolittins to trigger drug cargo release from liposomes, *in vivo,* we next test mock translational scenarios. Based on the data above, we hypothesized that macrolittins could be used to trigger macromolecular cargo release from POPC-PEG2K liposomes in the presence of cells without directly affecting the cells and without causing vesicle aggregation or fusion with cells. To test this idea, we used fluorescein-labelled cholera toxin subunit B (Fl-CTXB) as a macromolecular cargo. Fl-CTXB has a molecular weight of 11.6 kDa, which is a good model cargo because it is a protein cargo that will not escape from POPC vesicles spontaneously. Yet, once released by macrolittins CTXB will bind strongly to GM1 sphingolipids and will be

actively endocytosed into cells.[79] Thus, we can measure cargo release and subsequent uptake using flow cytometry and we can verify the cellular location of the released cargo by confocal microscopy. Fl-CTXB, at 0.7 μg/ml, was encapsulated in POPC vesicles containing 5% PEG2K-PE. We tested release by adding vesicles with entrapped CTXB to live HepG2 human liver cells followed by addition of M159. For a positive control we used direct addition of the same amount of non-encapsulated CTXB and vesicles. For negative controls we used vesicles and cells plus either no peptide addition, or the addition of the inert peptide ONEG.

The imaging results and quantification of flow results indicated that M159 readily released significantly higher amount of Fl-CTXB from vesicles and that the released protein was intact and was quickly uptaken into cells by endocytosis compared to negative controls (**Fig. 4-2A&B**). To investigate cell uptake of Fl-CTXB caused by liposome fusion with cell membrane, we utilized the same amount of R18, a non-toxic rhodamine labeled lipid which insert into cell membrane spontaneously as a positive control for lipid fusion. We found that very little of the lipid remained associated with cells, verifying that fusion and aggregation with cells do not take place under these conditions (**Fig. 4-2C**). This experiment constitutes a demonstration that the selectivity of the macrolittins is sufficient to trigger the release macromolecules from liposomes in the presence of cells, such that the cargo, but not the macrolittin peptide or the vesicle lipids, is immediately made available to cells.

M159 releases doxorubicin from liposomes in cell culture

Next, we encapsulated the classic small molecule chemotherapy drug, doxorubicin (DXR), into liposomes using remote loading method by a transmembrane phosphate

gradient.[80] In the clinic, DXR is often administered as vesicle encapsulated drug called Doxil.[81] DXR release is a more challenging system because its stable encapsulation in liposomes requires cholesterol, which reduces M159 activity. Nonetheless, M159 is still active against cholesterol-containing bilayers at concentrations where it has no toxicity to cells, enabling us to test this system in cell culture. DXR is a DNA intercalator that crosses cell plasma membranes spontaneously and diffuses to the nucleus where it induces apoptosis and cell senescence.[82] Conveniently, it is also fluorescent, so its cellular location can be determined. First, we confirmed that DXR encapsulation in these liposomes is stable for at least 24 hours (**Fig. 4-3A**). Then we measured peptide-induced leakage at 37°C and showed that M159 can induce release of DXR from these PC/cholesterol vesicles (**Fig. 4-4A**). Subsequently, we identified that the minimal exposure time for 200 μM free DXR to enter HeLa cells and cause measurable Hela cell toxicity is 12 minutes (**Fig. 4-4B**). We note that DXR does not kill most cells because it induces cell senescence. However, the fractional cytotoxicity is highly reproducible and can be used as measure of DXR biological effects. In these experiments, we added 200 μM vesicle-encapsulated DXR to HeLa cells and then induced drug release by adding M159 to the system for only 15 minutes before washing off vesicle and peptide. Positive control was 200 μM free DXR. Negative control was vesicle-encapsulated DXR plus the inert peptide ONEG. Confocal microscopy showed that that DXR was released from liposomes by M159 and was bound to DNA in cell nucleus after 15 min incubation (**Fig. 4-4C**). To quantify the cell toxicity induced by DXR, cells were incubated for 24 hours after 15 minutes with free DXR or encapsulated DXR plus peptides and then cytotoxicity was measured with Alamar Blue a sensor of metabolically active mitochondria. Treatment of HeLa cells for 15 minutes with 200 μM

encapsulated DXR had the same toxic effect as 200 μM free DXR (**Fig. 4-3B & 4-4D**), demonstrating that M159 readily made ~100% of the vesicle entrapped cargo molecules available in the presence of cells.

M159 decreases DNA transfection efficiency

In addition to liposome delivery, many other methods have been widely used for drug delivery. For example, cell penetrating peptides (CPP) can be conjugated with Peptide nucleic acid (PNA) and uptaken by cells efficiently[83]. Lipid nanoparticles have become very popular to deliver vaccines against viruses in vivo.[84] In terms of plasmid transfection, Lipofectamine 3000 has gained a lot of attention as a successful commercial product, which can form lipid nanoparticles with plasmid, driving uptake by various cell lines. To determine if M159 can affect the plasmid transfection by Lipofectamine 3000, we incubated a series of concentrations of M159 with plasmid-reagent complex and detected the difference in GFP plasmid expression. Interestingly, the results from confocal microscopy showed that significantly higher GFP expression was observed without M159 or with the inert peptide Oneg incubation while low GFP intensity was detected in the presence of M159. Thus GFP expression was inversely dependent on M159 concentration (**Fig. 4-5A**). Consistently, the blotting results indicated that higher concentration of M159 incubation during cell transfection did block GFP plasmid expression (**Fig. 4-5B**). Next, we tested if this low expression can be explained by inability of plasmid-reagent entry by M159 disruption. We firstly labeled the plasmid with Rhodamine and performed cell transfections. According to the confocal images (**Fig. 4-6**), the transfected cells without M159 or with Oneg had labeled DNA within the cell boundary, by contrast, little labeled DNA could be observed within cells with M159 treatment. Collectively, these results

suggested that M159 blocked plasmid expression by inhibiting DNA-Lipofectamine complex entry into cells, which might be caused by interrupting the compact structure of this complex. Further experiments will be required to elucidate the structure change of the complex potentially induced by M159.

DISCUSSION

To establish a peptide-triggered cargo release model, we already determined that the peptide M159 is very potent at permeabilizing POPC liposomes and it is not toxic to cells, as shown in previous chapters. In this chapter, our results constitute a demonstration that the selectivity of the macrolittins is sufficient to trigger the release of both small molecules and macromolecules from liposomes in the presence of cells, such that the cargo is immediately accessible to interact with cells at the microenvironment while neither macrolittin nor liposomes significantly interact with cells. Encapsulation of acutely toxic drugs increases the therapeutic index by sustaining their release and reducing their side effects systematically. Liposomal encapsulation of degradable compounds protects them in the body and increases circulation time. For instance, the recently approved SARS-CoV2 mRNA vaccines are delivered as liposome encapsulated mRNA for stability.[85] Liposomes can also accumulate passively in some tissues, especially tumors due EPR effect, where liposome accumulation followed by drug release is beneficial.[86]

From MelP5 to M159, we discover that non-toxic M159 has very high affinity to bind POPC liposome, and to cause both liposome leakage and fusion (**Fig. 4-7A**). In addition, M159 can induce interactions between heterogenous lipid (liposome and cell plasma membrane). Although we did not investigate the mechanism of this fusion further,

we could deduce that M159 induces some sub-visible lipid aggregates, and these compact lipid nanoparticles might subject to cell endocytosis, whereby POPC liposome fuse with cell membrane. Importantly, this fusion effect can be inhibited by inclusion of PEK2K labeled lipid, which can also increase liposome circulation time in vivo.

We have successfully encapsulated a toxin subunit and doxorubicin in liposomes, and showed that M159 could trigger their release from POPC or POPC/Cholesterol liposomes (**Fig. 4-7B**). However, while useful, these types of liposomes may not encapsulate all kinds of small and large cargoes without yielding toxic effect to cells, and we did try to encapsulate some small fluorescent cargo molecules that would remain entrapped. Therefore, the optimization of encapsulation method is needed for different cargoes, via factors such as buffer, temperature, lipid composition, purification method, and cargo property. In fact, the lipid dipalmitopyl-PC (DPPC) is more frequently used to prepare liposome formulations for drug delivery, partly because it does not have double bonds in fatty acid tails, and creates a much more stable bilayer because DPPC exists in a solid-like gel phase at physiological temperatures. M159 is highly selective to POPC liposomes but it cannot permeabilize DPPC or DOPC liposomes, so future peptide screening will be required to discover peptides specific to different lipid with altered tail length or double bonds.

In this work, we have proved the feasibility of the concept of utilizing the extraordinary membrane selectivity of the macrolittins to release cargos from liposomes in the presence of cells. However, there are some considerations for utilizing this model in vivo. Firstly, the first administration (injection) can be drug-containing liposomes, which could accumulate at a tumor site at some timepoint, and PK/PD characteristics such as time

of arrival at tumor site will be recorded; secondly, we should begin peptide administration after the majority of liposomes arrive at tumor cells, and determine the peptide properties in vivo. These are under ideal situations in which M159 has no systematic toxicity and is not degraded by protease in a short time. Importantly, the limitations of this model cannot be ignored. One is that the liposomes have no target effects despite EPR effect, which might lead to some undesirable effect, and a potential solution is to tether cancer cell surface antibody on liposomes. The other limitation is that the final peptide concentration will be extremely low due to systematic distribution and degradation by protease in vivo. The possible solution is to use D type peptide as a stimulus instead of L type peptide as mentioned in chapter 2. However, it is difficult to achieve targeting effect of peptides due to its small size.

Taken together, this work shows that the controlled release of macromolecular cargoes from PEG-POPC liposomes by the macrolittins is a delivery strategy that may be applicable in translational applications. Future technologies to be developed in support of this application include optimization of enhanced permeability and retention of vesicles and better targeting of vesicles and/or peptides to sites of interest.

Figure 4-1
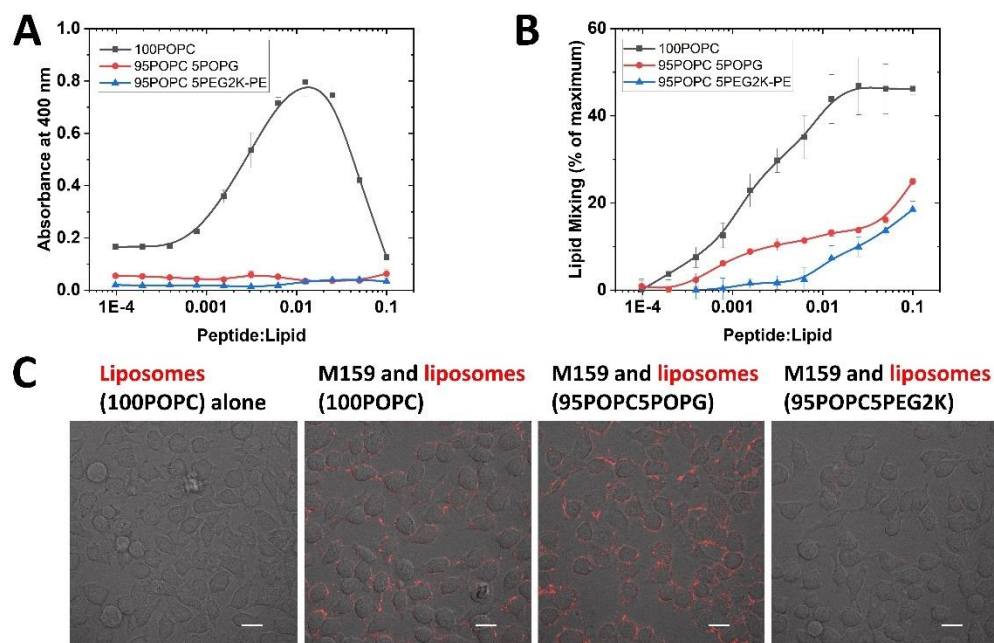
Figure 4-1. Inhibition of lipid-lipid aggregation and fusion. **A.** Light scattering of different compositions (100% POPC, 95% POPC and 5% POPG, 95% POPC and 5% PEG2K-PE) of liposomes with M159 treatments. 2 mM liposomes were incubated with M159 for 3 h different peptide to lipid ratios. **B.** FRET between dual labeled different liposomes and non-labeled different liposomes (100% POPC, 95% POPC and 5% POPG, 95% POPC and 5% PEG2K-PE). 0.4 mM Liposomes containing 0.5% NBD-PE and 0.5% rhodamine-PE dyes mixed with 2 mM unlabeled liposomes were incubated with M159 for 3 h at different peptide to lipid ratios. **C.** 32 µM M159 were incubated with different compositions of 1.6 mM 0.1% rhodamine-labelled liposomes in the presence of HepG2 cells and cells were washed and observed by a confocal microscope (from left to right: 100% POPC alone; 100% POPC and M159; 95% POPC, 5% POPG and M159; 95% POPC, 5% PEG2K and M159. ex/em = 512/560 nm). Scale bar = 20 µm. (Figure and legend are adapted from Sun, Hristova and Wimley, Nanoscale, 2021[31])

Figure 4-2
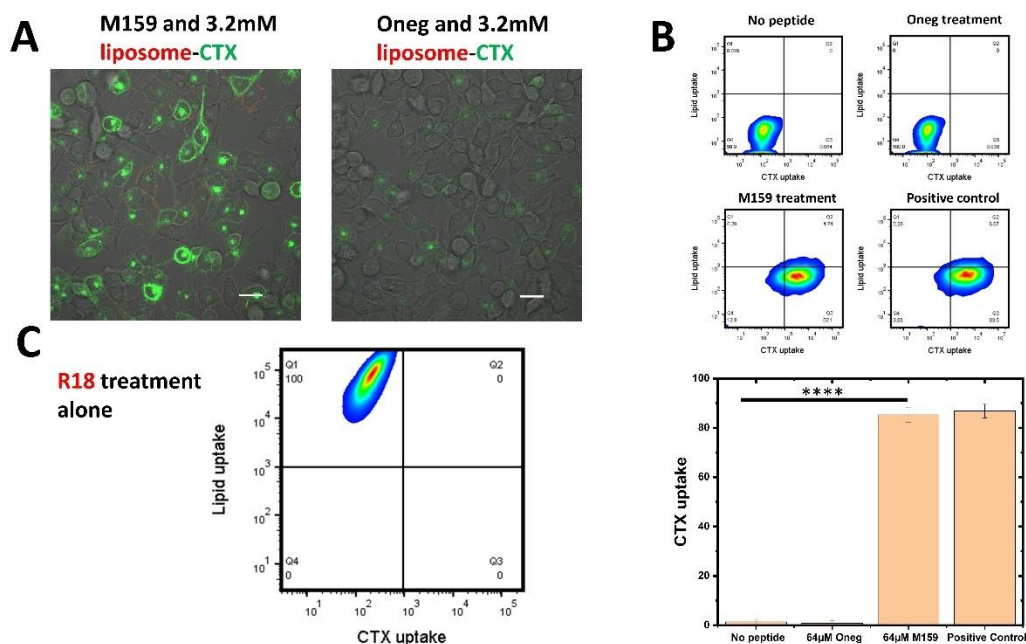
Figure 4-2. The effect of M159 on liposomes containing cholera toxin subunit B (CTXB). **A.** 3.2 mM 0.1% rhodamine-labeled liposomes (95% POPC, 5% PEG2k-PE) containing 0.7 mg/L FITC-CTXB were incubated with cells for 5 min and then 64 µM M159 or Oneg were added to HepG2 cells at around 80% cell confluency. After 25 min, cells were washed and observed in a confocal microscope (ex/em = 488/512 nm) (left: M159 treatment; right: Oneg treatment). Scale bar = 20 µm. **B.** Quantification of CTXB and lipid uptake in A by cells, using flow cytometry (from left to right: M159 and liposome-CTXB; M159, 0.7 mg/L free CTXB and empty liposomes; liposome-CTXB only; Oneg and liposome-CTXB; 3.2 µM rhodamine R18 lipid). **C.** Quantification of individual lipid uptake. Each measurement was repeated three times (****, p < 0.0001). (Figure and legend are adapted from Sun, Hristova and Wimley, Nanoscale, 2021[31])

Figure 4-3
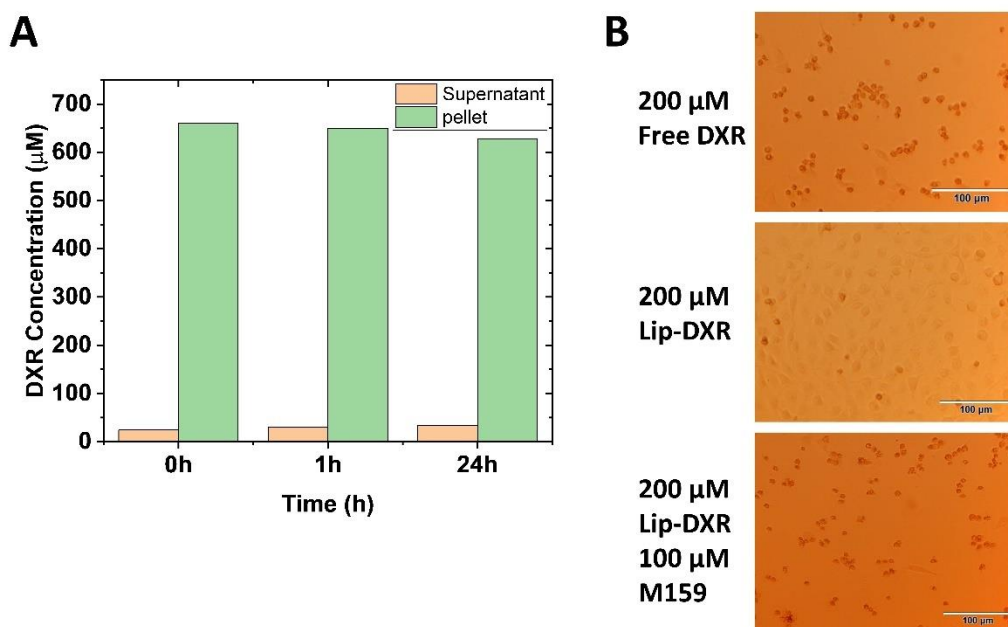
Figure 4-3. M159 and liposomes containing DXR. **A.** The stability of liposome-DXR. Doxorubicin was encapsulated into liposomes containing 70% POPC and 30% cholesterol by remote loading method. After preparation, at specific time points, liposome-DXR was ultracentrifuged (130000 x g) and DXR concentrations in the supernatant and in liposomes (pellet) were measured using a nanodrop. **B.** Hela cells were treated with 200 µM free DXR (upper), 200 µM liposome-DXR (middle) and 200 µM liposome-DXR plus 100 µM M159 (bottom) for 15 min respectively. After 24 h, cell morphology was observed by an optic microscope. Scale bar = 100 µm. (Figure and legend are adapted from Sun, Hristova and Wimley, Nanoscale, 2021[31])

Figure 4-4
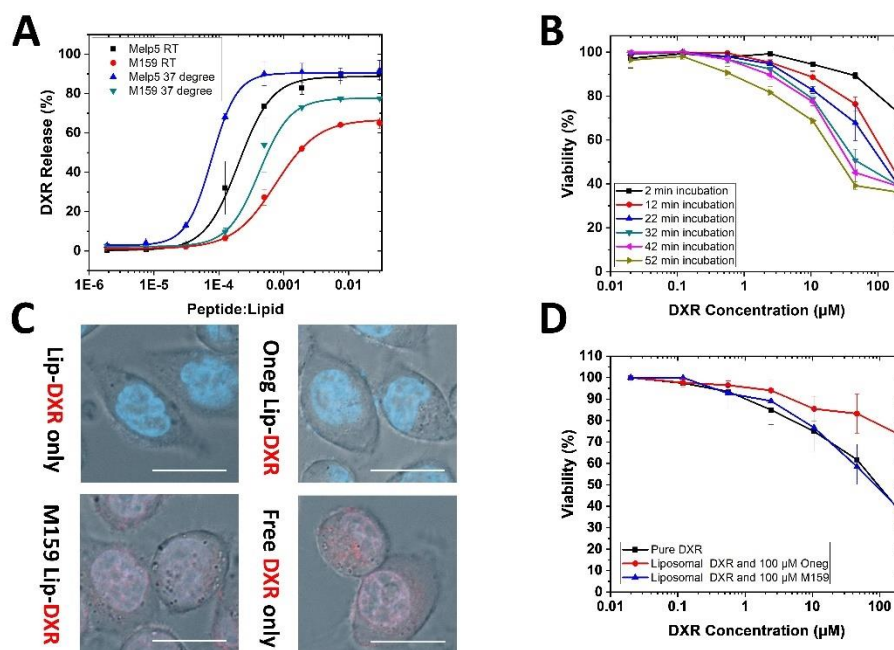
Figure 4-4. M159 and liposomes containing Doxorubicin (DXR). **A.** 6 mM liposomes (70% POPC, 30% Chol) containing 600 µM DXR were incubated with increasing concentrations of MelP5 or M159 for 1 h at room temperature or 37 degrees. After ultra-centrifugation, supernatants were measured photometrically at 495 nm by as released DXR. DXR from the lysis of liposomes with Triton X-100 was set as 100% DXR release. **B.** Increasing concentrations of free DXR (0.02 to 200 µM) were incubated with Hela cells for different time points (2 to 52 min). Cells were washed and subject to Alamar blue assay for viability measurements. **C.** 2 mM liposomes containing 200 µM DXR were incubated with cells for 5 min, then 100 µM M159 or ONEG was added onto cells. After 15 min, cells were washed and observed using a confocal microscope (top left: no peptide addition; top right: ONEG treatment; bottom left: M159 treatment; bottom right: 200 µM free DXR. Scale bar = 20 µm. **D.** Quantification of DXR-induced cell toxicity. Increasing concentrations of liposomes containing increasing concentrations of DXR or increasing concentrations of

free DXR were incubated with cells for 5 min, then 100 µM M159 or Oneg was added onto cells. After 15 min, cells were washed and replaced with complete media. After 24 hours, cells were subject to the cell viability assay. (Figure and legend are adapted from Sun, Hristova and Wimley, Nanoscale, 2021[31])

Figure 4-5
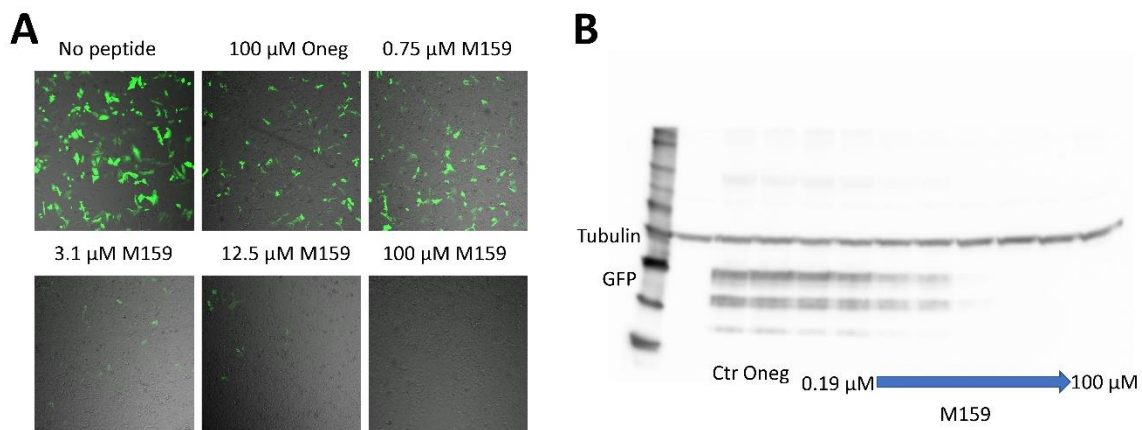
Figure 4-5. Effect of M159 on DNA plasmid transfection. **A.** 500 ng GFP plasmids were transfected into Hela cells by Lipofectamine 3000 reagents in the presence of peptide (Oneg or gradient concentrations of M159 shown). After 24 h, GFP expression were observed by confocal microscopy (ex488/em520). **B.** 2 µg GFP plasmids were transfected into Hela cells by Lipofectamine 3000 reagents in the presence of peptide (Oneg or gradient concentrations of M159 shown). After 24 h, GFP expression are seen by Western-blot, and tubulin served as a housekeeping protein.

Figure 4-6
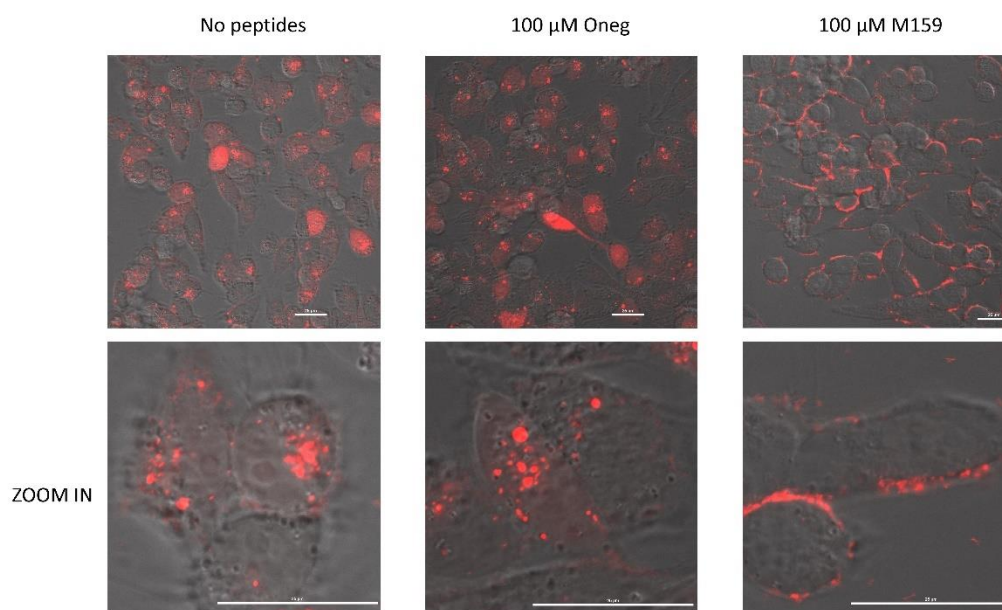
Figure 4-6. Effect of M159 on DNA plasmid entry into cells. 500 ng GFP plasmids were firstly labeled with Rhodamine and then transfected into Hela cells by Lipofectamine 3000 reagents without peptide incubation (left), in the presence of 100 µM Oneg (middle) or 100 µM M159 (right). After 24 h, DNA plasmid were observed by confocal microscopy (ex546/em576). (Top: full-size images; bottom: zoom in images, Scale bar = 20 µm)
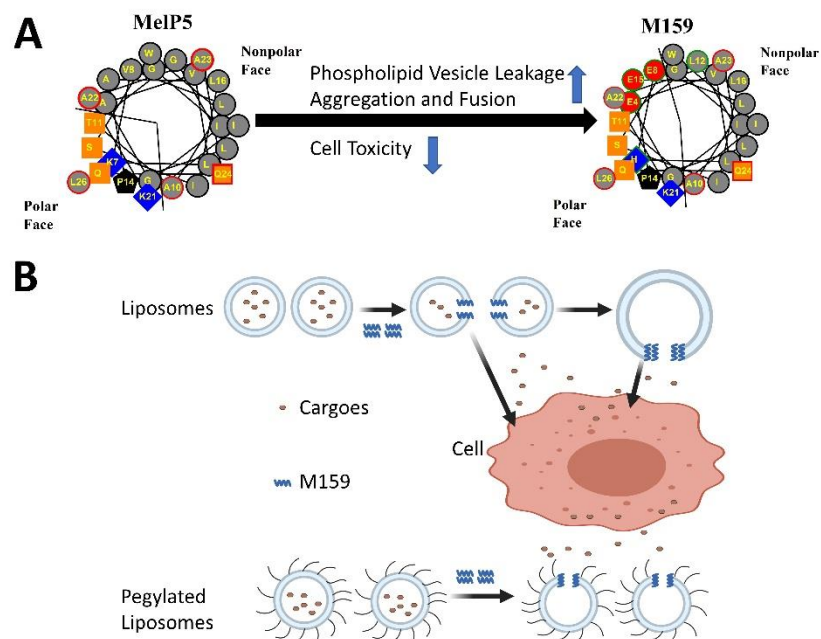
Figure 4-7

Figure 4-7. Schematic illustration of M159-induced cargo release from vesicles. **A.** Daughter M159 has a higher membrane selectivity than parent MelP5. **B.** In addition to causing PC vesicle leakage, M159 induces vesicle–vesicle fusion and vesicle–plasma membrane association, but these are inhibited by PEG on vesicles. (Figure and legend are adapted from Sun, Hristova and Wimley, Nanoscale, 2021[31])

CHAPTER 5: Screening an M159-based library for permeabilization of liposomes with different membrane thickness

INTRODUCTION

For membrane-permeabilizing peptide evolution, the laboratory has designed and screened at least two peptide libraries and discovered three generations of unique pore-forming peptides, including the macrolittins, studied here. All of these peptides are gain-of-function analogues of the natural venom toxin melittin. These peptides have diverse characteristics such as pH-dependent activity, high potency of permeabilization, and non-toxicity, and these features of peptides can be potentially useful in a variety of biotechnological applications, such as peptide-triggered drug release as discussed in previous chapters. However, it is not yet possible to predict the sequence-structure-function relationships for these peptides, because our understanding is mostly experimental and descriptive, due to the lack of reliable rules and algorithms for designing and engineering the functions of membrane active peptides.

From the peptide screening experience and the comparison of the different melittin-derived membrane active peptides, we found some clues and potential rules that might contribute to the pore-forming properties of these peptides. For example, both melittin and Melp5 have high percentage of non-polar amino acids that have high affinity to bind lipid membranes, including cell membranes, and cause high toxicity to mammalian cells. On the other hand, the daughter peptides pHD108 and M159 have fewer non-polar residues and cause minimal cell toxicity at pH 7. At pH 5, both pHD108 and M159 adopt α-helix

secondary structure in solution, even in the absence of lipid vesicles, suggesting that they self-assemble into oligomers. Melp5 and melittin, on the other hand, only adopt α-helix secondary structure in the presence of POPC when they partition into bilayers. In addition, molecular dynamic simulations, a computer simulation method used to analyze the structure and dynamics of atoms and molecules, enables us to better understand the interaction between peptide and lipid with details. Below, we will discuss sequence-structure-function of these membrane active peptides.

Importantly, we previously found that M159 has lower potency to enable macromolecules to pass membranes consisting of either thinner or thicker phospholipid (diC14:1PC and diC20:1PC), compared to POPC, C16:0-C18:1PC. The most significant effect observed was a dramatically lower pore forming potency for C20 liposomes, **Fig. 3-3**. In this chapter, we will describe a new peptide library, based on the sequence of M159, to screen peptide hits which permeabilize both C14 and C20 liposomes with high potency. We will focus on two key points: firstly, α-helical structure as peptide secondary structure should be maintained to partition into membranes perpendicularly; secondly, the length of peptides should be increased to get through thick membranes so that pores can be formed to enable the passage of macromolecules. Therefore, in the library, we i) maintained the hydrophobic/hydrophilic spacings of **3 to 4** amino acids for α-helix structure and pore formation on the liposomes, and ii) increased the length of M159 peptide at N terminus and/or C terminus. In addition, we made some specific residue substitutions in the library to modify overall net charge or hydrophobicity while some critical residues will not change according to **Chapter 3**. Finally, a peptide library containing 1728 peptides will be synthesized and screened for release of macromolecules in both thin (C14) and thick (C20)

liposomes. Sequences of peptide hits that can permeabilize thicker liposomes with high potency, will be compared to see if they share some similarities which are consistent to our design strategy for longer, α-helix peptides. Such potential rules can be utilized to engineer more membrane-permeabilizing peptides in the future.

MATERIALS AND METHODS

Piperidine, hexafluorophosphate (HATU), 1-Hydroxybenzotriazole (HOBT), protected amino acids, photolabile linker were purchased from Advanced Chemtech; DMF, DCM, DIPEA, phenol, TFA were purchased from Sigma.

Library construction

Peptide_Librarian is a custom software developed by Thomas C Freeman, and it was used to establish and display all the peptides in the library. This software can automatically generate all the sequences and molecular weights of the library after those amino acid variation of sequences was inputted, and they can be directly copied and pasted into Excel.

Solid phase peptide synthesis (SPPS)

Peptide synthesis was performed as described previously using a one-bead-one-peptide and a split-and-recombine approach.[87] 5 g of Tentagel MB NH2 polystyrene resin (0.3 mm diameter, 0.23 mmol/g loading capacity, Rapp Polymere MB30002) were swelled in dichloromethane (DCM) overnight, and then washed by dimethylformamide (DMF) for five times, then they were Fmoc deprotected with 30% piperidine in DMF. Resin was washed with DMF for five times, then an amino acid mixture containing individual amino acid and the coupling agent HATU, amide condensing agent HOBT, DIPEA were added

to the resin. The UV-labile linker 4-(4-[1-(9-Fluorenylmethyloxycarbonylamino)ethyl]-2-methoxy-5-nitrophenoxy) butanoic acid was added this way as well. Deprotection and amino acid addition continued until the peptide was complete. Remaining protective groups were removed with cold 88% trifluoroacetic acid (TFA), 5% phenol, 5% water, and 2% triisopropylsilane. Photolinker was cleaved from dry resin for 4 hr under 365 nm UV light from a standard 120-watt nail polish dryer. Optimizing extraction conditions involved adding different solvent solutions to the resin and incubating them under UV for 2 hours until dry. Concentration was then estimated with HPLC. Peptides were then brought into buffer solution by first incubating with 20 µL TBD leakage assay buffer 10 µL of this solution was used for C14 liposome leakage assay, 10 µL for C20 liposome leakage assay.

Screening

TBD leakage assays were described in **Chapter 3**.

MALDI mass spectrometry

Peptide and peptide-dye conjugate synthesized were mass verified using a Bruker Autoflex III MALDI-TOF mass spectrometer (Bruker Daltonics, Billerica, MA). Mass spectra data were collected in both linear and reflector mode with positive ion detection. Typical sample preparation for MALDI-TOF data was performed by making stock solutions of 70% Acetonitrile: water + 30% water with 0.1% trifluoroacetic acid saturated with α-Cyano-4-hydroxycinnamic acid matrix (20 mg/mL). 1 µL stock solution was mixed with 1 µL peptide solution (solvent: 50% methanol and 50% acetic acid) , deposited onto the MALDI target plate and allowed to evaporate via the dried droplet method.

RESULTS

Library design

The objective of this new library screening is to discover peptides that can permeabilize liposomes with different thickness. The main difference between vesicles in the screen is the fatty acid tail length. For example, liposomes consisting of C20:1 fatty acid have a thicker membrane, and M159 is much less potent against these thicker membranes. We hypothesize that longer peptides with α-helical secondary structure will be able to permeabilize thicker liposomes with higher potency. Therefore, one of the primary design principles in the library will be to test the effect of increasing the peptide length while maintaining α-helix structure.

The design of this new generation of membrane-permeabilizing peptide library was based on our previous two library design. In addition, the results regarding key amino acids of M159 evolution in **Chapter 3** are also considered. Plus, the molecular dynamic simulation results from our collaborators are important clues to the important principles of macrolittin pore formation. Generally, we made some residue substitutions and additions by modifying peptide hydrophobicity, amphipathicity, length and charge while preserving the helical spacings of polar residues. Thus, the limitations and observations that were made in previous projects are critical to review.

Firstly, we compared the sequences of evolutionary membrane-permeabilizing peptides including melittin, Melp5, M159 and pHD108 (**Fig. 5-1A**). We found that some residues are highly conserved residues or motifs such glycine-isoleucine-glycine from 1st to 3rd residues, 5th valine-6th leucine, 13th leucine-14th proline, 19th tryptophan-20th isoleucine, and charged residues are substituted by similar charged residues such as 7th and

21st cationic amino acids. Around C-terminus from 22nd to 26th residues, the prototype peptide melittin is significantly different from other peptides which share the same motif alanine-alanine-glutamine-glutamine-leucine. As is indicated by Helical Wheel projections in **Fig. 5-1B**, those non-polar residues compose the hydrophobic part of peptides which interacts with hydrophobic membrane bilayers while the polar residues form the hydrophilic face of the peptides which enables formation of the large pores and passage of macromolecules across membrane bilayers. Therefore, the arrangement of these conserved motifs maintains the property of membrane partitioning and pore formation during peptide evolution. Secondly, for individual residues, results from simulation shows how the distributions of the outermost hydrophobes, Val5 and Ala23, align tightly with the inner edge of the bilayer interface, and the polar face is marked by His7 and His21.[88] Importantly, Pro14, a highly conserved residue, is likely to function as a kink to adjust the overall length of the peptide according to the membrane thickness (**Fig. 5-1C**), however, C20 liposomes are so thick that pHD peptide cannot penetrate it even though Pro14 adjusts the peptide to the maximal length, suggesting that the peptides should be elongated to cross C20 membrane bilayer.[88] Lastly, we made several peptides variants from M159 and Melp5 and found that the glutamate residues at 4th, 8th positions are crucial determinants of cell toxicity and potency to permeabilize POPC liposomes. In other words, these factors likely determine selectivity for cholesterol-containing or pure POPC liposomes. And this selectivity to POPC lipid over cholesterol should be maintained for this new library design.

According to those observations above, the secondary structure of α-helix displays the peptide in an ideal helix of 3.6 residues per turn, these anionic residues were strategically positioned to maximize the number of i to i+3, i to i+4, and i to i+7 helical

spacings throughout the sequence for the formation of hydrophilic face and maximal interactions within aqueous pores when the peptides partition into membrane or otherwise fold into an α-helix. And this rule should be followed to maintain this secondary structure, therefore, we positioned one anionic or polar residue to every other 2 or 3 residues. For the length of peptide library, the middle part of peptides is important to adjust peptide length and hydrophobicity. Therefore, we added the hydrophobic motif LAL or ALA or XXX (none) to the N-terminus from 4th to 7th residues, and we added another hydrophobic motif LTLA or ATLA or XXXX (none) at around the C-terminus (29th to 32nd residues). The range of peptide length is from 27 to 35 residues. To test the effect of individual amino acid on peptide properties, glutamic acids at 4th, 12th and 19th maintained in M159 can be substituted by non-polar amino acids such as alanine and valine, consistent with the MelP5 sequence. The polar amino acid threonine at 15th position can also be other charged residues such as glutamic acid and lysine; the isoleucine at the 22nd position can be modified as glutamine, consistent with the majority of members in the macrolittin and pHD peptide families. Leucine at 16th position can also be glycine to decrease the side group space when partitioning. Finally, alanine can be added at 20th residue to potentially maintain overall helix. To sum up, we replaced residues in 6 positions and made 3 additions, which gave a total of 1728 possible peptides in this library. All amino acids were L-form and the whole library was subdivided into three sublibraries (L, A, X) according to 29th residue (**Fig. 5-2**). The peptide sequences were generated using Peptide_librarian software (**Fig. 5-3A**), and the numbers of peptides with the same molecular weight were distributed by histogram for each sublibrary (**Fig. 5-3B**), in which X sublibrary has lower molecular weight of peptides due to lack of 4 residues.

Solid phase peptide synthesis

SPPS has long been used as a well-established peptide synthesis method.[89] We used polyethylene glycol (PEG) modified polystyrene resin beads as the solid phase for our library. An active amino group is at the end of PEG attached to the resin bead and can react with amino acids. These resin beads with 0.3 mm diameter have a large surface area for peptide synthesis because they are porous. Each bead has a loading capacity of ~2.8 nmol. For each resin bead, only one peptide sequence will be conjugated according to the one-bead, one-peptide method.

The peptide synthesis reaction for coupling individual amino acids or photo-linker is indicated in **Fig. 5-4A**. The synthesis direction is from C terminus to N terminus so that the active amino group of the preceding amino acid is reacted with a carboxyl group of new amino acid whose amino group is protected. After this amino acid is coupled successfully, the amino group is deprotected by strong base and then proceeds with next residue reaction. A UV cleavable photolabile linker is also added in this way in between the resin and the peptide so that the peptide can be released from the resin. Notably, two glycines are conjugated between resin bead and photo-linker to increase reaction rate of the first amino acid coupling. The split-and-recombine approach is used to synthesize all peptides in this library. Specifically, we split the resin into separate vessels evenly, each for one reaction with different amino acids coupling to ensure one-bead-one-peptide principle (**Fig. 5-4B**). The separation of beads is used when a position in peptide has multiple possible amino acids. After separation, all the resin beads are combined together in one vessel and conjugated with only one amino acid if there is no variability at a residue position of the library. For example, in our template there are two possible amino acids

glutamic acid and valine at 4th residue, then the beads are split to two equal groups and each is reacted with either E or V amino acids, after which they will be recombined and mixed, deprotected before adding the glutamine next. To decrease the number of residue determination in Edman degradation, this library is divided into three sublibrary at 32nd position, therefore, three vessels are used to make sublibrary finally. After synthesis is complete, all the resin beads are subject to final deprotection of the N-terminus and all sidechain protecting groups.

Screening results

At this point, all the peptides with deprotected sidechains attached to resin beads via a photolabile linker have been synthesized successfully. To test the library members, a resin bead was added into individual well in 96-well plate to meet the principle of one peptide, one bead, one well. After cleavage from the resin bead by UV light, the peptide must be extracted, therefore, the choice of extraction solvent is important. Here, we tested a variety of solvent combinations including water, acetic acid, methanol, ethanol, DMSO, DMF, ACN, and DIPEA for preliminary peptide extraction by UV. We extracted library peptides from beads using individual solvent combinations and then quantified the amount of peptide by reverse-phase high performance liquid chromatography (RP-HPLC). We found that the solvent containing 80% methanol and 20% glacial acetic acid could extract up to 0.5 nmol peptide /bead under UV light, which was the best yield we observed for the A and X sublibraries. However, for the L sublibrary, this solvent mixture only was able to extract peptide from ~20% of the beads, and the yield was low. Other solvents had even lower yield for extracting peptide from the L sublibrary. Fortunately, this solvent could extract high concentrations of peptides from the majority of the resin beads (80%) in the A

and X sublibraries. Although we do not know the reason why peptides in the L sublibrary are difficult to extract, this observation might be explained by low solubility of these more hydrophobic peptides. We opted to screen peptides only from the from A and X sublibraries. Thus, we eliminated L sublibrary from the following large-scale peptide extraction and screening, and we screened a total amount of 1152 peptides from sublibraries A and X, using the TBD leakage assays (**Fig. 5-5**).

We screened around 600 peptides from sublibrary A and 600 peptides from sublibrary X with a total of 12 96-well plates for TBD leakage screening. Specifically, beads containing peptides were extracted by the solvent under UV light for two hours and the solvent was evaporated. Then 20 µL aqueous buffer for TBD leakage assays were added to reconstitute peptides, and 10 µL peptide solution were used for TBD leakage from C14 liposomes, the other 10 µL peptide solution were used for TBD leakage from C20 liposomes to achieve final peptide concentration as 10 µmol/L. We also included 10 µmol/L M159 as control, tritonX-100 and buffer as positive control and negative control respectively for TBD leakage assays. Therefore, the total amount of volume for TBD leakage assays are 50 µL with 1 hour incubation time.

Although we screened 6 plates for each sublibrary, we only chose 4 plates to fully analyze because of the high quality of data from these plates. The potency of liposome permeabilization induced by peptide hits was analyzed by Z-values (library member – plate mean)/ (plate standard deviation) for each library member using TBD leakage assays (**Fig. 5-6A**). In each screen the two TBD leakage values were roughly linearly related, and ranged from little leakage to significant leakage. For the A or X sublibrary, we found that there were peptide hits that enabled potent macromolecule passage across membranes with

different thickness as shown at left bottom areas in the histograms. Subsequently, we determined the molecular weights of these hits using MALDI mass spectrometry and looked for peptide sequences with the closest molecular weight in the library (**Fig. 5-6B**). Finally, those hits are named as plate number followed by well location in the plate (For example, 2E8 means well E8 on the second plate), and their sequences are listed in **Table 5-1** for sublibrary A and **Table 5-2** for sublibrary X. Notably, a specific molecular weight can be associated with multiple peptides due to interchanged position of two amino acids such as glutamic acid and valine. To confirm the sequences of these peptide hits, Edman degradation will be required to identify the individual peptides.

According to the results from mass spectrometry, we concluded the residue frequency for eight positions in each sublibrary (**Fig. 5-7**). For peptide hits in A sublibrary, 4th residue is completely taken up by E (41E/0V); ALA are dominant from 5th to 7th residues (21ALA/13LAL/7XXX); E is dominant at 12th residue (30E/11A); 15th position is main occupied by T (24T/16E/1K); G is dominant at 16th position (37G/4L); E is dominant at 19th residue (39E/2V); 20th can be either X or A (19X/22A); Q takes up the 22nd position (39Q/2I). And for peptide hits in X sublibrary, 4th residue is mainly taken up by E (26E/6V); ALA, LAL and XXX are distributed on average from 5th to 7th residues (11ALA/12LAL/11XXX); E is dominant at 12th residue (22E/12A); 15th position is main occupied by T (20T/9E/5K); G is dominant at 16th position (23G/11L); E is dominant at 19th residue (28E/6V); 20th is dominated by X over A (21X/13A); Q and I is distributed on average at 22nd position (17Q/17I). Finally, the consensus sequences are shown and compared with M159. Collectively, these peptides that can potentially permeabilize thicker and thinner liposomes potently are generally longer (XXX frequency is relatively low), but

maintain amphiphilicity with anionic residue E occurring in the sequences every other 3 or 4 residues, which can also be polar residues such as T or Q, suggesting helix structure with both hydrophilic and hydrophobic faces of peptides. We also found that G is dominant in the middle of peptides, which might be explained by a better flexibility due to lack of side group.

DISSCUSSION

Synthetic molecular evolution (SME) has been used to discover new molecules with desirable functions.[90, 91] In addition to screening membrane-permeabilizing peptides, we have discovered other gain-of-function peptides. For example, the hybrid cell penetrating peptides were discovered to deliver peptide nucleic acids (PNA) into cells with high efficiency; the antimicrobial peptide D-CONGA was effective at sterilize multi-drug resistant bacteria in animal model by topical administration.[4, 83] In this Chapter, we utilized SME to identify peptides with high potency to permeabilize liposomes with different thickness other than POPC bilayers.

We have accumulated rich experience for discovery of analogues of the natural toxin melittin. From previous results and observations, we conclude that α-helix secondary structure is important for membrane-permeabilizing peptides to partition into membranes, and that hydrophilic and hydrophobic faces are needed to stabilize the pore formation within membrane and enable efficient molecule passage across bilayers, yet the exact mechanisms of these peptides remain elusive and there is no strict rule for design or engineering. Here, we focused on the interaction between peptides and phospholipids with different lengths of fatty acid tails, especially longer tails such as C20. Either potent peptide

M159 or MelP5 could not completely permeabilize C20 liposomes. Therefore, we hypothesized that elongation of M159 while maintaining helix of peptide could make pores within C20 membrane. Thus, we designed the third-generation library of membrane-permeabilizing peptides. Specifically, we inserted anionic residue glutamic acid or polar amino acid with helical spacings to create a hydrophilic face to form the aqueous surface of the pore for molecule passage. The majority of residues consisted of non-polar residues, which formed the hydrophobic face to associate tightly with lipid bilayers.

During peptide screening, we did not know the molecular weight and sequence of each peptide, and the concentration of each peptide is roughly estimated due to the difference of peptide extract efficiency and solubilization. However, we could still discover many peptide hits that permeabilize both C14 and C20 liposomes with high potency from A and X sublibrary. Then we determined the molecular weights of all peptide candidates and found potential peptide sequences accordingly, though there was some uncertainty due to different library members having the same molecular weight. Nonetheless, highly conserved consensus sequences were determined from the screen. The final peptide sequences will be confirmed by Edman degradation. From all the sequences of peptide hits, which is consistent to our hypothesis: the majority of peptides have glutamic acid or polar amino acid positioned every **three or four** residues regularly; those peptides tend to have longer sequence than parent peptide M159, suggesting that penetration of thicker membrane requires longer helix peptides.

After these peptide sequences are identified, we will confirm their potency to permeabilize C14 and C20 liposomes. These liposomes are likely to have different characteristics compared to POPC liposomes such as stability, encapsulation efficiency,

cargo preference and PK/PD in vivo. Therefore, the optimization of peptide-triggered cargo release model will be investigated using different peptides and lipids for more advanced strategies of drug delivery in the future.

Figure 5-1
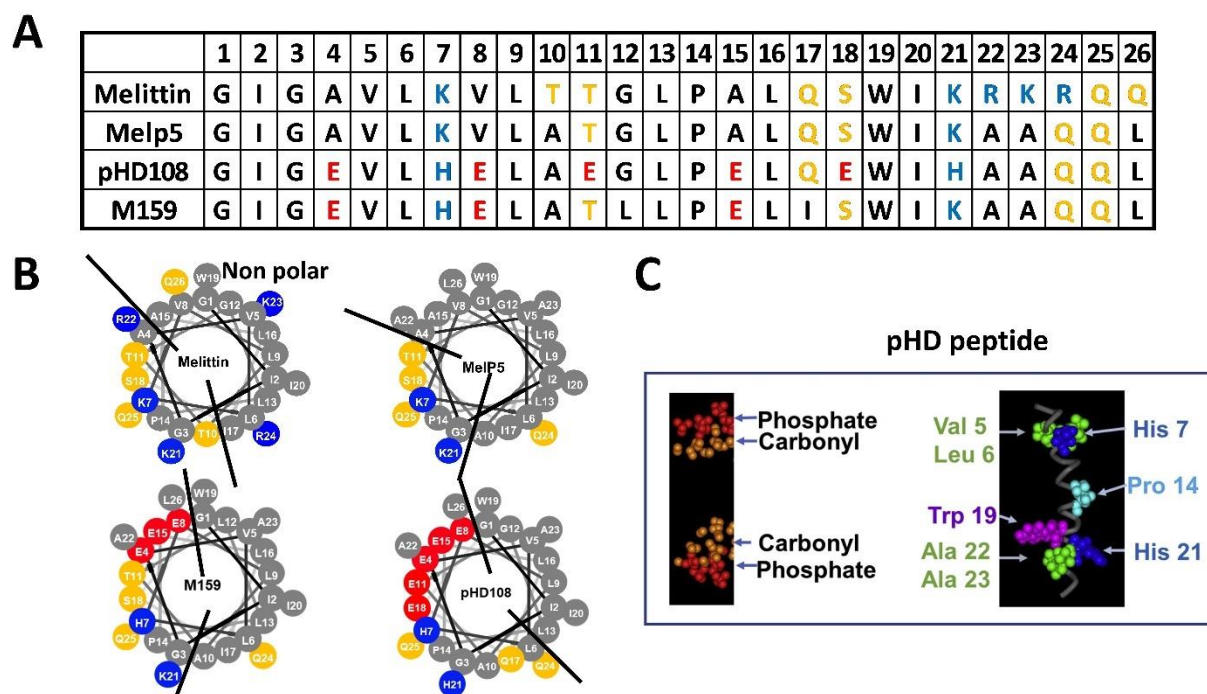
Figure 5-1. Sequence and structure of membrane-permeabilizing peptides. **A.** List of the amino acid sequences of generations of peptides. Acidic (red), basic (blue) and polar (yellow) residues are shown to highlight amphipathicity. **B.** Helical Wheel projections of the membrane-permeabilizing, non-polar side of α-helix is shown as grey color. C. Key residues of pHD108 are shown within POPC bilayer by MD simulation (figure was adapted from Kim SY, et al, *Biophys J*. 2021[88]).

Figure 5-2

	1	2	3	4	5	6	7	8	9	10	11	12	13	14	15	16	17	18	19	20	21	22	23	24	25	26	27	28	29	30	31	32	33	34	35
Whole library	G	I	G	E	(X	X	X)	E	V	L	H	E	L	A	T	L	L	P	E	X	L	I	S	W	I	K	A	A	(X	X	X	X)	Q	Q	L
				V	(L	A	L)					A			E	G			V	A		Q							(L	T	L	A)			
					(A	L	A)								K														(A	T	L	A)			
L sublibrary	G	I	G	E	(X	X	X)	E	V	L	H	E	L	A	T	L	L	P	E	X	L	I	S	W	I	K	A	A	L	T	L	A	Q	Q	L
				V	(L	A	L)					A			E	G			V	A		Q													
					(A	L	A)								K																				
A sublibrary	G	I	G	E	(X	X	X)	E	V	L	H	E	L	A	T	L	L	P	E	X	L	I	S	W	I	K	A	A	A	T	L	A	Q	Q	L
				V	(L	A	L)					A			E	G			V	A		Q													
					(A	L	A)								K																				
X sublibrary	G	I	G	E	(X	X	X)	E	V	L	H	E	L	A	T	L	L	P	E	X	L	I	S	W	I	K	A	A	X	X	X	X	Q	Q	L
				V	(L	A	L)					A			E	G			V	A		Q													
					(A	L	A)								K																				

Figure 5-2. Library design. This table indicates the template of this peptide library based on M159, and the length of peptides increases from 26 to 35 residues. Nine parts of this template were substituted (4th, 5th-7th, 12th, 15th, 16th, 19th, 20th, 22nd, 29th-32nd). Because solid phase peptide synthesis beginned from C terminus to N terminus, this library was subdivided into three sublibrary according to the residue at 29th (L as L sublibrary, A as A sublibrary, X as X sublibrary). The library was synthesized by split-and-combine strategy. Acidic (red), basic (blue) and polar (yellow) residues are shown to highlight amphipathicity.

Figure 5-3
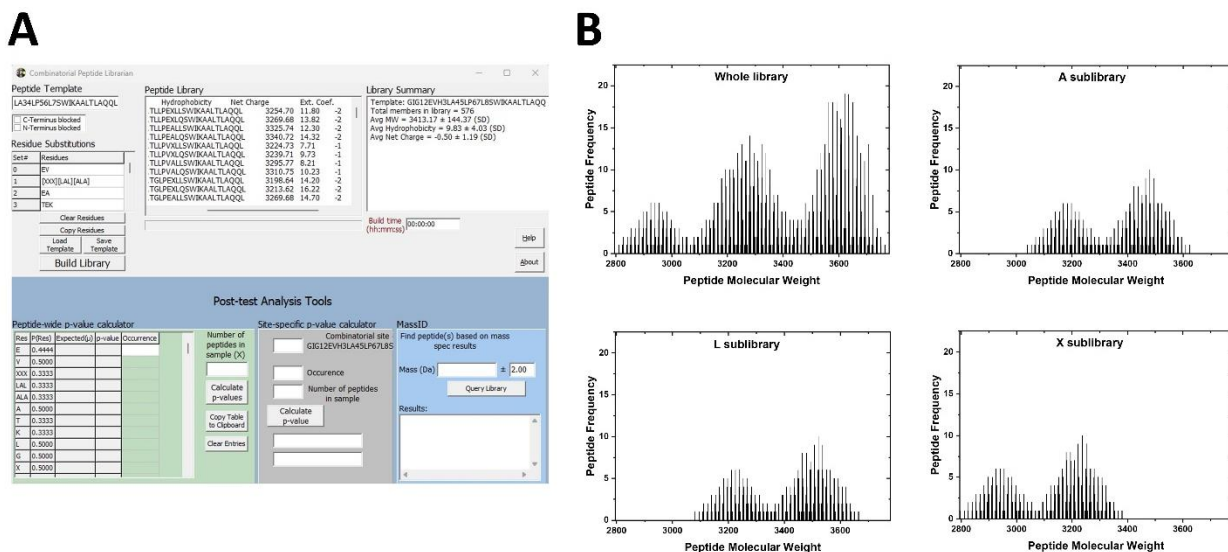
Figure 5-3. Peptide library generation. **A.** Peptide_Librarian is a custom software used to establish and display all the peptides in the library, and it also shows molecular weight, hydrophobicity, net charge and extinctive coefficient for each peptide. **B.** All the peptides in this library were generated, x axis indicated molecular weight of peptide and y axis showed number of different peptides with the same molecular weight. The whole peptide library was subdivided into L, A, X sublibrary.

Figure 5-4
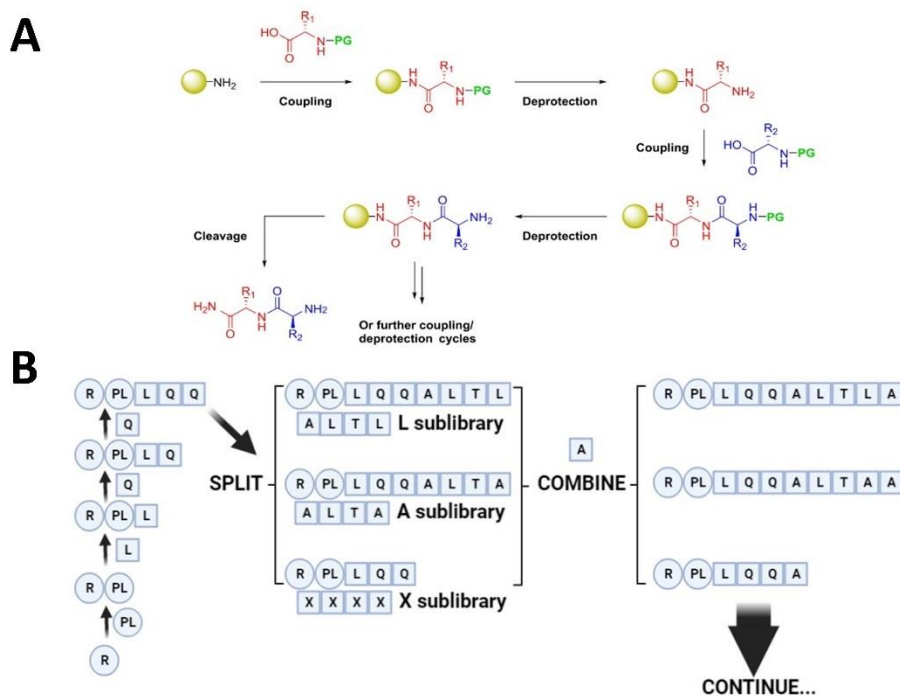
Figure 5-4. Solid phase peptide synthesis. **A.** The chemistry of SPPS proceeds by coupling new amino acid to amino group and then deprotection of the on-resin amino group, followed by addition of the next amino acid to that amino group. After all the residues were coupled, the polypeptide chain was deprotected and cleaved. (This figure is adapted from https://selekt.biotage.com/peptideblogs/what-is-solid-phase-peptide-synthesis) **B.** The split-and-recombine technique. This method splits the total amount of resins into separate reaction vessels evenly so that a different amino acid can be added to resins in individual vessel. Then all resins were recombined/mixed in one vessel again before the next set of the same amino acids were added. This figure shows the example of beginning of our library synthesis. (Created by Biorender)

Figure 5-5
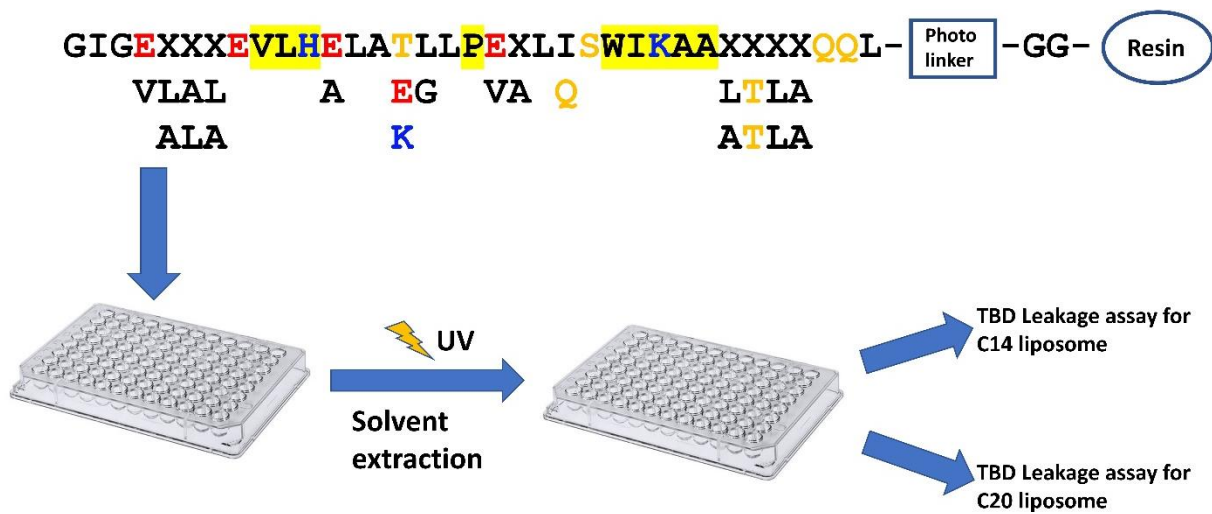
Figure 5-5. Workflow of peptide screening. When all the peptide syntheses on individual resin beads were completed and deprotected, individual beads were added into wells of 96-well plates (one bead, one peptide, one well), then resin beads were treated with extraction solvent (20% acetic acid, 80% methanol) under ultraviolet for 2 hours. After solvent evaporation, the extracted peptides were resuspended in aqueous buffers (0.025% acetic acid) for TBD leakage assays.

Figure 5-6
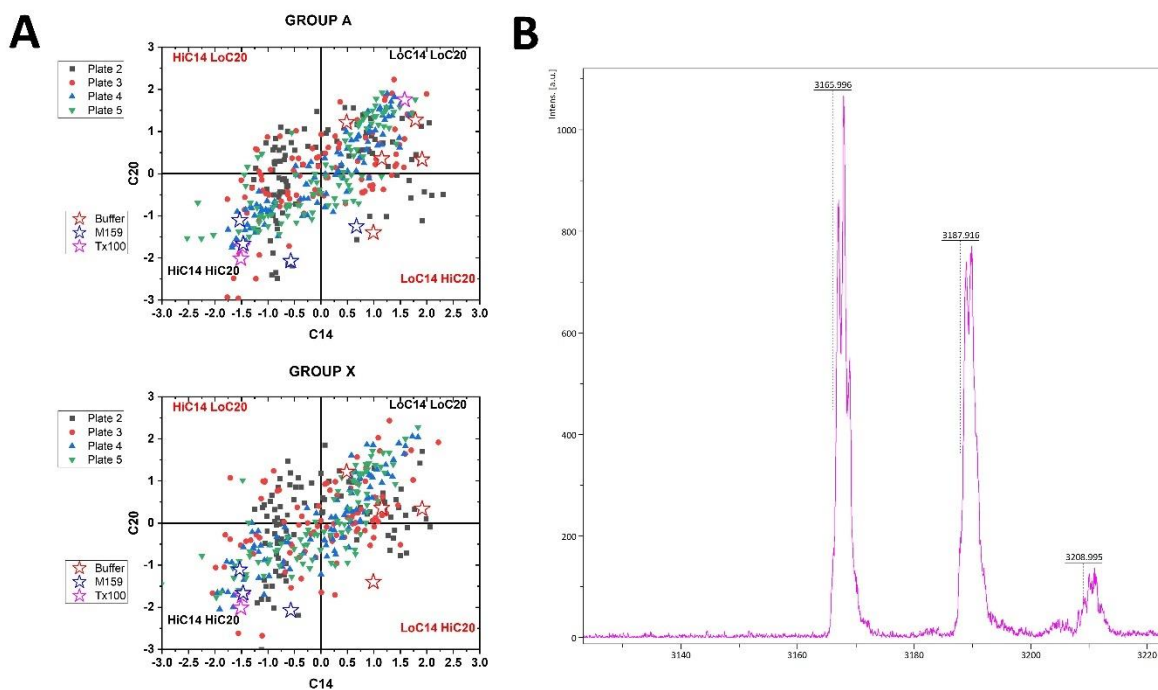
Figure 5-6. Peptide hits from library screening. **A.** The results of the screen. Z-values (library member – plate mean)/ (plate standard deviation) for each library member are shown. The peptides from sublibrary A (GROUP A, top) and sublibrary X (GROUP X bottom) were screened by TBD leakage assay using C14 and C20 liposomes. We selected potential peptide hits in area with both high potency for C14 and C20 (left bottom area) and measured their molecular weight by MALDI-TOF. **B.** An example of mass spectrometry figure of a peptide hit. The two larger peaks are Na adducts (+22) of the parent peak, indicating that this is a highly pure single sequence.

Figure 5-7
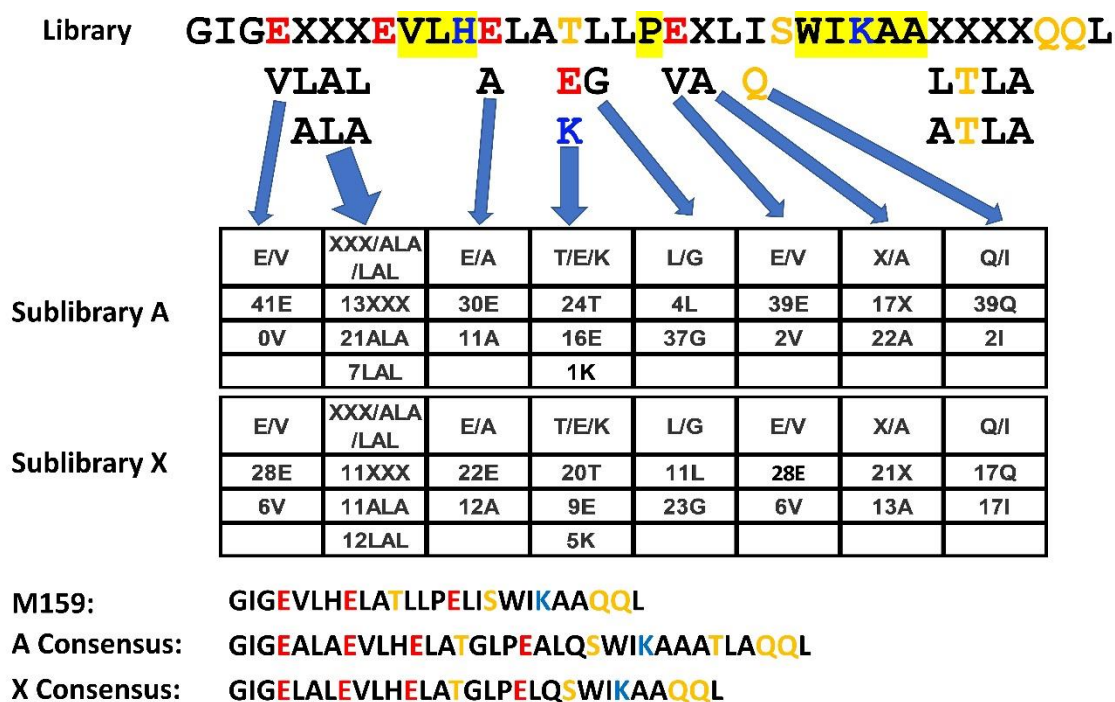
Figure 5-7. Residue comparison of potential peptide hits. For all peptide hits in sublibrary A and X, their molecular weights were measured and estimated in Table, and eight residue(s) variations were analyzed, and their frequency of occurrence were displayed in tables. The consensus sequences for each sublibrary are compared with parent peptide M159. The blue arrows from peptide template denoted residue substitution. Acidic (red), basic (blue) and polar (yellow) residues are shown.

Table 5-1

Peptide Hit	Potential Sequence
2C10	GIGELALEVLHELAEGLPEXLQSWIKAAATLAQQL
2D11	GIGEXXXEVLHELATGLPEALQSWIKAAATLAQQL
2E10	GIGEXXXEVLHALATGLPEALQSWIKAAATLAQQL
3A2	GIGVXXXEVLHELATGLPEXLQSWIKAAATLAQQL
3B3	GIGEALAEVLHELATGLPEXLQSWIKAAATLAQQL
3C11	GIGEXXXEVLHALATGLPEXLQSWIKAAATLAQQL
3C6	GIGEXXXEVLHALAEGLPEALQSWIKAAATLAQQL
3E11	GIGEALAEVLHALATGLPEALQSWIKAAATLAQQL
3E5	GIGEALAEVLHELATGLPEALQSWIKAAATLAQQL
3F5	GIGELALEVLHELAEGLPEALQSWIKAAATLAQQL
3G5	GIGEALAEVLHALAEGLPEXLQSWIKAAATLAQQL
3G8	GIGEALAEVLHELAEGLPEXLISWIKAAATLAQQL
4A5	GIGEXXXEVLHELATGLPEALQSWIKAAATLAQQL
4D6	GIGELALEVLHELATGLPEXLQSWIKAAATLAQQL
4E1	GIGEALAEVLHELATGLPEXLQSWIKAAATLAQQL
4E11	GIGELALEVLHELATGLPEXLQSWIKAAATLAQQL
4E6	GIGEALAEVLHELATGLPEXLQSWIKAAATLAQQL
4F9	GIGEALAEVLHELATGLPEALQSWIKAAATLAQQL
4G10	GIGEALAEVLHELATLLPEALQSWIKAAATLAQQL
4G5	GIGEXXXEVLHELAEGLPEALQSWIKAAATLAQQL
5B12	GIGEALAEVLHELATGLPEALQSWIKAAATLAQQL
5C1	GIGEALAEVLHALATGLPEALQSWIKAAATLAQQL
5C9	GIGEXXXEVLHELATLLPEALQSWIKAAATLAQQL
5D9	GIGEALAEVLHELAEGLPEALQSWIKAAATLAQQL
5E10	GIGEALAEVLHELAEGLPEALQSWIKAAATLAQQL
5F1	GIGELALEVLHELAEGLPEALQSWIKAAATLAQQL
2A10	GIGEXXXEVLHELAEGLPVXLISWIKAAATLAQQL
2A6	GIGEALAEVLHALATLLPEXLQSWIKAAATLAQQL
2B6	GIGELALEVLHELAEGLPEALQSWIKAAATLAQQL
2C10	GIGELALEVLHELAEGLPEXLQSWIKAAATLAQQL
2C11	GIGEALAEVLHELAKGLPEALQSWIKAAATLAQQL
2D11	GIGEXXXEVLHELATGLPEALQSWIKAAATLAQQL
2D6	GIGEALAEVLHALATGLPEXLQSWIKAAATLAQQL
2E10	GIGEXXXEVLHALATGLPEALQSWIKAAATLAQQL
2E9	GIGEALAEVLHALATGLPEALQSWIKAAATLAQQL
2F11	GIGEALAEVLHELAEGLPEXLQSWIKAAATLAQQL
2F12	GIGEXXXEVLHALAEGLPEXLQSWIKAAATLAQQL
2G11	GIGVXXXEVLHALATGLPVXLISWIKAAATLAQQL
2G3	GIGEXXXEVLHELATGLPEXLQSWIKAAATLAQQL
2H1	GIGEALAEVLHELATGLPEALISWIKAAATLAQQL
2H6	GIGEALAEVLHELAEGLPEXLQSWIKAAATLAQQL

Table 5-1. List of peptide hits in sublibrary A (First number is plate number followed by specific well).

Table 5-2

Peptide Hit	Potential Sequence
2B9	GIGELALEVLHALATLLPEXLQSWIKAAQQL
2B9	GIGELALEVLHALATGLPEALISWIKAAQQL
2C9	GIGELALEVLHELAEGLPVXLISWIKAAQQL
2C9	GIGVLALEVLHELAEGLPEXLISWIKAAQQL
2E8	GIGEALAEVLHELAKGLPVXLISWIKAAQQL
2E8	GIGVALAEVLHELAKGLPEXLISWIKAAQQL
2E8	GIGVLALEVLHELATGLPVXLQSWIKAAQQL
2F4	GIGEALAEVLHELAEGLPVXLISWIKAAQQL
2F4	GIGVALAEVLHELAEGLPEXLISWIKAAQQL
2F9	GIGEALAEVLHELAEGLPEXLISWIKAAQQL
3B2	GIGELALEVLHELATGLPEXLQSWIKAAQQL
3G10	GIGELALEVLHALATGLPEXLQSWIKAAQQL
3G3	GIGELALEVLHALAEGLPEXLISWIKAAQQL
3G4	GIGEALAEVLHELAEGLPEXLISWIKAAQQL
4C7	GIGEALAEVLHELATLLPEALQSWIKAAQQL
4D11	GIGEXXXEVLHALAKGLPEALQSWIKAAQQL
4D5	GIGEXXXEVLHELATGLPVALQSWIKAAQQL
4D5	GIGVXXXEVLHELATGLPEALQSWIKAAQQL
4D5	GIGEXXXEVLHELATLLPEXLISWIKAAQQL
4F3	GIGELALEVLHALATLLPEXLQSWIKAAQQL
4F3	GIGELALEVLHALATGLPEALISWIKAAQQL
4H4	GIGELALEVLHALATLLPEALQSWIKAAQQL
4H6	GIGEXXXEVLHELAELLPVALQSWIKAAQQL
4H6	GIGVXXXEVLHELAELLPEALQSWIKAAQQL
4H8	GIGEXXXEVLHALATLLPEXLQSWIKAAQQL
4H8	GIGEXXXEVLHALATGLPEALISWIKAAQQL
5B3	GIGEALAEVLHALATLLPEXLQSWIKAAQQL
5B3	GIGEALAEVLHALATGLPEALISWIKAAQQL
5C7	GIGELALEVLHELATGLPEXLQSWIKAAQQL
5D6	GIGEXXXEVLHELATGLPEXLISWIKAAQQL
5E4	GIGEXXXEVLHELAKLLPEXLQSWIKAAQQL
5E4	GIGEXXXEVLHELAKGLPEALISWIKAAQQL
5E9	GIGEALAEVLHELATLLPEXLQSWIKAAQQL
5E9	GIGEALAEVLHELATGLPEALISWIKAAQQL

Table 5-2. List of peptide hits in sublibrary X (First number is plate number followed by specific well).

REFERENCES

1.	S. L. Gerlach, R. Rathinakumar, G. Chakravarty, U. Göransson, W. C. Wimley, S. P. Darwin and D. Mondal, *Biopolymers*, 2010, **94**, 617-625.

2.	J. Suhorutsenko, N. Oskolkov, P. Arukuusk, K. Kurrikoff, E. Eriste, D.-M. Copolovici and Ü. Langel, *Bioconjugate Chemistry*, 2011, **22**, 2255-2262.

3.	H. Pan, N. R. Soman, P. H. Schlesinger, G. M. Lanza and S. A. Wickline, *Wiley Interdiscip Rev Nanomed Nanobiotechnol*, 2011, **3**, 318-327.

4.	C. G. Starr, J. Ghimire, S. Guha, J. P. Hoffmann, Y. Wang, L. Sun, B. N. Landreneau, Z. D. Kolansky, I. M. Kilanowski-Doroh, M. C. Sammarco, L. A. Morici and W. C. Wimley, *Proc Natl Acad Sci U S A*, 2020, **117**, 8437-8448.

5.	A. R. Hoffmann, S. Guha, E. Wu, J. Ghimire, Y. Wang, J. He, R. F. Garry and W. C. Wimley, *J Virol*, 2020, **94**.

6.	G. Bozzuto and A. Molinari, *Int J Nanomedicine*, 2015, **10**, 975-999.

7.	J. W. Park, *Breast Cancer Res*, 2002, **4**, 95-99.

8.	G. T. Noble, J. F. Stefanick, J. D. Ashley, T. Kiziltepe and B. Bilgicer, *Trends Biotechnol*, 2014, **32**, 32-45.

9.   W. C. Zamboni, A. C. Gervais, M. J. Egorin, J. H. Schellens, E. G. Zuhowski, D. Pluim, E. Joseph, D. R. Hamburger, P. K. Working, G. Colbern, M. E. Tonda, D. M. Potter and J. L. Eiseman, *Cancer Chemother Pharmacol*, 2004, **53**, 329-336.

10.   Y. Lee and D. H. Thompson, *Wiley Interdiscip Rev Nanomed Nanobiotechnol*, 2017, **9**.

11.   G. Kong, G. Anyarambhatla, W. P. Petros, R. D. Braun, O. M. Colvin, D. Needham and M. W. Dewhirst, *Cancer Res*, 2000, **60**, 6950-6957.

12.   H. L. Huang, P. H. Lu, H. C. Yang, G. D. Lee, H. R. Li and K. C. Liao, *Int J Nanomedicine*, 2015, **10**, 5171-5184.

13.   M. J. Barea, M. J. Jenkins, Y. S. Lee, P. Johnson and R. H. Bridson, *Int J Biomater*, 2012, **2012**, 458712.

14.   A. S. Ulrich, *Biosci Rep*, 2002, **22**, 129-150.

15.   S. Guha, J. Ghimire, E. Wu and W. C. Wimley, *Chem Rev*, 2019, **119**, 6040-6085.

16.   M. I. Sadowski and D. T. Jones, *Curr Opin Struct Biol*, 2009, **19**, 357-362.

17.   Y. Li, X. Han and L. K. Tamm, *Biochemistry*, 2003, **42**, 7245-7251.

18.   C. E. Dempsey, *Biochim Biophys Acta*, 1990, **1031**, 143-161.

19.   K. Matsuzaki, S. Yoneyama and K. Miyajima, *Biophys J*, 1997, **73**, 831-838.

20.   E. Jamasbi, S. Batinovic, R. A. Sharples, M. A. Sani, R. M. Robins-Browne, J. D. Wade, F. Separovic and M. A. Hossain, *Amino Acids*, 2014, **46**, 2759-2766.

21.   S. Dosler, E. Karaaslan and A. Alev Gerceker, *J Chemother*, 2016, **28**, 95-103.

22.   H. Memariani, M. Memariani, H. Moravvej and M. Shahidi-Dadras, *Eur J Clin Microbiol Infect Dis*, 2020, **39**, 5-17.

23.   H. Memariani and M. Memariani, *Appl Microbiol Biotechnol*, 2020, **104**, 6513-6526.

24.   S. Y. Woo and H. Lee, *Phys Chem Chem Phys*, 2017, **19**, 7195-7203.

25.   A. J. Krauson, J. He and W. C. Wimley, *J Am Chem Soc*, 2012, **134**, 12732-12741.

26.   G. Wiedman, T. Fuselier, J. He, P. C. Searson, K. Hristova and W. C. Wimley, *J Am Chem Soc*, 2014, **136**, 4724-4731.

27.   A. J. Krauson, O. M. Hall, T. Fuselier, C. G. Starr, W. B. Kauffman and W. C. Wimley, *J Am Chem Soc*, 2015, **137**, 16144-16152.

28.   S. Li, S. Y. Kim, A. E. Pittman, G. M. King, W. C. Wimley and K. Hristova, *J Am Chem Soc*, 2018, **140**, 6441-6447.

29.   G. Wiedman, S. Y. Kim, E. Zapata-Mercado, W. C. Wimley and K. Hristova, *J Am Chem Soc*, 2017, **139**, 937-945.

30.   Q. Lin and E. London, *PLoS One*, 2014, **9**, e87903.

31.   L. Sun, K. Hristova and W. C. Wimley, *Nanoscale*, 2021, **13**, 12185-12197.

32.   N. Oršolić, *Cancer Metastasis Rev*, 2012, **31**, 173-194.

33. S. F. Zhang and Z. Chen, *Mol Med Rep*, 2017, **16**, 3581-3586.

34. T. Yao and Y. Asayama, *Reprod Med Biol*, 2017, **16**, 99-117.

35. M. Liu, C. Li, M. Pazgier, Y. Mao, Y. Lv, B. Gu, G. Wei, W. Yuan, C. Zhan, W. Y. Lu and W. Lu, *Proc Natl Acad Sci U S A*, 2010, **107**, 14321-14326.

36. R. Akbari, M. Hakemi Vala, J. M. Sabatier and K. Pooshang Bagheri, *Amino Acids*, 2022, **54**, 1275-1285.

37. Z. V. Feng, I. L. Gunsolus, T. A. Qiu, K. R. Hurley, L. H. Nyberg, H. Frew, K. P. Johnson, A. M. Vartanian, L. M. Jacob, S. E. Lohse, M. D. Torelli, R. J. Hamers, C. J. Murphy and C. L. Haynes, *Chem Sci*, 2015, **6**, 5186-5196.

38. C. G. Starr, J. He and W. C. Wimley, *ACS Chem Biol*, 2016, **11**, 3391-3399.

39. J. Cruz, M. Mihailescu, G. Wiedman, K. Herman, P. C. Searson, W. C. Wimley and K. Hristova, *Biophys J*, 2013, **104**, 2419-2428.

40. J. Mejlvang, H. Olsvik, S. Svenning, J. A. Bruun, Y. P. Abudu, K. B. Larsen, A. Brech, T. E. Hansen, H. Brenne, T. Hansen, H. Stenmark and T. Johansen, *J Cell Biol*, 2018, **217**, 3640-3655.

41. G. Kroemer, L. Galluzzi, P. Vandenabeele, J. Abrams, E. S. Alnemri, E. H. Baehrecke, M. V. Blagosklonny, W. S. El-Deiry, P. Golstein, D. R. Green, M. Hengartner, R. A. Knight, S. Kumar, S. A. Lipton, W. Malorni, G. Nuñez, M. E. Peter, J. Tschopp, J. Yuan, M. Piacentini, B. Zhivotovsky and G. Melino, *Cell Death Differ*, 2009, **16**, 3-11.

42. Y. Chen, Y. Sun, Q. Zhao, C. Liu and C. Wang, *Cancer Drug Resist*, 2021, **4**, 1047-1060.

43. I. D. Solovyev, L. G. Maloshenok and A. P. Savitsky, *Materials (Basel)*, 2022, **15**.

44. W. Bursch, A. Ellinger, C. Gerner, U. Fröhwein and R. Schulte-Hermann, *Ann N Y Acad Sci*, 2000, **926**, 1-12.

45. Z. Zheng, J. Xie, L. Ma, Z. Hao, W. Zhang and L. Li, *Cell Mol Gastroenterol Hepatol*, 2022.

46. C. Mauvezin and T. P. Neufeld, *Autophagy*, 2015, **11**, 1437-1438.

47. J. M. Besterman and R. B. Low, *Biochem J*, 1983, **210**, 1-13.

48. A. Dautry-Varsat, *Biochimie*, 1986, **68**, 375-381.

49. S. Gordon, *Immunity*, 2016, **44**, 463-475.

50. P. Ridone, E. Pandzic, M. Vassalli, C. D. Cox, A. Macmillan, P. A. Gottlieb and B. Martinac, *J Gen Physiol*, 2020, **152**.

51. M. Kuzikov, J. Woens, A. Zaliani, J. Hambach, T. Eden, B. Fehse, B. Ellinger and K. Riecken, *Biomed Pharmacother*, 2022, **151**, 113104.

52. S. C. Maddila, C. Voshavar, P. Arjunan, R. P. Chowath, H. K. R. Rachamalla, B. Balakrishnan, P. Balasubramanian, R. Banerjee and S. Marepally, *Molecules*, 2021, **26**.

53. A. C. Quevedo, L. A. Ellis, I. Lynch and E. Valsami-Jones, *Nanomaterials (Basel)*, 2021, **11**.

54. E. Seaayfan, S. Nasrah, L. Quell, M. Kleim, S. Weber, H. Meyer, K. Laghmani and M. Kömhoff, *Cells*, 2022, **11**.

55. E. Sasabe, A. Tomomura, H. Liu, S. Sento, N. Kitamura and T. Yamamoto, *Cancer Sci*, 2022, **113**, 609-621.

56. I. Böhm and H. Schild, *Mol Imaging Biol*, 2003, **5**, 2-14.

57. X. Xie, Y. Li, H. Zhu, L. Chen, D. Chen, S. Lin and T. Fan, *Anticancer Agents Med Chem*, 2022, **22**, 3172-3181.

58. B. Vishnepolsky, G. Zaalishvili, M. Karapetian, T. Nasrashvili, N. Kuljanishvili, A. Gabrielian, A. Rosenthal, D. E. Hurt, M. Tartakovsky, M. Grigolava and M. Pirtskhalava, *Pharmaceuticals (Basel)*, 2019, **12**.

59. A. Prasad, A. Khatua, Y. K. Mohanta, M. Saravanan, R. Meena and I. Ghosh, *Nanoscale*, 2022, **14**, 10399-10417.

60. B. Wu, Q. Wang, X. Shi and M. Jiang, *Cell Commun Signal*, 2022, **20**, 161.

61. D. J. Klionsky, *Autophagy*, 2008, **4**, 740-743.

62. N. M. Sakhrani and H. Padh, *Drug Des Devel Ther*, 2013, **7**, 585-599.

63. S. Galdiero, A. Falanga, M. Cantisani, M. Vitiello, G. Morelli and M. Galdiero, *Int J Mol Sci*, 2013, **14**, 18758-18789.

64.   W. C. Wimley, *Methods Mol Biol*, 2015, **1324**, 89-106.

65.   J. C. Stewart, *Anal Biochem*, 1980, **104**, 10-14.

66.   T. Yeung, G. E. Gilbert, J. Shi, J. Silvius, A. Kapus and S. Grinstein, *Science*, 2008, **319**, 210-213.

67.   S. Raffy and J. Teissié, *Biophys J*, 1999, **76**, 2072-2080.

68.   J. Chen, J. Gao, M. Cai, H. Xu, J. Jiang, Z. Tian and H. Wang, *Nanoscale*, 2016, **8**, 13611-13619.

69.   O. Garbuzenko, Y. Barenholz and A. Priev, *Chem Phys Lipids*, 2005, **135**, 117-129.

70.   G. Cevc and H. Richardsen, *Adv Drug Deliv Rev*, 1999, **38**, 207-232.

71.   C. S. Chong and K. Colbow, *Biochim Biophys Acta*, 1976, **436**, 260-282.

72.   D. K. Struck, D. Hoekstra and R. E. Pagano, *Biochemistry*, 1981, **20**, 4093-4099.

73.   T. Hevonoja, M. O. Pentikäinen, M. T. Hyvönen, P. T. Kovanen and M. Ala-Korpela, *Biochim Biophys Acta*, 2000, **1488**, 189-210.

74.   S. H. White, W. C. Wimley, A. S. Ladokhin and K. Hristova, *Methods Enzymol*, 1998, **295**, 62-87.

75.   W. C. Wimley, *ACS Chem Biol*, 2010, **5**, 905-917.

76.   S. Y. Kim, A. E. Pittman, E. Zapata-Mercado, G. M. King, W. C. Wimley and K. Hristova, *J Am Chem Soc*, 2019, **141**, 6706-6718.

77.   C. Palm, M. Jayamanne, M. Kjellander and M. Hällbrink, *Biochim Biophys Acta*, 2007, **1768**, 1769-1776.

78.   J. N. Reginald-Opara, M. Tang, D. Svirskis, L. Chamley and Z. Wu, *Int J Pharm*, 2022, **626**, 122152.

79.   I. Basu and C. Mukhopadhyay, *Langmuir*, 2014, **30**, 15244-15252.

80.   A. Fritze, F. Hens, A. Kimpfler, R. Schubert and R. Peschka-Süss, *Biochim Biophys Acta*, 2006, **1758**, 1633-1640.

81.   Y. Barenholz, *J Control Release*, 2012, **160**, 117-134.

82.   F. Yang, S. S. Teves, C. J. Kemp and S. Henikoff, *Biochim Biophys Acta*, 2014, **1845**, 84-89.

83.   W. B. Kauffman, S. Guha and W. C. Wimley, *Nat Commun*, 2018, **9**, 2568.

84.   M. McMahon, G. O'Dell, J. Tan, A. Sárközy, M. Vadovics, J. M. Carreño, E. Puente-Massaguer, H. Muramatsu, C. Bajusz, W. Rijnink, M. Beattie, Y. K. Tam, E. Kirkpatrick Roubidoux, I. Francisco, S. Strohmeier, M. Kanekiyo, B. S. Graham, F. Krammer and N. Pardi, *Proc Natl Acad Sci U S A*, 2022, **119**, e2206333119.

85.   F. Wang, R. M. Kream and G. B. Stefano, *Med Sci Monit*, 2020, **26**, e924700.

86.   T. L. Andresen, S. S. Jensen and K. Jørgensen, *Prog Lipid Res*, 2005, **44**, 68-97.

87.   J. R. Marks, J. Placone, K. Hristova and W. C. Wimley, *J Am Chem Soc*, 2011, **133**, 8995-9004.

88.   S. Y. Kim, A. N. Bondar, W. C. Wimley and K. Hristova, *Biophys J*, 2021, **120**, 618-630.

89.   M. Amblard, J. A. Fehrentz, J. Martinez and G. Subra, *Mol Biotechnol*, 2006, **33**, 239-254.

90.   J. M. Rausch, J. R. Marks and W. C. Wimley, *Proc Natl Acad Sci U S A*, 2005, **102**, 10511-10515.

91.   R. Rathinakumar and W. C. Wimley, *J Am Chem Soc*, 2008, **130**, 9849-9858.

BIOGRAPY

Leisheng Sun was born on May 10, 1992 in Hunan Province, China, the only child of Zhiliang Sun and Libin Mo. He received his middle and high school from Hunan Agricultural Middle School and Yali Senior High School respectively, both located in Changsha city. Then He moved to Nanjing city in 2010 and obtained his Bachelor degree at China Pharmaceutical University in 2014, where he learned a lot of basic knowledge about biochemistry and pharmacology and developed his interest in human health sciences. Therefore, he came to Minneapolis and majored in pharmacology for a Master degree. And he selected Dr. Marchant as his advisor and joined his lab to study protein-protein interaction involved in cell autophagy, where he accumulated rich research experience about cell biology and biochemistry. Subsequently, he realized that his future goal is to development specific therapeutics to help patients who are suffering from diseases, and the ability to conduct independent and innovative research is really important. Therefore, he pursued a PhD at Tulane University in Dr. Wimley lab to discover active peptides that can be used as biotechnologies such antimicrobial therapy, drug delivery. Leisheng Sun has been focusing on membrane selectivity of peptide and developed a peptide-triggered cargo release model successfully, which was published on the cover on journal *Nanoscale*. And the rest of his work in the lab will be published soon. In addition, Leisheng Sun helped other lab members with their work and his names are in the authorship of several high-impact publications. Currently, Leisheng has already passed the final thesis defense and will get his PhD very soon. In the future, Leisheng Sun will continue his scientific projects to discover more functional peptides whose optimization will be used in a variety of treatment.